POLITECNICO DI TORINO

Corso di Laurea in Mechatronic Engineering

Tesi di Laurea Magistrale

Nonlinear analysis of stability and safety of Optimal Velocity Model vehicle groups on ring roads

Relatore
prof. Diego Regruto Tomalino

Correlatori:
prof. Francesco Paolo Deflorio
prof. Paolo Frasca
prof. Maria Laura Delle Monache
prof. Francesco Ferrante

Candidato
Cristina Magnetti Gisolo

A.A.2020/2021

Abstract

In the context of traffic control, modern techniques involve the presence of autonomous vehicles (AVs) implementing control strategies with the objective of stabilizing traffic flow and avoiding congestion. This approach has proven to be effective through experiments where a small number of AVs is inserted within a group of human-driven vehicles travelling on a ring road. With the objective of unveiling the key factors underlying experiments, we select a mathematical description of traffic flow and study its properties.

In this work, the well-known Optimal Velocity model, or Bando model, is adopted to model the behaviour of a group of N vehicles driving on a closed ring road without being fed by any external input signal. The main feature of this dynamical model is the definition of a velocity function for each vehicle, computed on the basis of the current distance with respect to the preceding vehicle. The dependence of the velocity, or optimal velocity, on the headway involves the hyperbolic tangent function, which makes the whole dynamical model nonlinear.

Beside Bando model, the analysis of a modified Optimal Velocity model is developed. This model is somehow a simplification, because it substitutes the hyperbolic tangent with a piecewise linear function in the definition of the velocity. In this way, the resulting Optimal Velocity model is significantly simplified and it can be studied as a linear system subject to saturated control law.

The objective of the proposed control law is to steer the system towards a particular equilibrium state, called speed equilibrium or uniform flow equilibrium, in which the N vehicles travel at the same speed and move on the ring keeping the same inter-vehicle distance. To study the stability of this particular equilibrium, both models are rewritten in a new set of state variables. In particular, the relative velocities of each couple of adjacent vehicles and their relative distances with respect to the distance at the uniform flow equilibrium. As a first step, the stability analysis is carried out by linearizing the model around the speed equilibrium and studying how the model parameters affect the eigenvalues of the linearized system. For Bando model, we apply results from the literature and state the relationship between the model parameters that must be satisfied to ensure local asymptotic stability of the uniform flow equilibrium to be asymptotically stable. Moreover, the same relationship is derived for groups of three, four and five vehicles by applying Routh criterion.

In the second part, the analysis is carried out on the original nonlinear models. Through the definition of local sector conditions on the nonlinearities of the models, it is possible to state a result that allows to determine an ellipsoidal estimate of the region of attraction. It is shown that the choice of the model parameters affects the size of the estimate, thereby validating the relationships between the stability and the model parameters that is observed through the former analysis based on linear approximation. The ellipsoids are then constrained to lie inside a polytope that forces a lower bound on the inter-vehicle distances. In this way, it is possible to define an invariant set from which collision is avoided.

Contents

1 Introduction 5

2 Optimal Velocity Model 11
- 2.1 Bando model . . . 11
  - 2.1.1 Experimental setup . . . 12
  - 2.1.2 Uniform flow equilibrium . . . 14
  - 2.1.3 Time simulation . . . 14
  - 2.1.4 Model in error coordinates . . . 17
- 2.2 Optimal Velocity model with saturation . . . 21
  - 2.2.1 Time simulation . . . 22
  - 2.2.2 Model in error coordinates . . . 24
- 2.3 Comparison of the two models . . . 25

3 Linear analysis 31
- 3.1 Linearization of Bando model . . . 31
  - 3.1.1 Time simulation . . . 39
- 3.2 Linear analysis of the model with saturation . . . 40
  - 3.2.1 Time simulation . . . 45
- 3.3 Comparison of the linear models . . . 51

4 Stability and safety analysis of the Optimal Velocity model with saturation 53
- 4.1 Linear systems subject to saturated control law . . . 53
- 4.2 Ellipsoidal estimate of the region of asymptotic stability . . . 59
- 4.3 Dependence of the RAS on the model parameters . . . 62
- 4.4 Safe region of asymptotic stability . . . 67

5 Stability and safety analysis of the Bando Optimal Velocity model 71
- 5.1 LTI systems with Neural Network Controller . . . 71
- 5.2 Ellipsoidal estimate of the region of attraction . . . 76
  - 5.2.1 Local sector condition on tanh . . . 76
  - 5.2.2 Offset local sector condition on tanh . . . 82
- 5.3 Dependence of the ROA on the model parameters . . . 84
- 5.4 Safe region of attraction . . . 87

6 Conclusion and future work 91
6.1 Summary and comparison of the models 91
6.2 Improvement of the analyses and future work 94

Bibliography 97

Chapter 1

Introduction

The interaction of groups of vehicles travelling on a roadway concerns everyday life and, in particular, traffic congestion is a usual phenomenon that may occur.
Traffic jams may have several causes, such as bottlenecks, lane changes or accidents, but in the experiment [1] carried out by Sugiyama et al. it is demonstrated that the behaviour of human drivers alone can lead to congestion.
In this experiment, shown in Figure 1.1, a group of 22 vehicles driven by humans travel on a ring road, starting at equally spaced positions. At first the flow is uniform, but, after some time, the vehicles speed up and slow down periodically, being too close with one another and then having too large headways. As a result, traffic flow is not uniform anymore and the travel is uncomfortable and unsafe, possibly leading to accidents. These phenomena where vehicles accelerate and then suddenly brake are known in the literature as stop-and-go waves. In the absence of changes to the roadway, since the behaviour of human drivers is sufficient to cause traffic jams, if there exists the chance to influence the driving of people, it is possible to improve traffic conditions, make drivers more comfortable and avoid accidents.
Several techniques have been employed in order to estimate and control traffic flow and handle and prevent traffic congestion.
Traffic control may rely on Eulerian systems at fixed locations, such as ramp metering [2], [3] and variable speed limits [4], [5], [6]. Both these techniques may show some limitations, because speed limits may not be attended by drivers and traffic congestion could occur on the access ramp of the road. Moreover, between two points where these systems are installed, there is no control on traffic.
In addiction to these fixed devices, the usage of Lagrangian or mobile systems is a common solution, both in control [7], [8], [9], [10] and sensing [11], [12]. It consists in the introduction in traffic flow of a certain number of controlled vehicles that, if needed, help to make the flow uniform, dampen stop-and-go waves, increase the road capacity and avoid traffic congestion. Of course, these vehicles need suitable sensing devices in order to localize other cars, measure their velocities and detect the presence of a possible traffic jam, and they must implement a control strategy able to stabilize traffic.
Nowadays, the main approaches in the usage of Lagrangian systems in traffic flow are variable speed limit control, platooning and mixed traffic.
Variable speed limit (VSL) strategies may be implemented at fixed points along the road

(a) $t = 0\ s$

(b) $t = 0.04\ s$

(c) $t = 0.08\ s$

(d) $t = 0.13\ s$

(e) $t = 0.18\ s$

(f) $t = 0.24\ s$

Figure 1.1: Experimental evidence for the physical mechanism of forming a jam. "The Mathematical Society of Traffic Flow", Yuki Sugiyama et al., New Journal of Physics, 2008, Multimedia supplement.

or they could be implemented by employing connected automated vehicles that adjust the speed of traffic flow [13], [14].
Platooning refers to the employment of only controlled vehicles, that form 'a platoon'. Examples of control techniques specific for this kind of system are the well known Adaptive Cruise Control (ACC) and Cooperative Adaptive Cruise Control (CACC). In a platoon, all

vehicles implement the same control strategy in order to reduce their inter-vehicle distance and keeping it safe or reaching high velocities avoiding accidents.
Mixed traffic refers to the usage of a possibly small percentage of autonomous vehicles that travel along side human drivers. A typical penetration rate representing the percentage of these vehicles with respect to the others is

$$penetration\ rate = 3 - 5\%.$$

As shown in [10], the presence of a small number of autonomous vehicles (AVs) may keep traffic flow fluid, avoid sudden acceleration and braking, prevent the occurrence of stop-and-go waves and make the travel safe and comfortable.
In Figure 1.2 is shown the experiment by Stern et al., with a setup similar to Sugiyama et al. one, where 22 vehicles travel on a ring road and only one of them is automated. At the beginning, the vehicles start equally spaced on the ring and the control action of the AV is switched off. Then, after some time, a wave arises, making some cars too close and others too far. During the experiment, the AV turns on its control strategy and dampens the wave, restoring the previous uniform flow.
Usually, the objective of traffic stabilizing is having all vehicles travelling at the same constant speed and keeping a safe headway.

(a) $t = 0\ s$

(b) $t = 93\ s$

(c) $t = 321\ s$

Figure 1.2: Ring road experiment with one AV by Stern et al.

Whatever is the selected control strategy, first of all there is need of a mathematical model able to describe the behaviour of any group of vehicles.
Traffic flow may be modeled by two kinds of mathematical descriptions:

- **Macroscopic modelling**
  Traffic is considered as a continuous flow and what is highlighted is the collective

behaviour of the group, without focusing on how the single vehicle behaves.
The mathematical description of these models includes nonlinear partial derivative equations (PDEs) that resemble the fluid-dynamics (i.e. conservation of mass equation). In this framework, the quantities of interest are traffic density, flow and average speed of the whole group and the result is the density distribution of the vehicles.
An example of macroscopic model is LWR model [15], [16], which exploits the conservation of cars mass law and it is based on the assumption that the average speed of the group of vehicles depends only on its density.

- **Microscopic modelling**
  The attention focuses on the dynamics of the single vehicle and the mathematical description of the whole group consists of a system of ordinary derivative equations (ODEs) for each car. The result is the trajectory of each vehicle and the quantities of interest are positions, velocities and accelerations of the vehicles.
  Car-following models are microscopic models, where the dynamics of the single vehicle depends only on the behaviour of the preceding one. Since each vehicle gets information only from the one in front of it, neglecting what happens behind, the information flow is unidirectional and therefore this kind of model is said to be 'unidirectional'.
  Two car-following models are the Follow-the-leader model [17], [18] and the Optimal velocity model [19]. In both mathematical descriptions, the acceleration of the i-th car depends on the position and/or the velocity of the preceding vehicle (i+1) in a nonlinear way (see Figure 1.3).

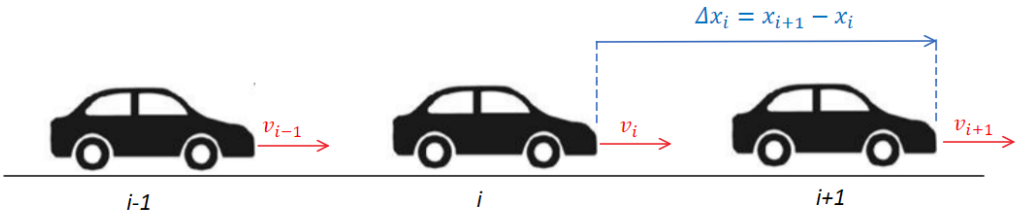

Figure 1.3: Three vehicles of the platoon

1. *Follow-the-leader model*
   Suppose the platoon is composed by N vehicles, x_i is the position of each vehicle and v_i is its absolute velocity.

$$\begin{cases} \dot{x}_i = v_i \\ \dot{v}_i = C \frac{v_{i+1} - v_i}{x_{i+1} - x_i}, \quad \forall\, i = 1, ..., N \end{cases} \tag{1.1}$$

   The acceleration of each car is linear with its relative speed with respect to the preceding vehicle $\Delta v = v_{i+1} - v_i$ and it is inversely proportional to their relative distance $\Delta x = x_{i+1} - x_i$. C is a constant with dimension [m/s].
   The drawback of this model is that, if two adjacent vehicles have the same velocity, the following vehicle does not speed up or slow down, whatever is their

relative distance. So, if the headway is too large, the following vehicle does not speed up in order to catch the leading one, and, if the headway is too small, the following vehicle does not brake in order to make the distance safer.

2. *Optimal velocity model*
   In order to solve the drawback of the Follow-the-leader model, the speed of each vehicle is compared with an optimal velocity value, computed on the basis of the headway with respect to the preceding vehicle. For instance, a possible optimal velocity function is defined in (1.2).

$$V_{opt}(x_{i+1} - x_i) = V_{\max} \frac{\tanh(x_{i+1} - x_i - l_v - d_s) + \tanh(l_v + d_s)}{1 + \tanh(l_v + d_s)} \tag{1.2}$$

$$\begin{cases} \dot{x}_i = v_i \\ \dot{v}_i = b\left[V_{opt}(x_{i+1} - x_i) - v_i\right], \quad \forall\ i = 1, ..., N \end{cases} \tag{1.3}$$

   b is a constant with dimension $[s^{-1}]$ representing the sensitivity of the driver, $\Delta x = x_{i+1} - x_i$ is the headway, d_s is the safe inter-vehicle distance and l_v is the length of each vehicle. Whenever the headway with respect to the preceding vehicle is small, the optimal velocity function tends to zero; on the contrary, if the inter-vehicle distance is very large, the optimal velocity tends to $V_{\max}$, which is the maximum allowable value.

- **Macro/microscopic modelling**
  It is possible to describe traffic flow as a collective phenomenon and add the dynamics of each single vehicle in order to both have an idea of the behaviour of the platoon and track the single car. These models mix macroscopic and microscopic descriptions of traffic and coupling equations that allow to combine them together.

Chapter 2

Optimal Velocity Model

2.1 Bando model

The Optimal Velocity model or the Bando model [19] is a microscopic description of traffic flow, where the acceleration of each single vehicle depends on an 'optimal' velocity function as described in (2.1). With this dynamical model, the velocity function of each car depends only on the headway with respect to the preceding vehicle.

$$\begin{cases} \dot{x}_i = v_i \\ \dot{v}_i = b\left[V_{opt}\left(x_{i+1} - x_i\right) - v_i\right], \quad \forall\ i = 1, ..., N \end{cases} \tag{2.1}$$

$b\ [s^{-1}]$ is a constant representing the sensitivity of the driver, x_i and v_i are the absolute position and velocity of the i-th vehicle and $\Delta x_i = x_{i+1} - x_i$ is the headway with respect to the preceding vehicle (i+1).
In the dynamical model introduced by Bando et al. the optimal velocity $V_{opt}(\Delta x_i)$ may be any monotonically increasing function that tends to zero when Δx_i is 'too small' and it tends to a maximum value when Δx_i is 'too large'. In this way, when the distance between the i-th vehicle and the vehicle i+1 is too small, the i-th vehicle slows down and it speeds up when its headway with respect to vehicle i+1 is too large.
A realistic function for the optimal velocity is

$$V_{opt}(x_{i+1} - x_i) = V_{\max}\frac{\tanh\left(x_{i+1} - x_i - l_v - d_s\right) + \tanh\left(l_v + d_s\right)}{1 + \tanh\left(l_v + d_s\right)} \tag{2.2}$$

where $V_{\max}$ is the maximum speed, l_v is the vehicle length and d_s is the safe distance between vehicles i and i+1. It is depicted in Figure 2.1. If $\Delta x_i = x_{i+1} - x_i \gg l_v + d_s$ so the inter-vehicle distance between the i-th vehicle and its preceding car is large, then $\tanh\left(x_{i+1} - x_i - l_v - d_s\right)$ tends to 1 and $V_{opt}(\Delta x_i)$ asymptotically converges to its maximum value $V_{\max}$. In this way, the i-th vehicle accelerates in order to reduce the gap in front of it.
If $\Delta x_i = x_{i+1} - x_i \ll l_v + d_s$, the headway between the i-th vehicle and its preceding car is too small, then $\tanh\left(x_{i+1} - x_i - l_v - d_s\right)$ tends to -1 and $V_{opt}(\Delta x_i)$ is low. In this way, the i-th vehicle slows down and the inter-vehicle distance with respect to the preceding vehicle increases.

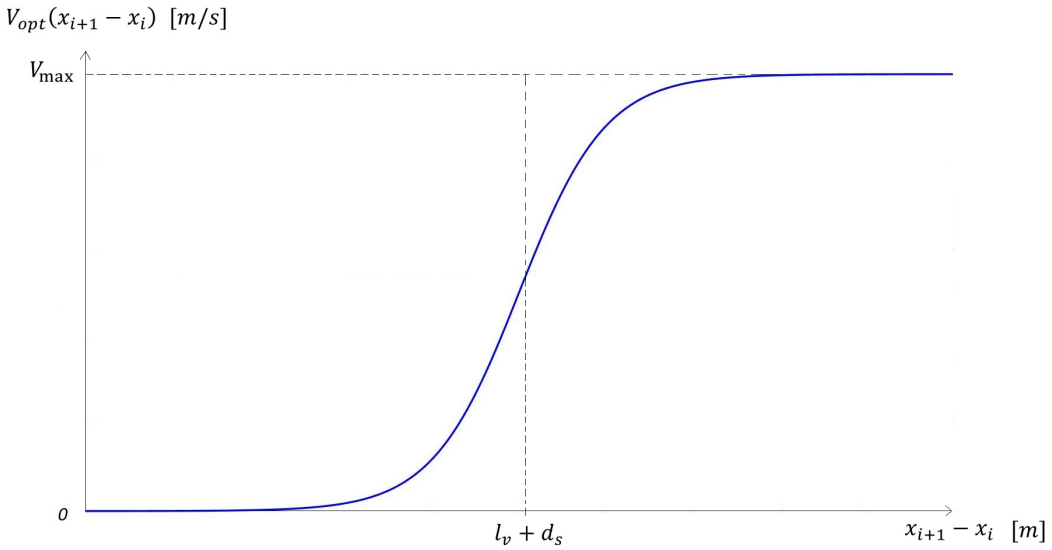

Figure 2.1: $V_{opt}(x_{i+1} - x_i)$ of the Bando model

The optimal velocity function (2.2) makes the model nonlinear and it shows only a dependence on the headway. More complex Optimal Velocity models describe the velocity as function of both the headway and the relative velocity with respect to the preceding vehicle:

$$V_{opt}(\Delta x_i, \Delta v_i)$$

In this way, the model shows the dependence of the acceleration of each car not only on the distance between itself and the vehicle in front, but also on the difference of their velocities.

2.1.1 Experimental setup

In the following chapters, the Optimal Velocity model will be employed to describe the behaviour of a platoon of N vehicles that travel on a ring road, as shown in Figure 2.2. Even if a closed ring road is not a realistic setup and it neglects some phenomena that may arise in real life (like a narrowing of the roadway or a crossroad) this framework represents a sort of infinite road. Moreover, it allows to see the presence of the so-called stop-and-go waves, as shown in [1] and [10].

Since the vehicles travel on a closed ring and the acceleration of the i-th vehicle depends on the headway with respect to its preceding vehicle, the model described in (2.1) and (2.2) becomes as follows.
Let us call one car of the platoon as the 1^{st} vehicle, then its acceleration $\dot{v}_1$ depends on the headway $\Delta x_1 = x_2 - x_1$ as follows.

$$\begin{cases} \dot{x}_1 = v_1 \\ \dot{v}_1 = b \left[V_{\max} \frac{\tanh(x_2 - x_1 - l_v - d_s) + \tanh(l_v + d_s)}{1 + \tanh(l_v + d_s)} - v_1 \right], \end{cases} \tag{2.3}$$

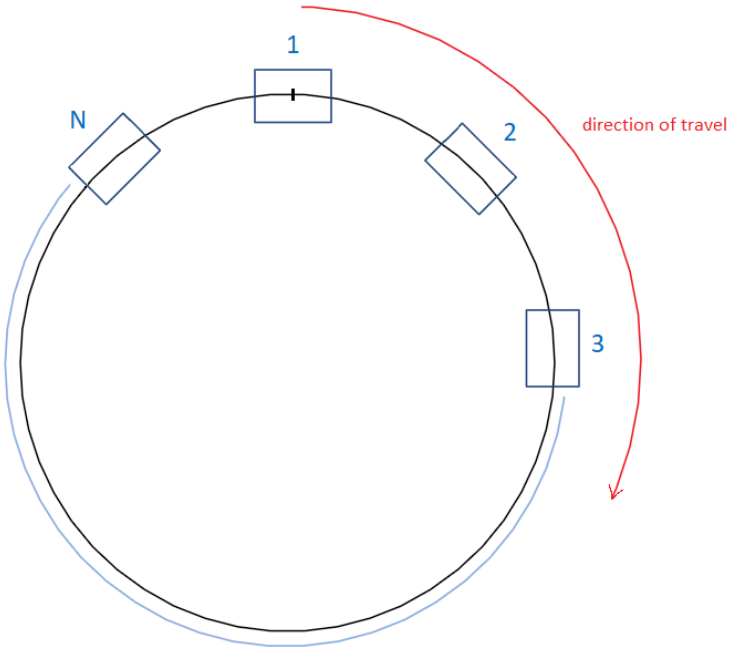

Figure 2.2: Sketch of 4 vehicles of the platoon that travel clockwise on a ring road

where x_2 is the position of the 2^{nd} vehicle, x_1 is the position of the 1^{st} vehicle and the 2^{nd} vehicle is in front of the 1^{st} one. See Figure 2.2.
In an analogue way, the acceleration of the 2^{nd} vehicle depends on the headway with respect to the 3^{rd} car, as shown in (2.4), where x_3 is the position of the 3^{rd} vehicle in front of the 2^{nd} one,

$$\begin{cases} \dot{x}_2 = v_2 \\ \dot{v}_2 = b\left[V_{\max}\frac{\tanh(x_3-x_2-l_v-d_s)+\tanh(l_v+d_s)}{1+\tanh(l_v+d_s)} - v_2\right], \end{cases} \tag{2.4}$$

and so on. Since there are N vehicles and they travel on a closed ring, the 1^{st} vehicle is placed in front of the N-th and then $\dot{v}_N$ depends on the headway $\Delta x_N = x_1 - x_N$.

$$\begin{cases} \dot{x}_N = v_N \\ \dot{v}_N = b\left[V_{\max}\frac{\tanh(x_1-x_N-l_v-d_s)+\tanh(l_v+d_s)}{1+\tanh(l_v+d_s)} - v_N\right], \end{cases} \tag{2.5}$$

Looking at Figure 2.2, the absolute positions of the vehicles are taken with respect to a zero reference, that is the position of the 1^{st} vehicle at the start of the experiment.

2.1.2 Uniform flow equilibrium

In [10] it is shown the Optimal Velocity model of N vehicles travelling on a ring road of length L, where the acceleration of the N-th vehicle depends on an external input u:

$$\begin{cases} \dot{x}_i = v_i, \quad \forall\ i = 1, ..., N \\ \dot{v}_i = b\left[V_{opt}\left(x_{i+1} - x_i\right) - v_i\right], \quad \forall\ i = 1, ..., N-1 \\ \dot{v}_N = u \end{cases} \tag{2.6}$$

The objective of the control strategy developed in this study is to drive the system to a particular equilibrium state, called uniform flow equilibrium or speed equilibrium, where all vehicles travel at the same absolute velocity.
Considering system (2.6), the vehicles may drive at the same speed $\bar{v}$ if $V_{opt}(\Delta x_i) = \bar{v},\ \forall\ i = 1, ..., N-1$. Since the velocity function of each vehicle strictly depends on its headway, the speed equilibrium is achieved when the uncontrolled $N-1$ vehicles have the same headway $\Delta x_i = d,\ \forall\ i = 1, ..., N-1$. The distance between the N-th vehicle and the 1^{st} one may be anyone. In this way, $V_{opt}(d) = \bar{v}$ and, if $\bar{v}$ is fixed, d is fixed as well.

Similarly, we want to define a speed equilibrium state for our autonomous Optimal Velocity model of N vehicles on a ring road.

$$\begin{cases} \dot{x}_i = v_i, \quad \forall\ i = 1, ..., N \\ \dot{v}_i = b\left[V_{opt}\left(x_{i+1} - x_i\right) - v_i\right], \quad \forall\ i = 1, ..., N \end{cases} \tag{2.7}$$

where $i + 1 = 1$ when $i = N$.
Since in model (2.7) the acceleration of the N-th vehicle is a function of its headway, the speed equilibrium is achieved when $V_{opt}(\Delta x_i) = \bar{v},\ \forall\ i = 1, ..., N$ and so when $\Delta x_i = d,\ \forall\ i = 1, ..., N$. This means that at the uniform flow equilibrium the vehicles are equally spaced on the ring road and, if the road has length L, their inter-vehicle distance is fixed and equal to $d = \frac{L}{N}$.

2.1.3 Time simulation

In this section, the Optimal Velocity model (2.7) is simulated in time domain, considering a platoon of $N = 10$ vehicles on a ring road of length L and setting the following parameters:

$$V_{\max} = 15\ m/s,\ b = 10\ s^{-1},\ d_0 = l_v + d_s = 10\ m$$

By construction, the state vector of the Optimal Velocity model

$$\boldsymbol{y} = [x_1, x_2, ..., x_N, v_1, v_2, ..., v_N] \in \mathbb{R}^{2N}$$

is limited for any initial condition. Absolute positions x_i are bounded because the vehicles travel on a closed ring of limited length and the absolute velocities are upper bounded because $V_{opt}(\Delta x_i)$ at most is equal to $V_{\max}$.
In order to reach the speed equilibrium, where all the vehicles share the same absolute velocity, the relative distances must be the same. So, on a ring road of length $L = 150\ m$, the final desired distance should be:

$$\Delta x_i = x_{i+1} - x_i = d = \frac{L}{N} = 15\ m$$

Let us run the simulation of model (2.7) starting from the initial conditions shown in Table 2.1. When the headway relative to one couple of vehicles is 'small' with respect to d_0, which

Table 2.1: Initial conditions

Vehicle number	Initial absolute positions [m]	Initial absolute velocities [m/s]
1	$x_1(0) = 0$	$v_1(0) = 5$
2	$x_2(0) = 12$	$v_2(0) = 7$
3	$x_3(0) = 23$	$v_3(0) = 6$
4	$x_4(0) = 30$	$v_4(0) = 4$
5	$x_5(0) = 36$	$v_5(0) = 8$
6	$x_6(0) = 63$	$v_6(0) = 5$
7	$x_7(0) = 76$	$v_7(0) = 6$
8	$x_8(0) = 93$	$v_8(0) = 8$
9	$x_9(0) = 112$	$v_9(0) = 12$
10	$x_{10}(0) = 136$	$v_{10}(0) = 6$

is the safety distance, the velocity function of the following vehicle tends to zero in order to slow it down and increase their relative distance.
For example, look at the inter-vehicle distance between the 4^{th} and the 5^{th} vehicle at the starting time:

$$\Delta x_4(0) = x_5(0) - x_4(0) = 6\ m \ll d_0$$

Since it is too small, the optimal velocity of the 4^{th} (the following car of the couple) should be low and in fact:

$$V_{opt}^4(0) = 0{,}005\ m/s$$

Since the initial velocity $v_4(0) = 4\ m/s$ is far larger than $V_{opt}^4(0)$, the 4^{th} vehicle (V_4) slows down in order to increase its relative distance with respect to its leading vehicle (V_5), as shown in Figure 2.3 and Figure 2.4.
As V_4 slows down, V_5 speeds up in order to reduce its distance with respect to V_6, so the relative distance between V_4 and V_5 increases and this causes V_{opt}^4 to increase with respect to its previous value, as shown in Figure 2.5. So V_4 speeds up because it tries to follow its optimal velocity and at the end it assumes the velocity of vehicle V_5.
On the contrary, when the headway relative to one couple of vehicles is 'large' with respect to d_0, the velocity function of the following vehicle tends to $V_{\max}$ in order to decrease their relative distance.
For example, look at couple of vehicles V_{10} and V_1 in Figures 2.6-2.8. At the beginning, their inter-vehicle distance is

$$\Delta x_{10}(0) = x_{10}(0) - x_1(0) = 14\ m \gg d_0,$$

so the velocity function of the following vehicle, V_{10}, is almost equal to $V_{\max}$.

$$V_{opt}^{10}(0) = 14{,}99\ m/s$$

This makes V_{10} to speed up and, since from $t = 0{,}28\ s$ V_1 slows down, their inter-vehicle distance, Δx_{10} decreases. When Δx_{10} is lower than $d_0 = 10\ m$, so the distance between

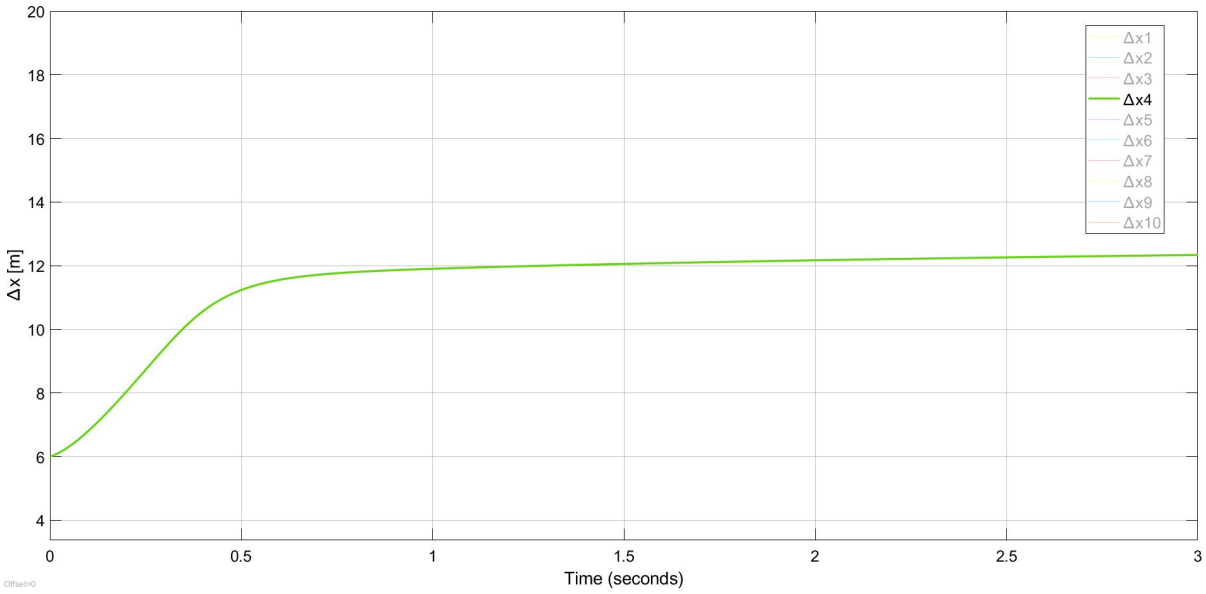

Figure 2.3: Relative distance between V_5 and V_4

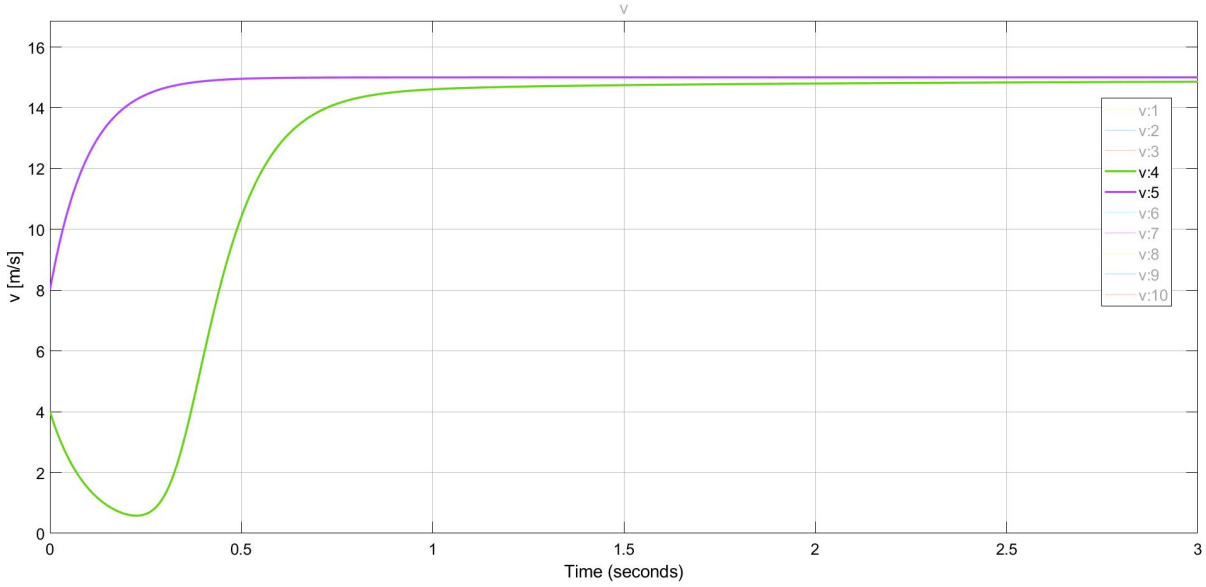

Figure 2.4: Absolute velocities of V_4 (green) and V_5 (purple)

V_1 and V_{10} is not safe, V_{opt}^{10} reduces and vehicle V_{10} slows down in order to increase the headway. Then, as Δx_{10} increases, V_{opt}^{10} increases as well and vehicle V_{10} speeds up until it assumes a velocity similar to vehicle V_1 and an almost constant inter-vehicle distance.
After the transient, all vehicles assume equally spaced positions, as shown in Figure 2.9, and the same constant velocity, so they reach the uniform flow equilibrium state. Since their final inter-vehicle distance is $d = \frac{L}{N} = 15\ m$, which is larger than d_0, their absolute

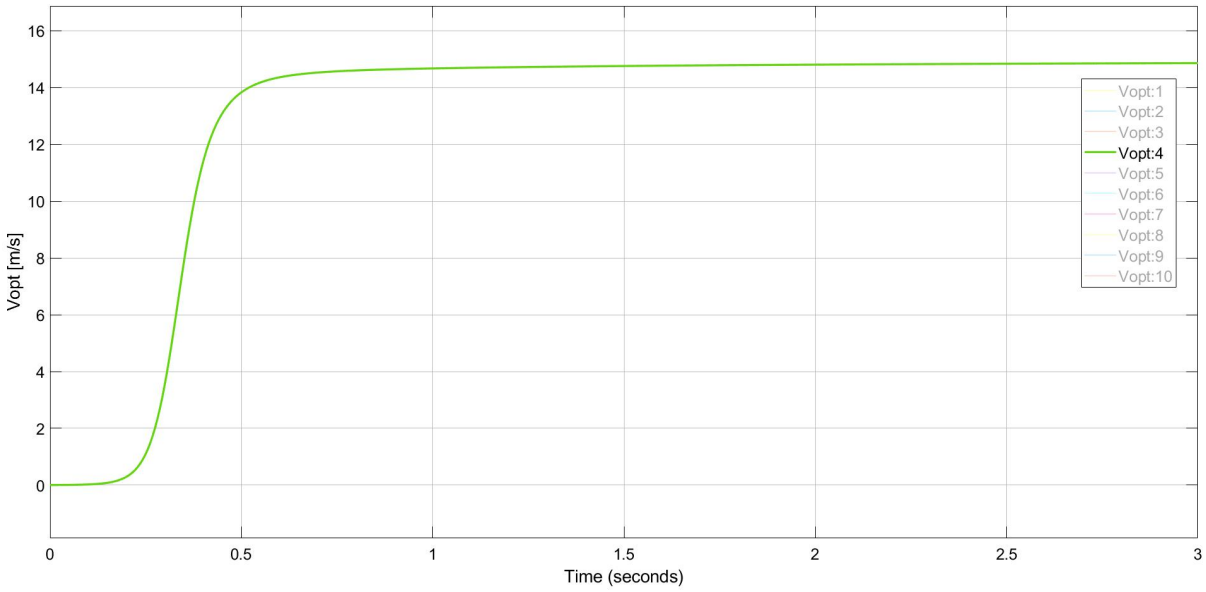

Figure 2.5: Optimal velocity $V_{opt}^4(t)$

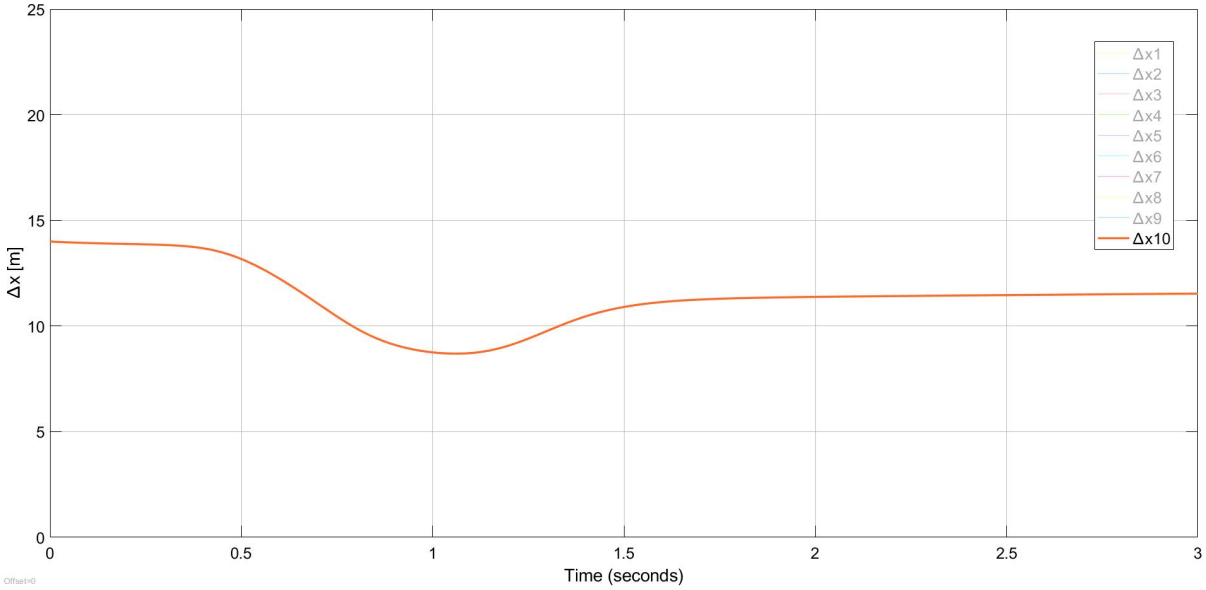

Figure 2.6: Relative distance between V_{10} and V_1

velocity will be almost equal to $V_{\max}$.

2.1.4 Model in error coordinates

In order to study how the Optimal Velocity model (2.7) behaves with respect to the uniform flow equilibrium state, it is rewritten in other state variables.

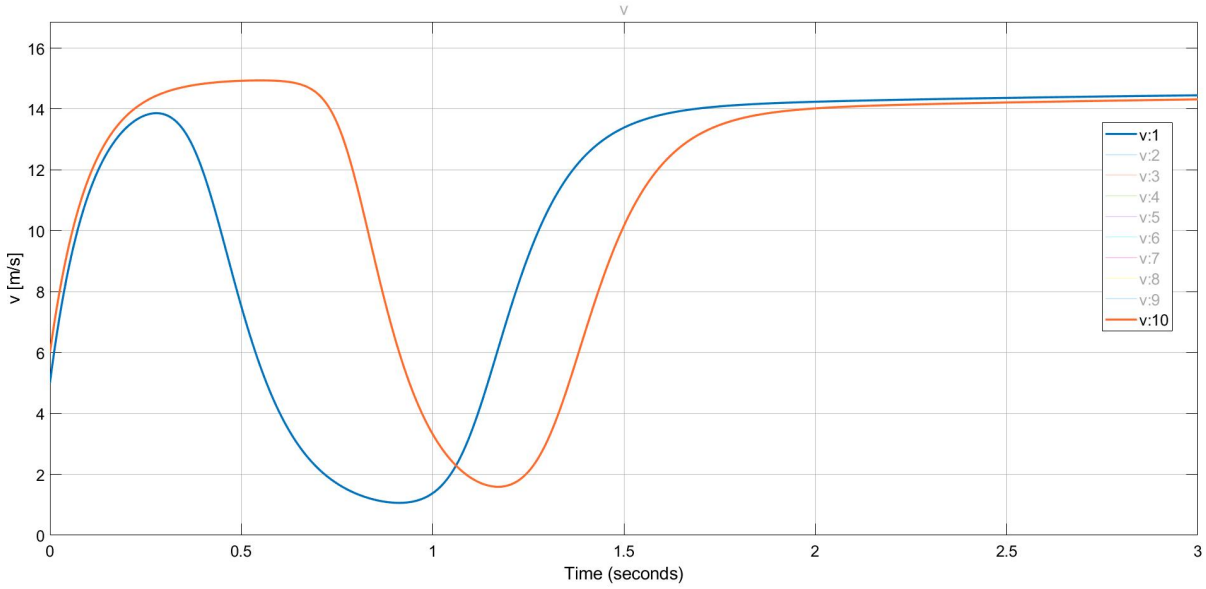

Figure 2.7: Absolute velocities of V_{10} (red) and V_1 (blue)

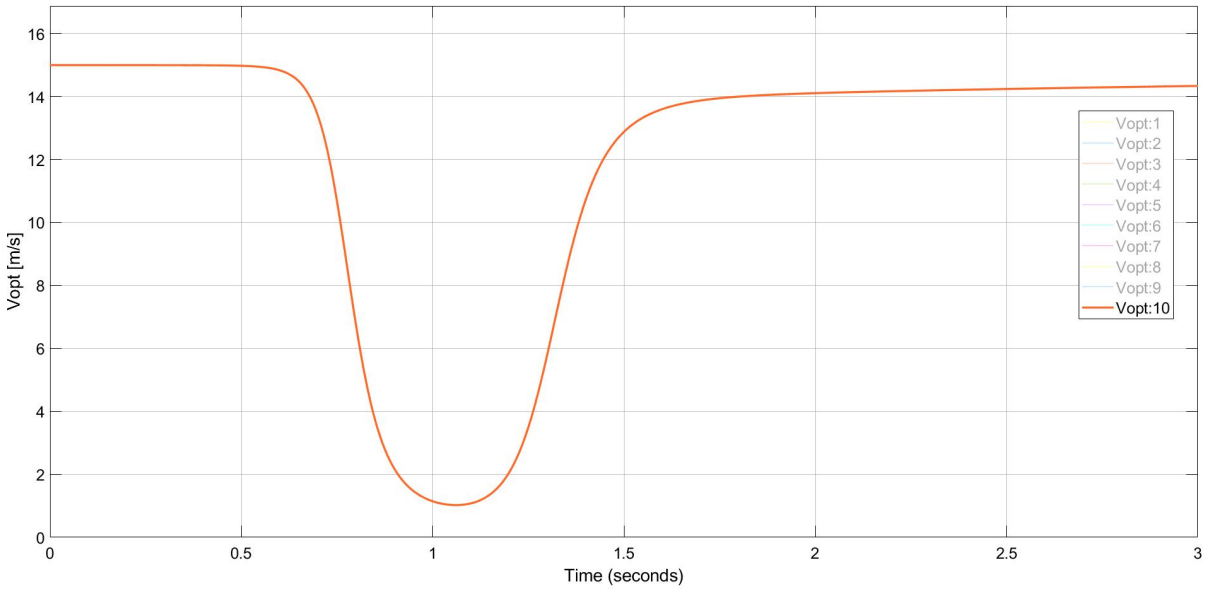

Figure 2.8: Optimal velocity $V_{opt}^{10}(t)$

The new state variables are the relative velocities y_i of one vehicle with respect to its following one and the spacing errors z_i that represent the gap between the relative distances of each couple of vehicles and the desired distance $d = \frac{L}{N}$ at the speed equilibrium.

$$z_i = x_{i+1} - x_i - d = \Delta x_i - d$$

$$y_i = v_{i+1} - v_i$$

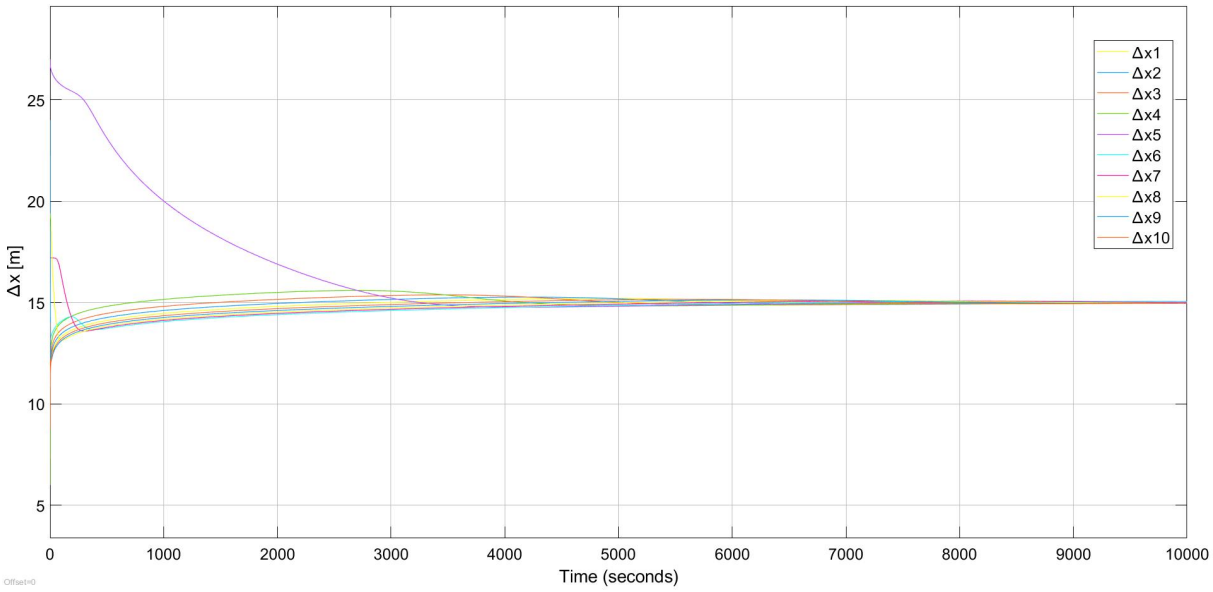

Figure 2.9: Relative distances of the platoon

When $i = N$, they are equal to $z_N = x_1 - x_N - d$ and $y_N = v_1 - v_N$.
In these coordinates, the differential equations of model (2.7) become:

$$\begin{cases} \dot{z}_i = y_i, \quad \forall\ i = 1, ..., N \\ \\ \dot{y}_i = b\left[V_{\max}\frac{\tanh(z_{i+1}+d-l_v-d_s)-\tanh(z_i+d-l_v-d_s)}{1+\tanh(l_v+d_s)} - y_i\right], \quad \forall\ i = 1, ..., N \end{cases} \tag{2.8}$$

where $i + 1 = 1$ when $i = N$.
For the sake of simplicity, let us call $d_0 = l_v + d_s$ and rewrite model (2.8) as

$$\begin{cases} \dot{z}_i = y_i, \quad \forall\ i = 1, ..., N \\ \\ \dot{y}_i = b\left[V_{\max}\frac{\tanh(z_{i+1}+d-d_0)-\tanh(z_i+d-d_0)}{1+\tanh(d_0)} - y_i\right], \quad \forall\ i = 1, ..., N \end{cases} \tag{2.9}$$

where $i + 1 = 1$ when $i = N$.
At the speed equilibrium, $\Delta x_i = d$ and $v_i = V_{opt}(d) = \bar{v}$, $\forall\ i = 1, ..., N$, because the vehicles travel at the same speed and are equally spaced. It means that

$$z_i = 0,\ y_i = 0,\ \forall\ i = 1, ..., N$$

In this new set of state variables,

$$\mathbf{x} = [z_1, z_2, ..., z_N, y_1, y_2, ..., y_N]^T \in \mathbb{R}^{2N}, \tag{2.10}$$

the speed equilibrium point of model (2.7) coincides with the origin of model (2.9) and, since the speed equilibrium is the desired state, z_i and y_i are referred to as 'error' coordinates.

In Section 3.1, it will be shown that the linearization of model (2.9) around the origin (i.e. uniform flow equilibrium) has a structural zero eigenvalue that prevents the uniform flow equilibrium to be asymptotically stable. In order to solve this drawback, we will consider a modification of this model.
Since in Figure 2.2 the vehicles travel on a closed ring road, their relative distances are not independent from one another, because their sum must be equal to the length L of the ring.

$$\sum_{i=1}^{N} \Delta x_i = \sum_{i=1}^{N} z_i + d = L$$

Since $L = Nd$, the sum of the spacing errors is equal to zero and this allows us to rewrite one state variable as function of the others.

$$\sum_{i=1}^{N} z_i = L - Nd = 0$$

$$z_N = -\sum_{i=1}^{N-1} z_i$$

Let us substitute it in model (2.9) and define a Reduced Optimal Velocity model (2.11) in $2N-1$ state variables (2.12).

$$\begin{cases} \dot{z}_i = y_i, \quad \forall\ i = 1, ..., N-1 \\ \dot{y}_i = b\left[V_{\max}\frac{\tanh(z_{i+1}+d-d_0)-\tanh(z_i+d-d_0)}{1+\tanh(d_0)} - y_i\right], \quad \forall\ i = 1, ..., N-2 \\ \dot{y}_{N-1} = b\left[V_{\max}\frac{\tanh\left(-\sum_{i=1}^{N-1} z_i+d-d_0\right)-\tanh(z_{N-1}+d-d_0)}{1+\tanh(d_0)} - y_{N-1}\right], \\ \dot{y}_N = b\left[V_{\max}\frac{\tanh(z_1+d-d_0)-\tanh\left(-\sum_{i=1}^{N-1} z_i+d-d_0\right)}{1+\tanh(d_0)} - y_N\right], \end{cases} \tag{2.11}$$

where $d_0 = l_v + d_s$. Having substituted one variable, the state vector has been reduced to

$$\tilde{\mathbf{x}} = [z_1, z_2, ..., z_{N-1}, y_1, y_2, ..., y_N]^T \in \mathbb{R}^{2N-1}, \tag{2.12}$$

As shown in Section 3.1, the Jacobian matrix of the linearization of this model around the origin (i.e. uniform flow equilibrium) can have all eigenvalues with negative real part if the parameters satisfy a necessary and sufficient condition, and thus the origin will be an asymptotically stable equilibrium point for the nonlinear model.

2.2 Optimal Velocity model with saturation

Let us consider the Bando Optimal Velocity model on a ring road, where $d_0 = l_v + d_s$:

$$\begin{cases} \dot{x}_i = v_i, \quad \forall\ i = 1, ..., N \\ \\ \dot{v}_i = b\left[V_{\max}\frac{\tanh(x_{i+1}-x_i-d_0)\ +\ \tanh(d_0)}{1\ +\ \tanh(d_0)} - v_i\right], \quad \forall\ i = 1, ..., N \end{cases} \tag{2.13}$$

where $i + 1 = 1$ when $i = N$.
Since $\tanh(\xi)$ is upper and lower bounded and linear around the origin, you may consider substituting it with the saturation function defined in (2.14) and shown in Figure 2.10.

$$\text{sat}(\xi) = \begin{cases} -u_{\min}, & \text{if } \xi < -u_{\min} \\ \xi, & \text{if } -u_{\min} \leq \xi \leq u_{\max} \\ u_{\max}, & \text{if } \xi > u_{\max} \end{cases} \tag{2.14}$$

The resulting optimal velocity function is still bounded and monotonically increasing and

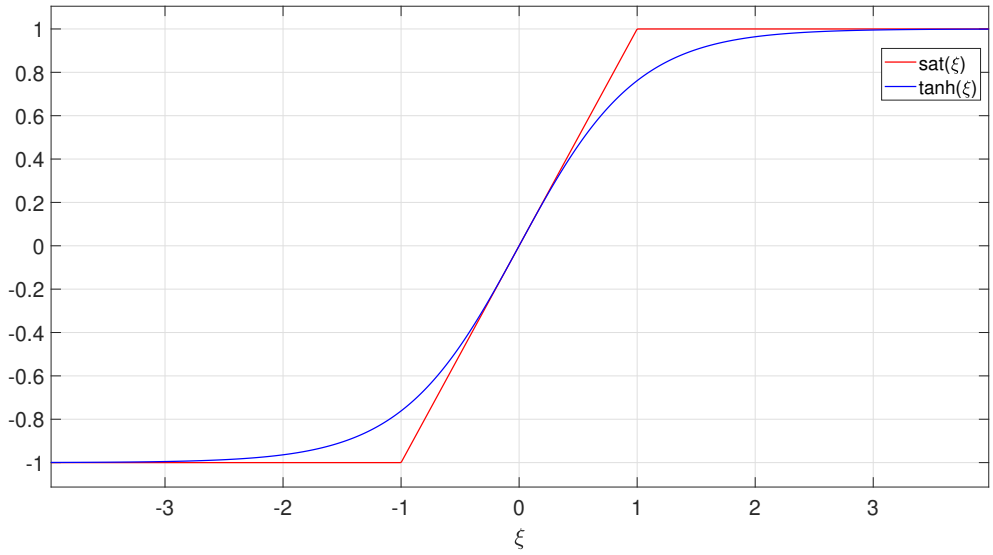

Figure 2.10: $\tanh(\xi)$ (blue) and $\text{sat}(\xi)$ (red)

the modified Optimal Velocity model is defined in (2.15).
The reason of the substitution will be clear in Chapter 4. Basically, a system like (2.15), where the nonlinearity is given by the saturation function (2.14), is simpler than a generic nonlinear system and its properties may be studied with particular techniques defined in [23].

$$\begin{cases} \dot{x}_i = v_i, \quad \forall\ i = 1, ..., N \\ \\ \dot{v}_i = b\left[V_{\max}\frac{\text{sat}(x_{i+1}-x_i-d_0)\ +\ \tanh(d_0)}{1\ +\ \tanh(d_0)} - v_i\right], \quad \forall\ i = 1, ..., N \end{cases} \tag{2.15}$$

where $i+1=1$ when $i=N$.
It is worthy to check if the modified Optimal Velocity model behaves similarly to the Bando model (2.13) and if it is able to describe the dynamics of traffic flow.
In particular, the modified optimal velocity (2.16) as function of the spacing is depicted in Figure 2.11 and the linear behaviour occurs for $\Delta x_i = x_{i+1} - x_i$ such that $d_0 - 1\ m \leq \Delta x_i \leq d_0 + 1\ m$.

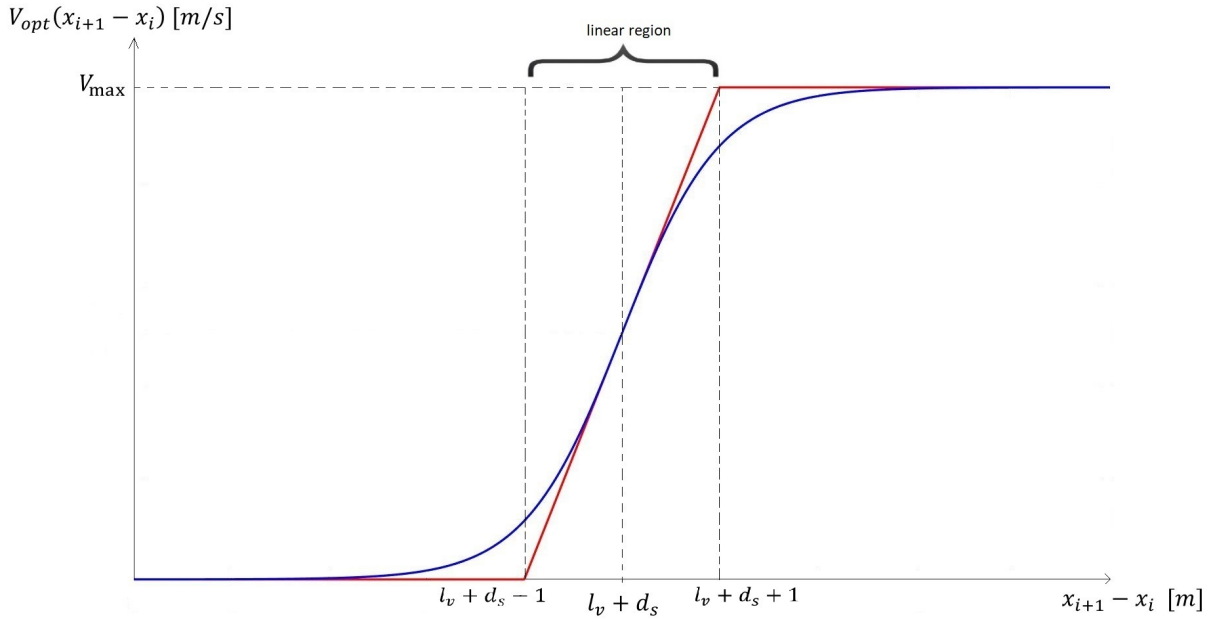

Figure 2.11: $V_{opt}(x_{i+1} - x_i)$ of the Bando model (blue) and of the Optimal Velocity model with saturation (red)

$$V_{opt}(x_{i+1} - x_i) = V_{\max} \frac{\text{sat}\,(x_{i+1} - x_i - d_0) + \tanh(d_0)}{1 + \tanh(d_0)} \tag{2.16}$$

2.2.1 Time simulation

Let us consider a platoon of $N = 10$ vehicles on a ring road of length $L = 150\ m$ where the dynamics of the vehicles is described by the modified Optimal Velocity model (2.15) with the following model parameters:

$$V_{\max} = 15\ m/s, \quad b = 10\ s^{-1}, \quad d_0 = l_v + d_s = 10\ m$$

With these parameters, the linear region of the saturated model occurs for $9\ m \leq \Delta x_i \leq 11\ m$.
Let us run a simulation of the behaviour of the platoon, where the velocity function is (2.16). The initial conditions are the same shown in Table 2.1.
For example, let us have a look at the 4^{th} vehicle, V_4. At the beginning, its headway is

$$\Delta x_4(0) = x_5(0) - x_4(0) = 6\ m < d_0 - 1\ m.$$

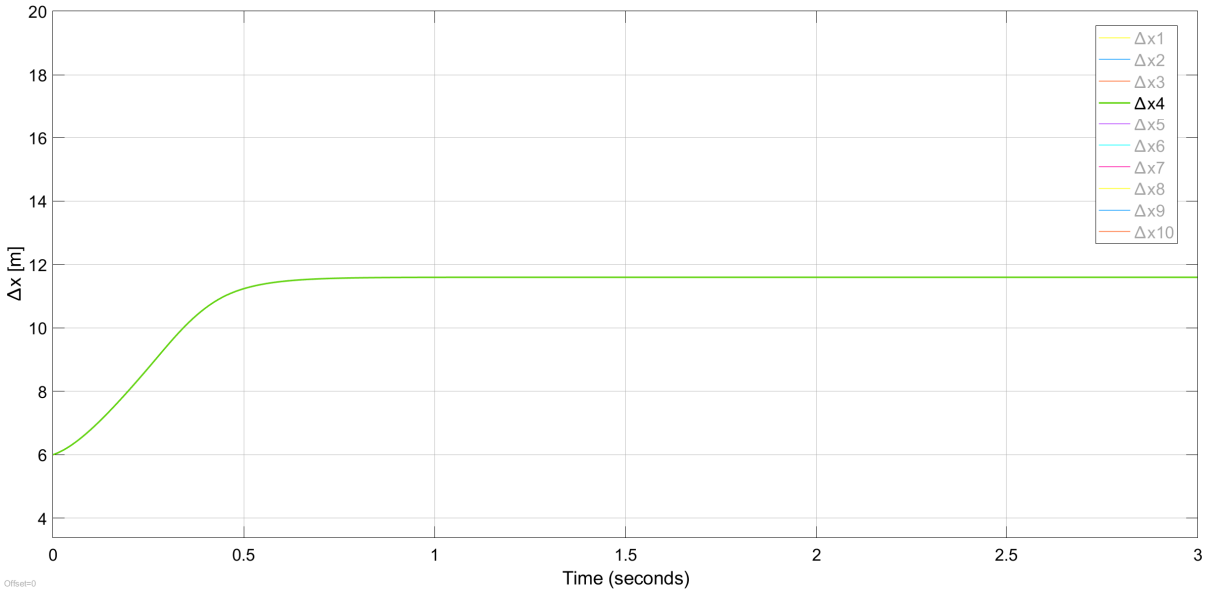

Figure 2.12: Relative distance between V_4 and V_4

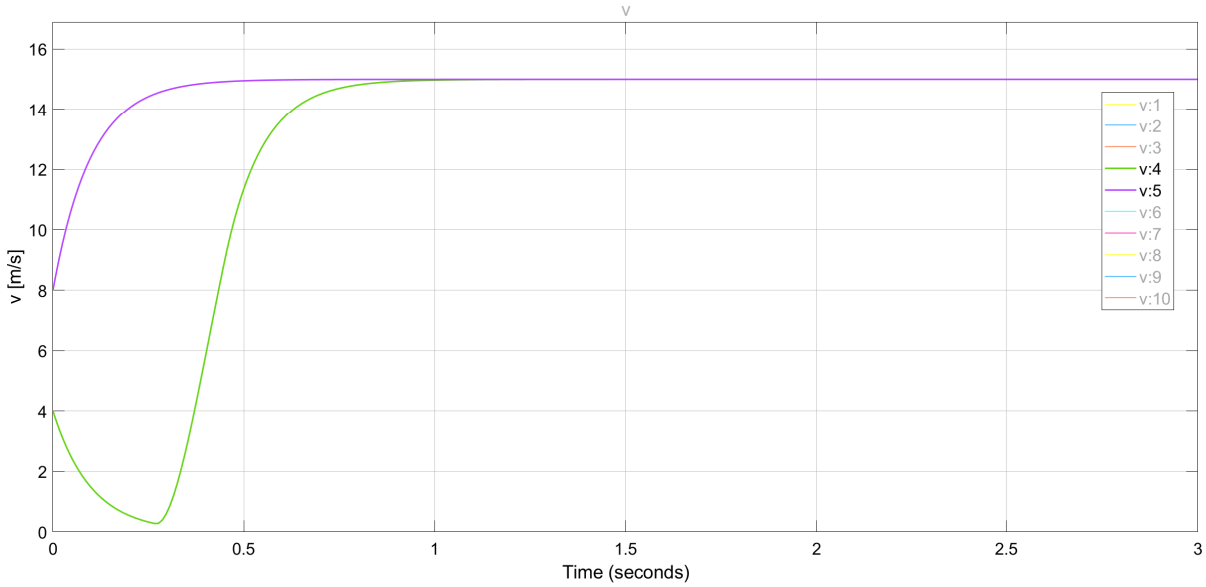

Figure 2.13: Absolute velocities of V_4 (green) and V_5 (purple)

Since this distance is less than $d_0 - 1\ m\ m$, as shown in Figure 2.11, the optimal velocity function of V_4 saturates to the lower bound and so $V^4_{opt}(0) = 0\ m/s$, as shown in Figure 2.14. Therefore, vehicle V_4 brakes and its headway increases. At $t = 0.27\ s$, Δx_4 becomes equal to $d_0 - 1\ m = 9\ m$, it enters the linearity region and the optimal velocity function is linearly dependent on the headway. At $t = 0.45\ s$, Δx_4 exceeds $d_0 + 1\ m = 11\ m$ and so the optimal velocity function saturates to the upper bound and becomes equal to $V_{\max}$.

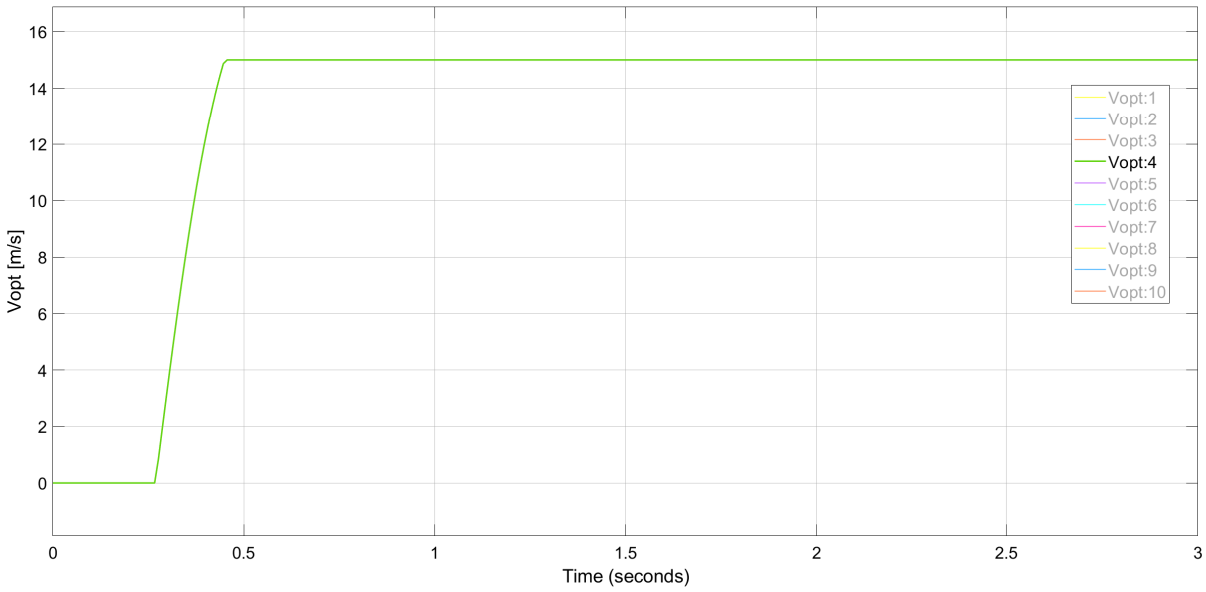

Figure 2.14: Optimal velocity $V_{opt}^4(t)$

When the transient is over, Δx_4 is equal to $d = \frac{L}{N} = 11.6\ m$, so the optimal velocity function of V_4 stays constant and equal to $V_{\max}$. With respect to the velocity function of the Bando Optimal Velocity model shown in Figure 2.5, V_{opt}^4 can saturate or be linear with the headway.
The model (2.15) behaves in a similar way with respect to Bando model (2.13) because the nonlinear functions that regulate the velocity of each vehicle with respect to the headway are similar and the principle is the same.

2.2.2 Model in error coordinates

As well as for Bando model, the Optimal Velocity model (2.15) with saturation function (2.16) may be rewritten in a new set of state variables: spacing errors with respect to the inter-vehicle distance at the uniform flow equilibrium and relative velocities.

$$z_i = x_{i+1} - x_i - d = \Delta x_i - d$$

$$y_i = v_{i+1} - v_i$$

The differential equations of the model in error coordinates is (2.17) and the new state vector is (2.18).

$$\begin{cases} \dot{z}_i = y_i, \quad \forall\ i = 1, ..., N \\ \\ \dot{y}_i = b\left[V_{\max}\frac{\text{sat}(z_{i+1}+d-d_0)-\text{sat}(z_i+d-d_0)}{1+\tanh(d_0)} - y_i\right], \quad \forall\ i = 1, ..., N \end{cases} \tag{2.17}$$

where $i + 1 = 1$ when $i = N$.

$$\mathbf{x} = [z_1, z_2, ..., z_N, y_1, y_2, ..., y_N]^T \in \mathbb{R}^{2N} \tag{2.18}$$

For the same reason as for the Bando model, it is convenient to consider that the spacing errors are not independent from one another, because the vehicles travel on a closed ring of length L. Thus, the sum of their inter-vehicle distances is equal to L and the sum of the spacing errors is equal to zero. This fact allows us to express one state variable as function of the others:

$$z_N = -\sum_{i=1}^{N-1} z_i$$

As a consequence, system (2.17) is reduced to model (2.19), whose state vector (2.20) has dimension $2N-1$.

$$\begin{cases} \dot{z}_i = y_i, \quad \forall\ i = 1, ..., N-1 \\ \dot{y}_i = b\left[V_{\max}\frac{\text{sat}(z_{i+1}+d-d_0)-\text{sat}(z_i+d-d_0)}{1+\tanh(d_0)} - y_i\right], \quad \forall\ i = 1, ..., N-2 \\ \dot{y}_{N-1} = b\left[V_{\max}\frac{\text{sat}\left(-\sum_{i=1}^{N-1} z_i+d-d_0\right)-\text{sat}(z_{N-1}+d-d_0)}{1+\tanh(d_0)} - y_{N-1}\right], \\ \dot{y}_N = b\left[V_{\max}\frac{\text{sat}(z_1+d-d_0)-\text{sat}\left(-\sum_{i=1}^{N-1} z_i+d-d_0\right)}{1+\tanh(d_0)} - y_N\right] \end{cases} \tag{2.19}$$

$$\tilde{\mathbf{x}} = [z_1, z_2, ..., z_{N-1}, y_1, y_2, ..., y_N]^T \in \mathbb{R}^{2N-1} \tag{2.20}$$

2.3 Comparison of the two models

In both the Bando model (2.13) and the Optimal Velocity model with saturation (2.15), the velocity function of each vehicle is computed on the basis of the current distance with respect to the preceding vehicle. Both the optimal velocity functions are nonlinear and they are lower and upper bounded. When the headway is too large, the velocity function tends to the maximum value and, when the headway is too short, the velocity function tends to zero. Thus, the idea at the basis of the models is the same. Nevertheless, substituting the saturation function (2.14) in the expression of the optimal velocity defined in Bando model could lead to some differences in the behaviour of the platoon.
In this section, both models are simulated in time domain, starting with the same initial conditions and same model parameters, in order to highlight their differences.

Simulation 1. Let us consider a platoon of $N = 5$ vehicles travelling on a ring road of length $L = 55\ m$. The parameters are:

$$b = 10\ s^{-1},\ V_{\max} = 15\ m/s,\ d_0 = l_v + d_s = 10\ m.$$

In Table 2.2 are shown the same initial conditions for both models. In Figure 2.15 and 2.16 are shown the relative distances of both models as they converge to the inter-vehicle

distance at the uniform flow equilibrium: $d = \frac{L}{N} = 11\ m$. It is clear that the convergence of the model with saturation function is faster with respect to Bando model.
Since the final inter-vehicle distance is equal to $d_0 + 1\ m = 11\ m$, the vehicles of the model with saturation function will drive at the maximum velocity $V_{\max}$, as shown in Figure 2.18. On the contrary, in Bando model, the absolute velocities of the vehicles are lower, because their velocity functions do not saturate, as shown in Figure 2.17. At steady state, the vehicles in Bando model drive at

$$v_i = V_{opt}(d) = \bar{v} = 13.2\ m/s.$$

The velocity of the convergence to the uniform flow equilibrium will be seen through the study of the linearization of both models in Chapter 3.

Table 2.2: Initial conditions

Vehicle number	Initial absolute positions [m]	Initial absolute velocities [m/s]
1	$x_1(0) = 0$	$v_1(0) = 5$
2	$x_2(0) = 9$	$v_2(0) = 7$
3	$x_3(0) = 22$	$v_3(0) = 6$
4	$x_4(0) = 36$	$v_4(0) = 4$
5	$x_5(0) = 47$	$v_5(0) = 3$

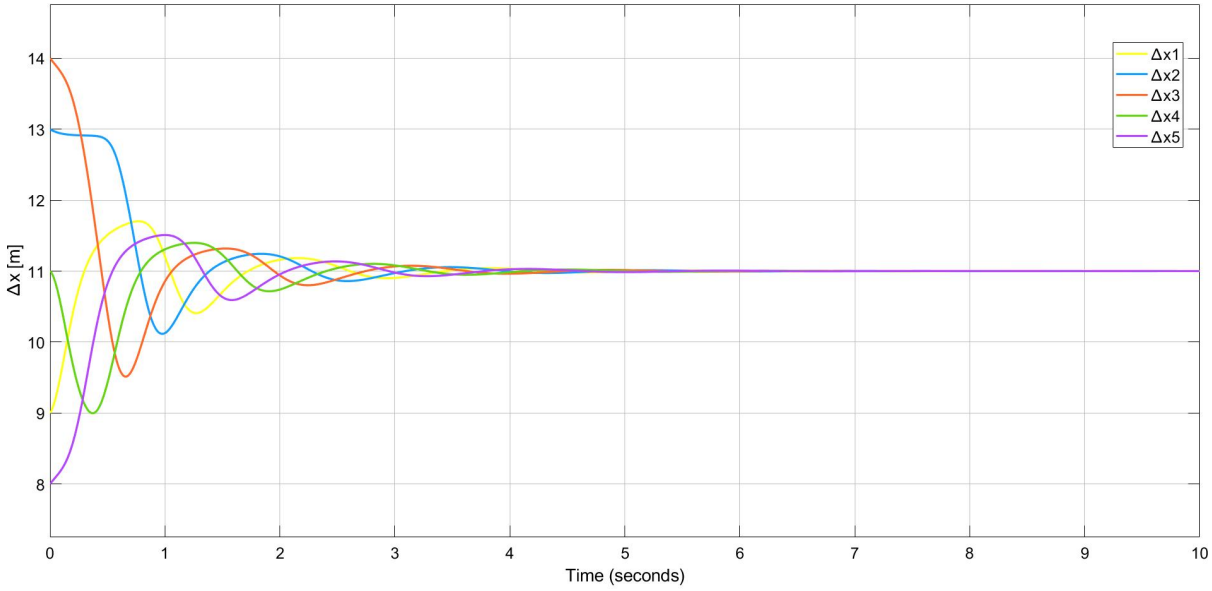

Figure 2.15: Relative distances of the model with tanh in Simulation 1

Simulation 2. Let us consider again a platoon of $N = 5$ vehicles, that travel on a ring road of longer length: $L = 75\ m$. The parameters are the same:

$$b = 10\ s^{-1},\ V_{\max} = 15\ m/s,\ d_0 = l_v + d_s = 10\ m.$$

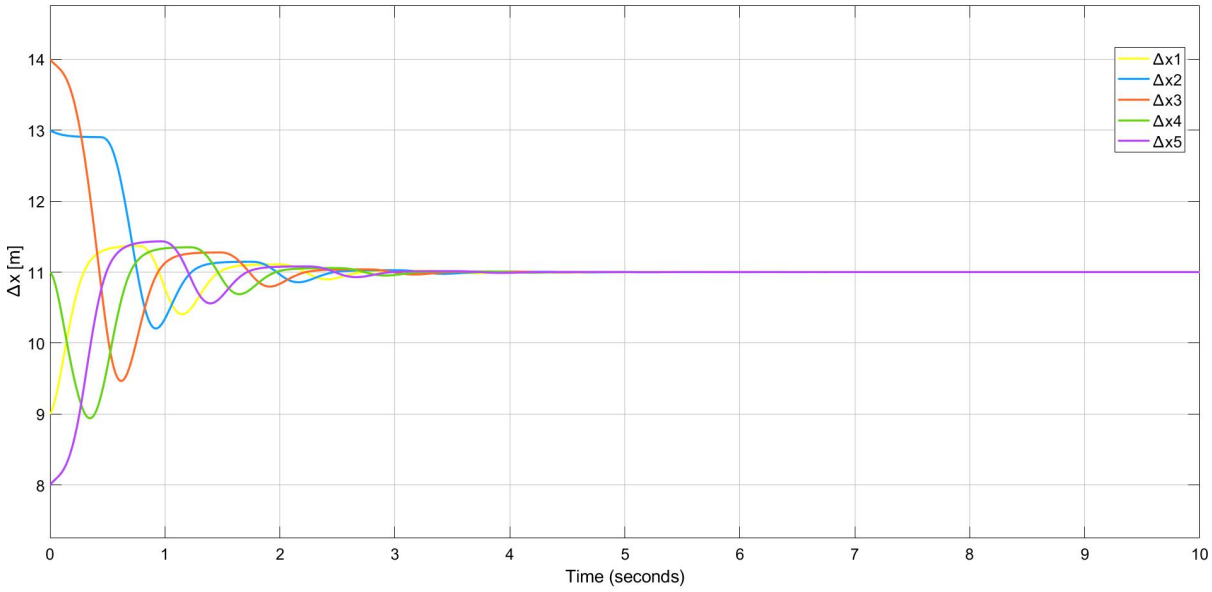

Figure 2.16: Relative distances of the model with sat in Simulation 1

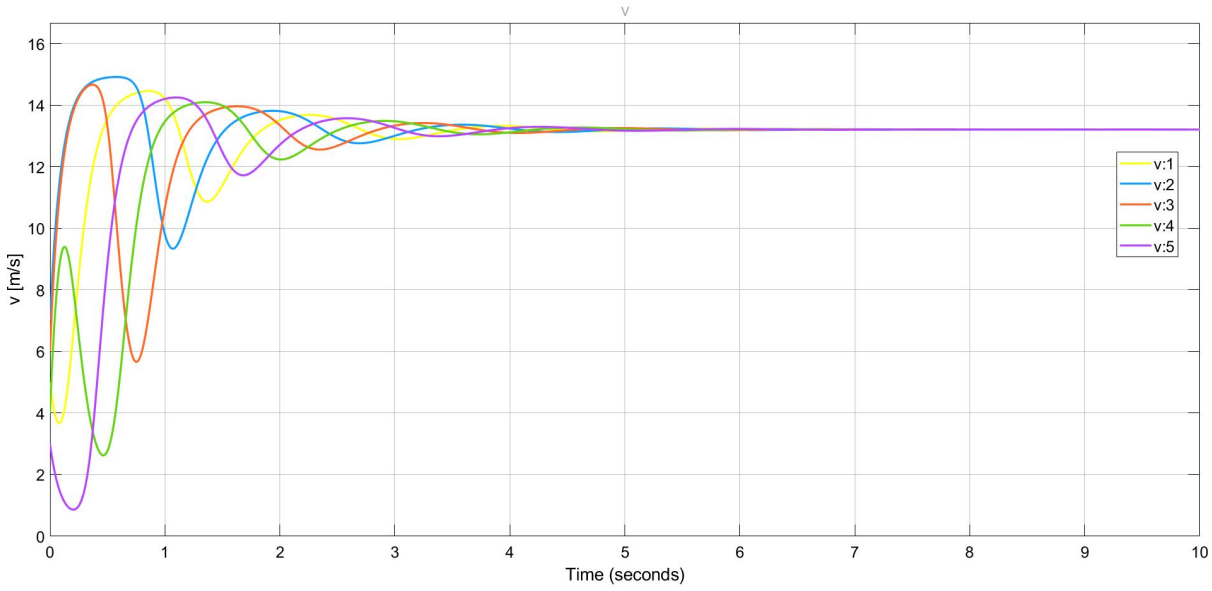

Figure 2.17: Absolute velocities of the model with tanh in Simulation 1

In Table 2.3 are shown the initial conditions of both models and in Figure 2.19 and 2.20 are shown the relative distances in time domain. With the choice of parameters shown above, the Bando model converges to the uniform flow equilibrium, as the vehicles assume equally spaced positions at the end of the transient. Since their inter-vehicle distances converge to $d = \frac{L}{N} = 15\ m$, their velocity functions will be almost equal to $V_{\max}$:

$$v_i = V_{opt}(d) = \bar{v} = 14.99\ m/s.$$

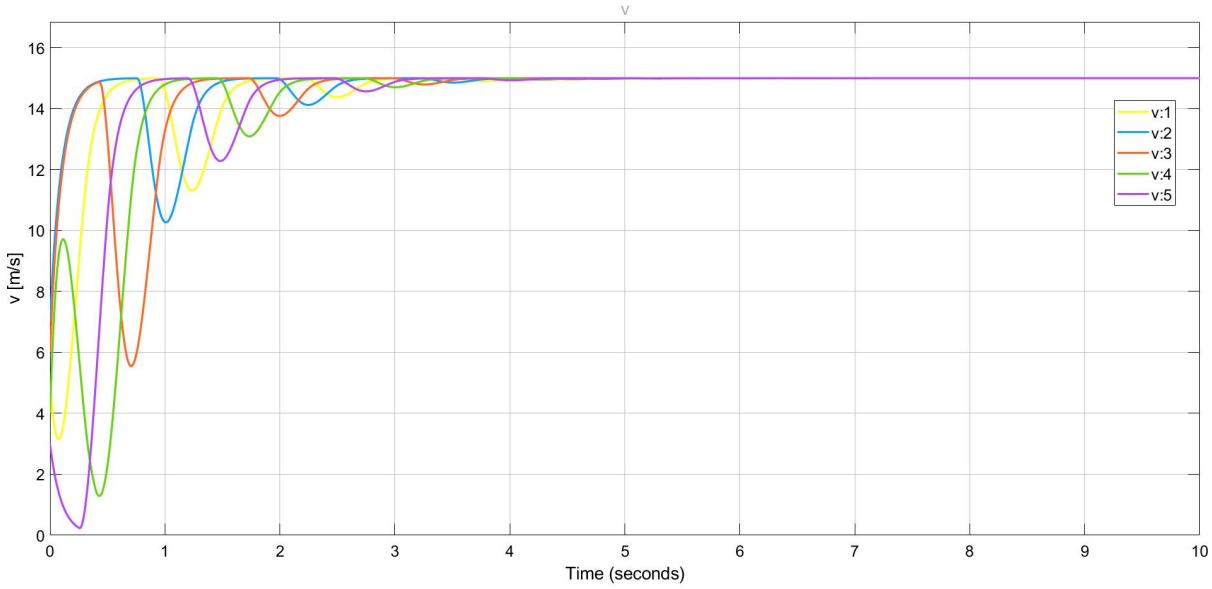

Figure 2.18: Absolute velocities of the model with sat in Simulation 1

On the contrary, the vehicles of the Optimal Velocity model with saturation function drive at constant and equal absolute velocities, but they assume any inter-vehicle distances, as shown in Figure 2.20. This drawback of the Optimal Velocity model with saturation

Table 2.3: Initial conditions

Vehicle number	Initial absolute positions [m]	Initial absolute velocities [m/s]
1	$x_1(0) = 0$	$v_1(0) = 5$
2	$x_2(0) = 12$	$v_2(0) = 7$
3	$x_3(0) = 24$	$v_3(0) = 6$
4	$x_4(0) = 38$	$v_4(0) = 4$
5	$x_5(0) = 56$	$v_5(0) = 3$

function will be explained better in Section 3.2, but, with a larger length of the ring road, the vehicles assume inter-vehicle distances that exceeds the linearity region of the optimal velocity function shown in Figure 2.11. This makes the velocity functions saturate up to $V_{\max}$ and be independent on the current headways, so that the headways do not play any role in the computation of the time derivative of the velocities. Basically, in this way, the main feature of Bando model fails and it is like having no information on the current headways in order to regulate the velocities of vehicles.

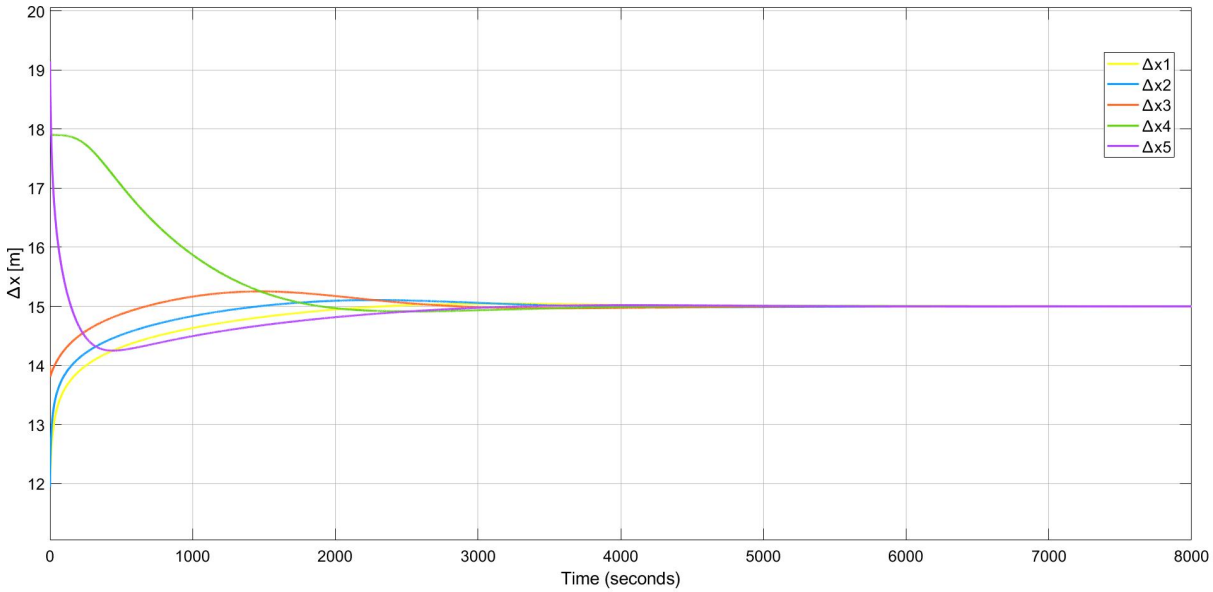

Figure 2.19: Relative distances of the model with tanh in Simulation 2

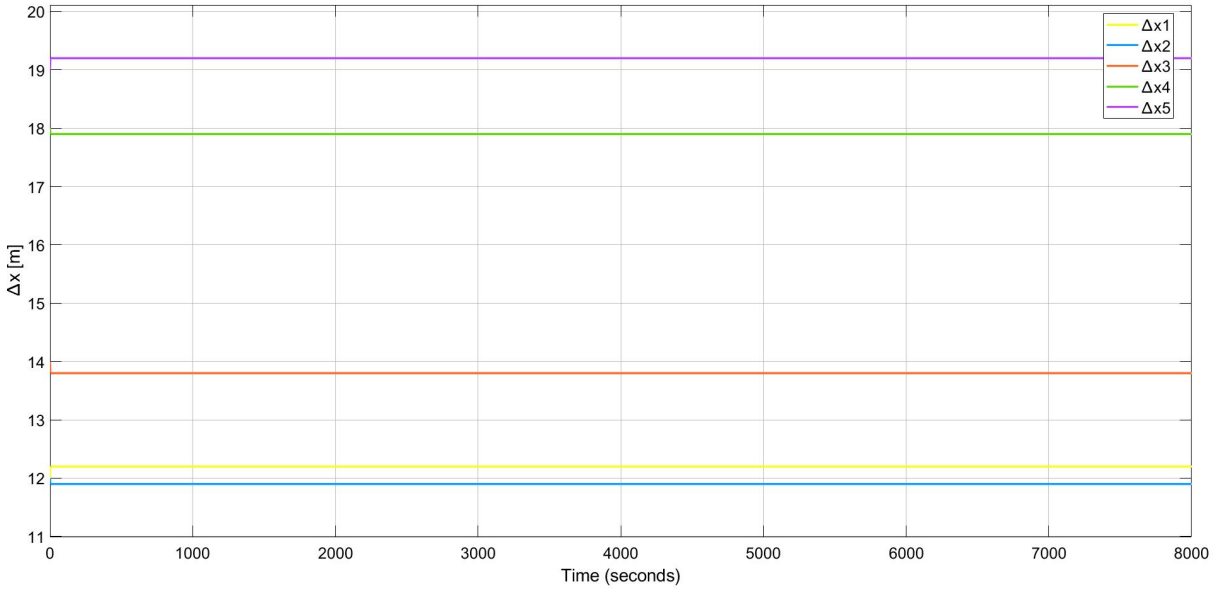

Figure 2.20: Relative distances of the model with sat in Simulation 2

Chapter 3

Linear analysis

3.1 Linearization of Bando model

In this section is presented the linearization of the Optimal Velocity traffic model by Bando et al. on a ring road of length L. In particular, the model that will be linearized is the Optimal Velocity model (3.1) of N vehicles in error coordinates (3.2).

$$\begin{cases} \dot{z}_i = y_i, \quad \forall\ i = 1, ..., N \\ \\ \dot{y}_i = b\left[V_{\max}\frac{\tanh(z_{i+1}+d-d_0)-\tanh(z_i+d-d_0)}{1+\tanh(d_0)} - y_i\right], \quad \forall\ i = 1, ..., N \end{cases} \tag{3.1}$$

where $i + 1 = 1$ when $i = N$.

$$\mathbf{x} = [z_1, z_2, ..., z_N, y_1, y_2, ..., y_N]^T \in \mathbb{R}^{2N}, \tag{3.2}$$

where $d_0 = l_v + d_s$ is the safety inter-vehicle distance, b is the sensitivity of the drivers, $V_{\max}$ is the maximum value of the optimal velocity function, z_i are the spacing errors with respect to the distance $d = \frac{L}{N}$ at the uniform flow equilibrium and y_i are the relative velocities of each couple of adjacent vehicles.

$$z_i = x_{i+1} - x_i - d = \Delta x_i - d$$

$$y_i = v_{i+1} - v_i$$

Since our aim is to let the group of vehicles reach the uniform flow equilibrium, where all of them drive at the same velocity and keep the same constant distances, we are interested on the properties of this equilibrium point. For this reason, model (3.1) is linearized around the uniform flow equilibrium.
At the uniform flow equilibrium,

$$\begin{aligned} x_{i+1} - x_i = \Delta x_* = d = \frac{L}{N} \\ v_i = v_* = V_{opt}(d), \end{aligned} \tag{3.3}$$

which corresponds to

$$\begin{aligned} z_i &= z_* = 0 \\ y_i &= y_* = 0 \end{aligned} \tag{3.4}$$

Therefore, the uniform flow equilibrium point for model (3.1) corresponds to the origin and its linearization around this equilibrium is

$$\begin{aligned} \dot{z_i} &= y_i, && \forall\ i = 1, .., N \\ \dot{y_i} &= -\gamma z_i + \gamma z_{i+1} - b y_i, && \forall\ i = 1, ..., N \end{aligned} \tag{3.5}$$

where $\gamma = b\frac{\partial V_{opt}(d)}{\partial z_i} = \frac{bV_{\max}}{1+\tanh(d_0)}\operatorname{sech}^2(d - d_0)$ and $i + 1 = 1$ when $i = N$.

Given the state vector (3.2), the linearized model in matrix form is

$$\dot{\mathbf{x}} = J\mathbf{x}, \tag{3.6}$$

where the Jacobian matrix is equal to

$$J = \begin{bmatrix} 0 & I_N \\ J_{yz} & -bI_N \end{bmatrix} \in \mathbb{R}^{2N\times 2N}$$

with I_N that is the identity matrix $N \times N$,

$$J_{yz} = \frac{bV_{\max}\operatorname{sech}^2(d - d_0)}{1 + \tanh(d_0)} \begin{bmatrix} -1 & 1 & & (0) \\ & \ddots & \ddots & \\ (0) & & -1 & 1 \\ 1 & 0 & \dots & -1 \end{bmatrix} \in \mathbb{R}^{N\times N}.$$

Let us perform the analysis of the eigenvalues of the linearized model (3.5) by determining the characteristic polynomial of J. We compute $\det(J - \lambda I_{2N})$ through the Schur's complement S of $J - \lambda I_{2N}$.

$$J - \lambda I_{2N} = \begin{bmatrix} -\lambda I_N & I_N \\ J_{yz} & (-b - \lambda)I_N \end{bmatrix}$$

Being $\gamma = \frac{bV_{\max}}{1+\tanh(d_0)}\operatorname{sech}^2(d - d_0)$, its Schur's complement is

$$S = \frac{1}{\lambda + b} \begin{bmatrix} -\lambda^2 - b\lambda - \gamma & \gamma & & (0) \\ & \ddots & \ddots & \\ (0) & & -\lambda^2 - b\lambda - \gamma & \gamma \\ \gamma & 0 & \dots & -\lambda^2 - b\lambda - \gamma \end{bmatrix}.$$

We exploit the following property of the Schur's complement:

$$\det(J - \lambda I_{2N}) = \det(S)\ \det((-b - \lambda)I_N).$$

Since S is a block circulant matrix, its determinant is

$$\det(S) = -\frac{\lambda}{(\lambda + b)^{N-1}} \prod_{k=1}^{N-1} (-\lambda^2 - b\lambda - \gamma + \gamma e^{\frac{2k\pi j}{N}})$$

and the resulting characteristic polynomial of J is

$$\det(J - \lambda I_{2N}) = \lambda(\lambda + b) \prod_{k=1}^{N-1} (\lambda^2 + b\lambda + \gamma - \gamma e^{\frac{2k\pi j}{N}}). \tag{3.7}$$

where $\gamma = \frac{bV_{\max}}{1+\tanh(d_0)} \operatorname{sech}^2(d - d_0)$.
The characteristic polynomial shows a structural eigenvalue in the origin. Moreover, it is the same expression of the characteristic polynomial shown in [20]. Therefore, the same necessary and sufficient conditions may be considered in order to state whether the remaining roots have negative real part. By considering only the Optimal Velocity model, we can rewrite the conditions in [20] as

$$\frac{V_{\max}}{b} \frac{\operatorname{sech}^2(d - d_0)}{1 + \tanh(d_0)} < \frac{1}{1 + \cos\left(\frac{2\pi(i-1)}{N}\right)}, \ \forall\ i = 2, ..., N. \tag{3.8}$$

For a fixed N, we solve a system of $N - 1$ inequalities (3.8) and get the resulting stability constraint. The most restrictive constraint is obtained for $i = 2$, thus, for any N, the non-zero roots of J have negative real part if and only if the following condition is satisfied.

$$\frac{V_{\max}}{b} \frac{\operatorname{sech}^2(d - d_0)}{1 + \tanh(d_0)} < \frac{1}{1 + \cos(\frac{2\pi}{N})} \tag{3.9}$$

Since J has one structural zero eigenvalue, we cannot state whether the origin is an asymptotically stable equilibrium point for model (3.1). For this reason, let us switch to the Reduced Optimal Velocity model (3.10).

$$\begin{cases} \dot{z}_i = y_i, \quad \forall\ i = 1, ..., N-1 \\ \dot{y}_i = b\left[V_{\max} \frac{\tanh(z_{i+1}+d-d_0) - \tanh(z_i+d-d_0)}{1+\tanh(d_0)} - y_i\right], \quad \forall\ i = 1, ..., N-2 \\ \dot{y}_{N-1} = b\left[V_{\max} \frac{\tanh\left(-\sum_{i=1}^{N-1} z_i + d - d_0\right) - \tanh(z_{N-1}+d-d_0)}{1+\tanh(d_0)} - y_{N-1}\right], \\ \dot{y}_N = b\left[V_{\max} \frac{\tanh(z_1+d-d_0) - \tanh\left(-\sum_{i=1}^{N-1} z_i + d - d_0\right)}{1+\tanh(d_0)} - y_N\right], \end{cases} \tag{3.10}$$

where $d_0 = l_v + d_s$. Having substituted one variable, the state vector has been reduced to

$$\tilde{\mathbf{x}} = [z_1, z_2, ..., z_{N-1}, y_1, y_2, ..., y_N]^T \in \mathbb{R}^{2N-1}. \tag{3.11}$$

As before, the uniform flow equilibrium point corresponds to the origin of model (3.10), therefore, we linearize it around the same equilibrium. The linearized model of (3.10) is

$$\begin{aligned}
&\dot{z}_i = y_i, \quad \forall\ i = 1, .., N-1 \\
&\dot{y}_i = -\gamma z_i + \gamma z_{i+1} - b y_i, \quad \forall\ i = 1, ..., N-2 \\
&\dot{y}_{N-1} = -\gamma \sum_{j=1}^{N-2} z_j \ - 2\gamma z_{N-1} \ - b y_{N-1} \\
&\dot{y}_N = 2\gamma z_1 + \gamma \sum_{j=1}^{N-2} z_j \ - b y_N
\end{aligned} \tag{3.12}$$

where $\gamma = b\frac{\partial V_{opt}(d)}{\partial z_i} = \frac{bV_{\max}}{1+\tanh(d_0)} \operatorname{sech}^2(d - d_0)$. The linear system (3.12) may be rewritten in matrix form as

$$\dot{\tilde{\mathbf{x}}} = \tilde{J}\tilde{\mathbf{x}}. \tag{3.13}$$

The Jacobian matrix is equal to

$$\tilde{J} = \begin{bmatrix} 0 & \tilde{J}_{zy} \\ \tilde{J}_{yz} & -bI_N \end{bmatrix},$$

where

$$\tilde{J}_{yz} = \frac{bV_{\max} \operatorname{sech}^2(d - d_0)}{1 + \tanh(d_0)} \begin{bmatrix} -1 & 1 & & & (0) \\ & -1 & 1 & & \\ & & \ddots & \ddots & \\ (0) & & & -1 & 1 \\ -1 & -1 & -1 & \dots & -2 \\ 2 & 1 & 1 & \dots & 1 \end{bmatrix} \in \mathbb{R}^{N \times N-1},$$

and

$$\tilde{J}_{zy} = \begin{bmatrix} 1 & & & (0) & 0 \\ & 1 & & & \vdots \\ & & \ddots & & \vdots \\ (0) & & & 1 & 0 \end{bmatrix} \in \mathbb{R}^{N-1 \times N}.$$

The eigenvalues of $\tilde{J}$ depend on the parameters $V_{\max}$, b and $d - d_0$. For a given number N of vehicles, we fix d_0 and vary d by changing the length L of the ring road. Through numerical simulation, we see that all the eigenvalues have negative real part if the parameters belong to certain ranges. In this case, the linearized system (3.12) around the origin is asymptotically stable and the uniform flow equilibrium is an asymptotically stable equilibrium point for the nonlinear system (3.10). The equilibrium point may become unstable if b decreases, $V_{\max}$ increases or $|d - d_0|$ decreases.
We are interested in understanding which is the relationship between the model parameters and the eigenvalues of $\tilde{J}$ and which constraints the model parameters must satisfy in order to guarantee asymptotic stability of the uniform flow equilibrium. To answer this questions, for a specific number of vehicles, we compute the characteristic polynomial of $\tilde{J}$ and apply Routh stability criterion [21],[22].

N = 3. Let us consider a group of three vehicles as the smallest size of the platoon. In this case, the characteristic polynomial is

$$\det(\tilde{J} - \lambda I_5) = -(\lambda + b)\left[\lambda^4 + 2b\lambda^3 + (3\gamma + b^2)\lambda^2 + 3b\gamma\lambda + 3\gamma^2\right], \tag{3.14}$$

where $\gamma = \frac{bV_{\max}}{1+\tanh(d_0)}\operatorname{sech}^2(d - d_0)$. As expected, it does not shown any structural zero eigenvalue and it is such that the characteristic polynomial of the non-reduced linear model (3.5) with $N = 3$ is

$$\det(J - \lambda I_6) = -\lambda \ \det(\tilde{J} - \lambda I_5).$$

In fact, the reduction of the original model (3.1) has the objective of avoiding the structural zero eigenvalue, while the rest of the polynomial doesn't change. Therefore, the characteristic polynomial of $\tilde{J}$ is

$$\det(\tilde{J} - \lambda I) = -(\lambda + b)\prod_{k=1}^{N-1}(\lambda^2 + b\lambda + \gamma - \gamma e^{\frac{2k\pi j}{N}}).$$

By imposing the necessary and sufficient condition (3.9) derived from the results in [20], we can ensure that the eigenvalues of $\tilde{J}$ have negative real part. By considering the polynomial (3.14), we can derive the same constraint applying the Routh stability criterion. One eigenvalue of (3.14) is $\lambda_1 = -b$ and it is negative. For the remaining polynomial of 4^{th} order, let us fill the Routh table, Figure 3.1, and apply the criterion in order to derive a necessary and sufficient condition to guarantee that the polynomial have roots with negative real part and thus the origin is an asymptotically stable equilibrium point for the model with $N = 3$. In order for the polynomial to have all roots with negative real part,

4	1	$3\gamma + b^2$	$3\gamma^2$
3	$2b$	$3b\gamma$	0
2	$\frac{3}{2}\gamma + b^2$	$3\gamma^2$	0
1	$-\frac{3}{2}b\gamma^2 + 3b^3\gamma$	0	0
0	$3\gamma^2$	0	0

Figure 3.1: Routh table of the linearized model when $N = 3$

the elements of the first column of the table must be positive, which is true if $\gamma < 2b^2$.

This condition is equivalent to

$$\frac{V_{\max}}{b}\frac{\operatorname{sech}^2(d-d_0)}{1+\tanh(d_0)} < 2. \tag{3.15}$$

The same condition can be derived from (3.9) when $N = 3$. If the parameters of the model with $N = 3$ are chosen such that (3.15) holds, then the eigenvalues of the linearization around the origin have negative real part, so the linearized model (3.12) is asymptotically stable and the uniform flow equilibrium is asymptotically stable for the original nonlinear model (3.10) when $N = 3$.

N = 4. As well as before, we compute the characteristic polynomial of $\tilde{J}$ when $N = 4$.

$$\det(\tilde{J} - \lambda I_7) =$$

$$-(\lambda+b)\left[\lambda^6 + 3b\lambda^5 + (4\gamma+3b^2)\lambda^4 + (8b\gamma+b^3)\lambda^3 + (6\gamma^2+4b^2\gamma)\lambda^2 + 6b\gamma^2\lambda + 4\gamma^3\right],$$

Again, it has the following relationship with the characteristic polynomial of the original model (3.1).

$$\det(J - \lambda I_8) = -\lambda \ \det(\tilde{J} - \lambda I_7),$$

so the condition (3.9) ensures asymptotic stability of the reduced model (3.10). $\tilde{J}$ has again an eigenvalue equal to $\lambda_1 = -b$. For the remaining part of the polynomial we build the Routh table, Figure 3.2, and apply the Routh stability criterion. We derive the inequalities

6	1	$4\gamma + 3b^2$	$6\gamma^2 + 4b^2\gamma$	$4\gamma^3$
5	$3b$	$8b\gamma + b^3$	$6b\gamma^2$	0
4	$\frac{4}{3}\gamma + \frac{8}{3}b^2$	$4\gamma^2 + 4b^2\gamma$	$4\gamma^3$	0
3	$\frac{-b\gamma^2 + 8b^3\gamma + 2b^5}{\gamma + 2b^2}$	$\frac{12b^3\gamma^2 - 3b\gamma^3}{\gamma + 2b^2}$	0	0
2	$\frac{20b^3\gamma^3 + 8b^5\gamma^2 + 8b^7\gamma}{-b\gamma^2 + 8b^3\gamma + 2b^5}$	$4\gamma^3$	0	0
1	$\frac{-6b^6\gamma^5 + b^4\gamma^6 - 14b^8\gamma^4 + 20b^{10}\gamma^3 - b^2\gamma^7}{(5b^3\gamma^3 + 2b^5\gamma^2 + 2b^7\gamma)(\gamma + 2b^2)}$	0	0	0
0	$4\gamma^3$	0	0	0

Figure 3.2: Routh table of the linearized model when $N = 4$

that guarantee that the elements of the 1^{st} column of the table are positive. The necessary

and sufficient condition to satisfy in order for the roots of the polynomial to have negative real part is (3.16).

$$\frac{V_{\max}}{b}\frac{\operatorname{sech}^2(d-d_0)}{1+\tanh(d_0)} < 1 \tag{3.16}$$

This stability condition is equivalent to (3.9) when $N = 4$.

N = 5. We follow the same procedure for a model with $N = 5$, computing $\det(\tilde{J} - \lambda I_9)$, filling the Routh table of the characteristic polynomial without $-(\lambda + b)$ and applying the criterion. The roots of the characteristic polynomial have negative real part if the following constraint is satisfied.

$$\frac{V_{\max}}{b}\frac{\operatorname{sech}^2(d-d_0)}{1+\tanh(d_0)} < \frac{987}{1292} \tag{3.17}$$

From constraints (3.15)-(3.17) we end up to particular cases of condition (3.9), thus the a necessary and sufficient condition for asymptotic stability of the uniform flow equilibrium for the Reduced Optimal Velocity model (3.10) is

$$\frac{V_{\max}}{b}\frac{\operatorname{sech}^2(d-d_0)}{1+\tanh(d_0)} < \frac{1}{1+\cos(\frac{2\pi}{N})} = \kappa_N, \tag{3.18}$$

where κ_N depends only on the number of vehicles. Moreover, as the number of vehicles increases, κ_N reduces and the condition is more restrictive. Anyway,

$$\lim_{N\to\infty} \kappa_N = \frac{1}{2},$$

so, for any N, there always exists a set of parameters (b, $V_{\max}$, d, d_0) that ensures asymptotic stability of the uniform flow equilibrium.
Looking at (3.18), for a fixed N, the uniform flow equilibrium may become unstable if b decreases, $V_{\max}$ increases or $|d - d_0|$ reduces, because the right-hand term increases. By fixing $d_0 = l_v + d_s$, the stability of the uniform flow equilibrium for the model of a given number N of vehicles depends on the length L of the ring road. If the length of the ring road is such that $d \gg d_0$ or $d \ll d_0$ then, for any b and $V_{\max}$, the left-hand side term of (3.18) is almost equal to zero. Thus, the stability constraint is satisfied, but the eigenvalues of $\tilde{J}$ tend to the imaginary axis.
The relationship of stability on the parameters is confirmed also by the numerical analyses. Varying the parameters, b, $V_{\max}$ and $d-d_0$ we perform a numerical analysis computing the real part of the most critical eigenvalue, $\lambda_{\max}$, and focus on the level set of $Re(\lambda_{\max}) = 0$. In Figure 3.3 are depicted the level sets for a group of 10 vehicles. In the borderline case,

$$\frac{V_{\max}}{b}\frac{\operatorname{sech}^2(d-d_0)}{1+\tanh(d_0)} = \kappa_N, \tag{3.19}$$

we have marginal stability, which means that at least two eigenvalues of $\tilde{J}$ lie on the imaginary axis. When this scenario occurs, $Re(\lambda_{\max}) = 0$, so it is exactly the situation shown in Figure 3.3. In the borderline case, b and $V_{\max}$ are linearly dependent when $d-d_0$ is fixed and this is confirmed by the curves in Figure 3.3. If $V_{\max}$ is fixed, b is proportional

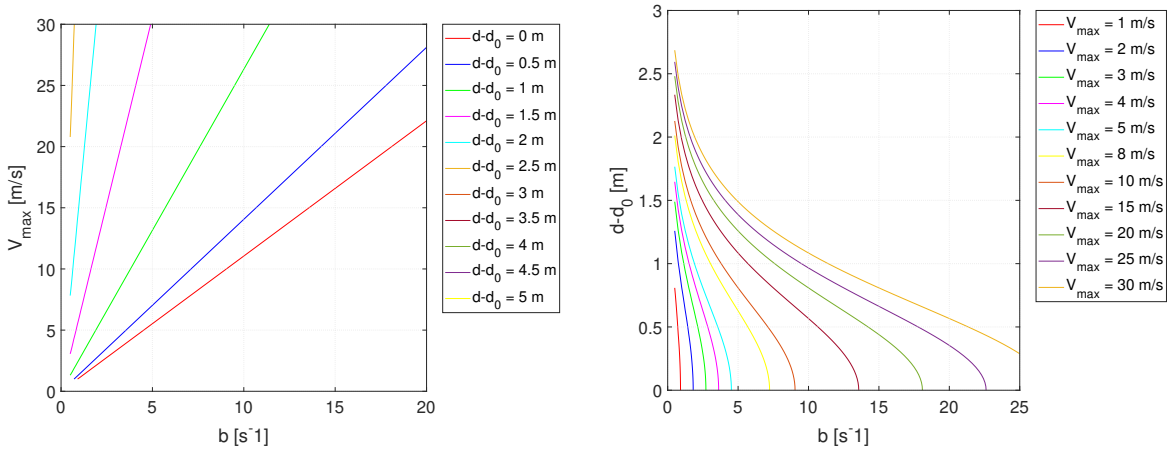

(a) (b)

Figure 3.3: Zero level of $Re(\lambda_{\max})$ when $N = 10$

to $\text{sech}^2(d - d_0)$ and this confirms the curves shown in Figure 3.3, whose profile resembles sech^2. Moreover, in Figure 3.3, beyond a certain value of $d - d_0$, $Re(\lambda_{\max}) < 0$, so for high values of $d - d_0$ the eigenvalues of $\tilde{J}$ are negative and the stability constraint (3.18) is satisfied.
From [20], the real part of the eigenvalues for the Optimal Velocity model is

$$Re(\lambda) = -\frac{b}{2} + \frac{1}{2}\left(\frac{\sqrt{b^4 + 32\gamma^2(1-\cos(\frac{2\pi}{N})) - 8b^2\gamma(1-\cos(\frac{2\pi}{N}))} + b^2 - 4\gamma(1-\cos(\frac{2\pi}{N}))}{2}\right)^{\frac{1}{2}},$$

where $\gamma = \frac{bV_{\max}}{1+\tanh(d_0)}\,\text{sech}^2(d - d_0)$.

$$\lim_{|d-d_0|\to\infty} Re(\lambda) = 0,$$

so the real part of the eigenvalues remains negative but tends to zero. Therefore, fixing d_0, if the ring road is too long ($d \gg d_0$) or too short ($d \ll d_0$), the trajectories reach the uniform flow equilibrium, but the convergence is slow.
Moreover, the stability of the uniform flow equilibrium depends on the size of the group of vehicles. Assume to increase N and the length L of the ring road such that $d = \frac{L}{N}$ is constant. Then,

$$\lim_{N\to\infty} Re(\lambda) = 0.$$

So, as the number of vehicles and the length of the ring increase, the stability of the uniform flow equilibrium worsens and the convergence to the equilibrium is slower. The dependence of stability on b, $V_{\max}$, $d - d_0$ and N shows off in the nonlinear framework, too, as described in Chapter 5.

3.1.1 Time simulation

We simulate the Optimal Velocity model (2.1) of a group of $N = 10$ vehicles on a ring road. It is simulated on a ring of length $L = 100\ m$, where $d_0 = l_v + d_s = 10\ m$, with two different choices of b and $V_{\max}$.

A - Asymptotically stable equilibrium point
In this first scenario, the model parameters are $b = 10\ s^{-1}$ and $V_{\max} = 10\ m/s$. With this choice, the stability condition (3.18) is satisfied, where $\kappa_{10} = 0.5528$, so the uniform flow equilibrium is an asymptotically stable point for the nonlinear system (2.1). Assume that the initial conditions are far from the equilibrium. Anyway, the trajectories of the model converge to the uniform flow equilibrium, where the vehicles keep the same inter-vehicle distances, as shown in Figure 3.4 and drive with the same velocity.

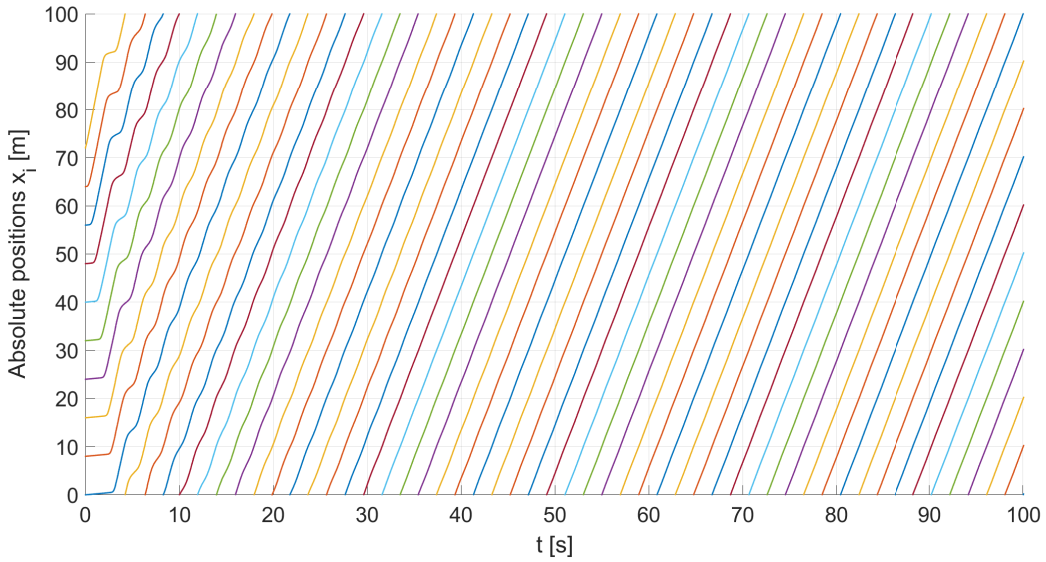

Figure 3.4: Simulation A - Evolution of the absolute positions x_i of a group of $N = 10$ vehicles with respect to time

B - Unstable equilibrium point
At the start of the simulation the vehicles are equally spaced and drive at the same velocity $v_i = V_{opt}(d)$, so the system starts at the uniform flow equilibrium. The parameters are $b = 3\ s^{-1}$ and $V_{\max} = 20\ m/s$, then

$$\frac{V_{\max}}{b}\frac{\operatorname{sech}^2(d - d_0)}{1 + \tanh(d_0)} > \kappa_{10}.$$

The stability condition (3.18) is not satisfied and the equilibrium point is unstable. In time simulation, the trajectories of (2.1) start from the uniform flow equilibrium and eventually the equilibrium is not kept and the stop-and-go waves rise up, as shown in Figure 3.5.

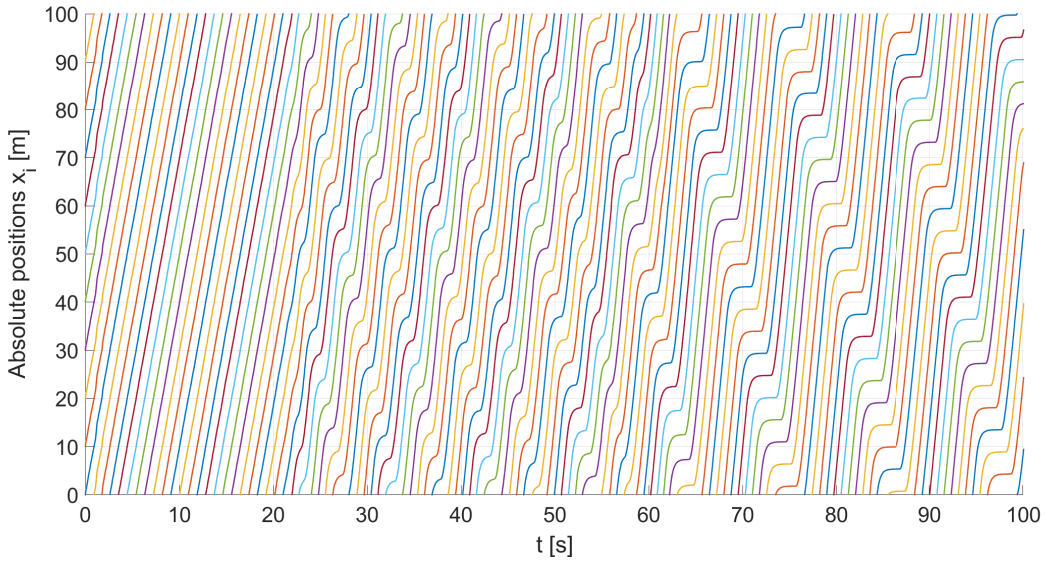

Figure 3.5: Simulation B - Evolution of the absolute positions x_i of a group of $N = 10$ vehicles with respect to time

3.2 Linear analysis of the model with saturation

In this section we study the properties of the Optimal Velocity model (3.20) with saturation function around the uniform flow equilibrium.

$$\begin{cases} \dot{x}_i = v_i, \quad \forall\ i = 1, ..., N \\ \\ \dot{v}_i = b\left[V_{\max}\frac{\text{sat}(x_{i+1}-x_i-d_0)\ +\ \tanh(d_0)}{1\ +\ \tanh(d_0)} - v_i\right], \quad \forall\ i = 1, ..., N \end{cases} \tag{3.20}$$

where $i + 1 = 1$ when $i = N$. We consider the model in error coordinates (3.22), so that the uniform flow equilibrium coincides with the origin:

$$\begin{cases} \dot{z}_i = y_i, \quad \forall\ i = 1, ..., N \\ \\ \dot{y}_i = b\left[V_{\max}\frac{\text{sat}(z_{i+1}+d-d_0)-\text{sat}(z_i+d-d_0)}{1+\tanh(d_0)} - y_i\right], \quad \forall\ i = 1, ..., N \end{cases} \tag{3.21}$$

where $i + 1 = 1$ when $i = N$.

$$\mathbf{x} = [z_1, z_2, ..., z_N, y_1, y_2, ..., y_N]^T \in \mathbb{R}^{2N} \tag{3.22}$$

If the state and $d - d_0$ are such that the saturation function (2.14) lies in the linear region, then model (3.21) is linear and equal to:

$$\begin{cases} \dot{z}_i = y_i, \quad \forall\ i = 1, ..., N \\ \\ \dot{y}_i = \frac{bV_{\max}}{1+\tanh(d_0)}z_{i+1} - \frac{bV_{\max}}{1+\tanh(d_0)}z_i - by_i, \quad \forall\ i = 1, ..., N, \end{cases} \tag{3.23}$$

which is similar to the linear model (3.5). Therefore, system (3.23) has a structural zero-eigenvalue and we cannot state whether the uniform flow equilibrium is an asymptotically stable equilibrium point for model (3.21). For this reason, we reduce the state vector (3.22) and define the following nonlinear model in the same way as for the Bando model in Section 3.1.

$$\begin{cases} \dot{z}_i = y_i, \quad \forall\ i = 1, ..., N-1 \\ \dot{y}_i = b\left[V_{\max}\frac{\text{sat}(z_{i+1}+d-d_0)-\text{sat}(z_i+d-d_0)}{1+\tanh(d_0)} - y_i\right], \quad \forall\ i = 1, ..., N-2 \\ \dot{y}_{N-1} = b\left[V_{\max}\frac{\text{sat}\left(-\sum_{i=1}^{N-1} z_i+d-d_0\right)-\text{sat}(z_{N-1}+d-d_0)}{1+\tanh(d_0)} - y_{N-1}\right], \\ \dot{y}_N = b\left[V_{\max}\frac{\text{sat}(z_1+d-d_0)-\text{sat}\left(-\sum_{i=1}^{N-1} z_i+d-d_0\right)}{1+\tanh(d_0)} - y_N\right] \end{cases} \tag{3.24}$$

$$\tilde{\mathbf{x}} = [z_1, z_2, ..., z_{N-1}, y_1, y_2, ..., y_N]^T \in \mathbb{R}^{2N-1} \tag{3.25}$$

System (3.24) may be written as

$$\dot{\tilde{\mathbf{x}}} = A\tilde{\mathbf{x}}(t) + B\,\text{sat}(K\tilde{\mathbf{x}}(t) + \bar{d}), \tag{3.26}$$

where $\bar{d} = (d - d_0)\mathbf{1}_N \in \mathbb{R}^N$,

$$A = \begin{bmatrix} 0 & A_{zy} \\ 0 & -bI_N \end{bmatrix},$$

with I_N the identity matrix $\in \mathbb{R}^{N\times N}$ and

$$A_{zy} = \begin{bmatrix} 1 & & & (0) & 0 \\ & 1 & & & \vdots \\ & & \ddots & & \vdots \\ (0) & & & 1 & 0 \end{bmatrix} \in \mathbb{R}^{N-1\times N},$$

$$B = \begin{bmatrix} 0_{N-1\text{x}N} \\ B_{yz} \end{bmatrix} \in \mathbb{R}^{2N-1\times N},$$

where

$$B_{yz} = \frac{bV_{\max}}{1+\tanh(d_0)} \begin{bmatrix} -1 & 1 & & & (0) \\ & -1 & 1 & & \\ & & \ddots & \ddots & \\ (0) & & & -1 & 1 \\ 1 & 0 & \dots & 0 & -1 \end{bmatrix} \in \mathbb{R}^{N\times N}$$

and

$$K = \begin{bmatrix} K_{yz} & 0_{N\text{x}2N-1} \end{bmatrix} \in \mathbb{R}^{N\times N-1},$$

where

$$K_{yz} = \begin{bmatrix} 1 & & & (0) \\ & 1 & & \\ & & \ddots & \\ (0) & & & 1 \\ -1 & \dots & \dots & -1 \end{bmatrix} \in \mathbb{R}^{N \times N}.$$

In order to find out the equilibrium points $\bar{\mathbf{x}}$ of system (3.26), let us solve the following equality:

$$A\bar{\mathbf{x}} + B\,\mathrm{sat}(K\bar{\mathbf{x}}(t) + \bar{d}) = 0. \tag{3.27}$$

1. Suppose $\bar{\mathbf{x}}$ and $\bar{d}$ are such that $\mathrm{sat}(K\bar{\mathbf{x}} + \bar{d})$ lies in the linearity region, then equation (3.27) is equal to

$$A\bar{\mathbf{x}} + B(K\bar{\mathbf{x}} + \bar{d}) = 0$$
$$(A + BK)\bar{\mathbf{x}} + B\bar{d} = 0$$
$$\bar{\mathbf{x}} = -(A + BK)^{-1}B\bar{d}$$

   Since $B\bar{d} = 0,\ \forall\ \bar{d},\ \bar{\mathbf{x}} = 0$ is the only equilibrium point for system (3.26), provided that each row of $\mathrm{sat}(K\bar{\mathbf{x}}(t) + \bar{d})$ lies in the linearity region.

$$\mathrm{sat}(K\bar{\mathbf{x}} + \bar{d}) = \begin{cases} 1, & \text{if } K\bar{\mathbf{x}}(t) + \bar{d} \succ 1 \\ K\bar{\mathbf{x}} + \bar{d}, & \text{if } -1 \preccurlyeq K\bar{\mathbf{x}} + \bar{d} \preccurlyeq 1 \\ -1, & \text{if } K\bar{\mathbf{x}} + \bar{d} \prec -1 \end{cases} \tag{3.28}$$

   In order to be in the linearity region, the following inequality must hold,

$$-1 \preccurlyeq K\bar{\mathbf{x}} + \bar{d} \preccurlyeq 1. \tag{3.29}$$

   Then $\bar{\mathbf{x}} = 0$ is an equilibrium point for system (3.26) in its linearity region if $\bar{d}$ is such that

$$-1 \preccurlyeq \bar{d} \preccurlyeq 1, \tag{3.30}$$

   then

$$-1 \leq d - d_0 \leq 1. \tag{3.31}$$

   Being $d_0 = l_v + d_s$ fixed, if L is such that $d = L/N$ satisfies inequality (3.31), the only equilibrium point of system (3.26) coincides with the uniform flow equilibrium, where all the vehicles travel at the same velocity and have constant and equal headway. If $\bar{d}$ doesn't satisfy inequality (3.31), the system doesn't work in the linearity region and the initial hypothesis doesn't hold anymore.

2. Suppose to be in the high saturation region, where $\bar{\mathbf{x}}$ and $\bar{d}$ are such that

$$\mathrm{sat}(K\bar{\mathbf{x}} + \bar{d}) = \mathbf{1}_N.$$

   Then equation (3.27) is equal to

$$A\bar{\mathbf{x}} + B\mathbf{1}_N = 0.$$

Since $B\mathbf{1}_N = 0$, then

$$A\bar{\mathbf{x}} = 0. \tag{3.32}$$

Any vector $\bar{\mathbf{x}}$ such that

$$\bar{\mathbf{x}} = [rand(N-1,1), zeros(N,1)]^T \tag{3.33}$$

solves equation (3.32). Therefore, if the system works in saturation, there are more equilibrium points in addiction to $\bar{\mathbf{x}} = 0$ and these equilibria are such that the vehicles are arbitrary spaced and travel with the same maximum velocity, $V_{\max}$.

3. Let us suppose to be in the low saturation region. In this case, since

$$\text{sat}(K\bar{\mathbf{x}} + \bar{d}) = -\mathbf{1}_N$$

and $B(-\mathbf{1})_N = 0$, again equation (3.27) is equal to (3.32) and it has the same set of solutions (3.33). In this case, if the velocity functions saturate to the lower value, it means that at the equilibrium all vehicles are still.

In conclusion, when system (3.26) works in the linearity region, the only equilibrium point is the uniform flow, where all the vehicles travel at the same velocity and are equally spaced. When it works in the saturation region, there are additional equilibria, where the vehicles have zero relative velocities and any spacing error.

Let us study the stability properties of the equilibrium points in the linearity region and in the saturation region.

1. *Linearity region*

In this case, model (3.26) is equal to

$$\dot{\tilde{\mathbf{x}}}(t) = A\tilde{\mathbf{x}}(t) + B(K\tilde{\mathbf{x}}(t) + \bar{d}) \tag{3.34}$$

and, since $B\bar{d} = 0$, it is equivalent to

$$\dot{\tilde{\mathbf{x}}}(t) = (A + BK)\tilde{\mathbf{x}}(t). \tag{3.35}$$

The stability properties of this linear system are given by the study of matrix $A+BK$.

$$A + BK = \begin{bmatrix} 0_{N-1\times N-1} & M_{zy} \\ M_{yz} & -bI_N \end{bmatrix},$$

where I_N is the identity matrix $\in \mathbb{R}^{N\times N}$,

$$M_{zy} = \begin{bmatrix} 1 & & & (0) & 0 \\ & 1 & & & \vdots \\ & & \ddots & & \vdots \\ (0) & & & 1 & 0 \end{bmatrix} \in \mathbb{R}^{N-1\times N}.$$

and

$$M_{yz} = \frac{bV_{\max}}{1+\tanh(d_0)} \begin{bmatrix} -1 & 1 & & & (0) \\ & -1 & 1 & & \\ & & \ddots & \ddots & \\ (0) & & & -1 & 1 \\ -1 & -1 & -1 & \dots & -2 \\ 2 & 1 & 1 & \dots & 1 \end{bmatrix} \in \mathbb{R}^{N \times N-1}.$$

In the linearity region, the only equilibrium point is $\bar{\mathbf{x}} = 0$ and, fixing $d_0 = l_v + d_s$, the stability of this equilibrium depends only on b and $V_{\max}$.
Moreover, matrix $A + BK$ is similar to the Jacobian matrix $\tilde{J}$ of the linearized Optimal Velocity model (3.12) except for the absence of $\text{sech}^2(d - d_0)$. Therefore, the eigenvalues of $A + BK$ have negative real part if and only if the following condition is true.

$$\frac{V_{\max}}{b} \frac{1}{1+\tanh(d_0)} < \frac{1}{1+\cos(\frac{2\pi}{N})} \tag{3.36}$$

Therefore, if model (3.24) works in the linearity region, the uniform flow equilibrium is the only equilibrium point and it is asymptotically stable if and only if the parameters satisfy condition (3.36).

2. *Saturation region*

When the state $\tilde{\mathbf{x}}(t)$ and $d - d_0$ are such that system (3.26) works in one of the two saturation regions, it is equal to

$$\dot{\tilde{\mathbf{x}}}(t) = A\tilde{\mathbf{x}}(t). \tag{3.37}$$

Basically, the derivative of the velocity of each vehicle does not depend on the distance with respect to the preceding vehicle, so the main feature of the Optimal Velocity model is lost. The linear system (3.37) may have several equilibrium points, including $\bar{\mathbf{x}} = 0$, and they correspond to have any inter-vehicle distances and absolute velocities that are all equal to $V_{\max}$ or equal to zero.
The stability properties of the equilibrium points depend on matrix A, which has N eigenvalues equal to $-b$ and $N - 1$ eigenvalues equal to zero. For this reason, all the equilibrium points of (3.37) are unstable and, if model (3.24) works in one of the two saturation regions, the uniform flow equilibrium is unstable.

Since in the saturation region the system has several equilibrium points besides the uniform flow equilibrium, the objective is to avoid that all the velocity functions of the nonlinear model (3.20) saturate to $V_{\max}$ or all saturate to zero. The parameter of the model that determines whether the velocity functions saturate is $d - d_0$. Therefore, by fixing $d_0 = l_v + d_s$, it's the length L of the ring road that makes the trajectories of (3.20) converge to the linearity region or the saturation region for a given number N of vehicles.
If $-1\ m \leq d - d_0 \leq 1\ m$, it is not possible that at the same time instant all the velocity functions saturate to $V_{\max}$ or to zero, for any initial condition. This is because, since the ring road is closed, the inter-vehicle distances cannot be such that $x_{i+1} - x_i - d_0 > 1\ m$ or $x_{i+1} - x_i - d_0 < -1\ m\ \forall\ i = 1, ..., N$ at the same time. Therefore, in the worst

case, even if $N-1$ velocity functions saturate up to $V_{\max}$, the last velocity function lies in the linearity region or in the low saturation region. Similarly, if $N-1$ velocity functions saturate down to zero, the remaining velocity function lies in the linearity region or in the high saturation region. In both cases, all the velocity functions will reach the linearity region and eventually the trajectories of (3.20) converge to the uniform flow equilibrium.
If $d - d_0 > 1\ m$, it means that the ring road is 'too long' and sooner or later all the inter-vehicle distances are such that

$$x_{i+1} - x_i - d_0 > 1\ m,$$

so the velocity functions of all vehicles reach the high saturation region at different times. Starting with any initial condition, all velocity functions saturate up to $V_{\max}$ because the inter-vehicle distances are too large. When they all lie in the saturation region, the derivatives of the velocities don't depend on the headways anymore, so they keep their velocities constant independently on the headways. The result is that the vehicles travel with the maximum velocity and assume any inter-vehicle distances.
If $d - d_0 < -1\ m$, the ring road is 'too short' and the inter-vehicle distance of at least one couple of vehicles is shorter than the safe distance:

$$x_{i+1} - x_i - d_0 < -1\ m.$$

When this happens, the following vehicle of the couple stops because its velocity function saturates to zero. All vehicles behind it brake and stop as well, so all velocity functions saturate to zero and the vehicles are still.

The three different scenarios are shown in the following time simulations.

3.2.1 Time simulation

Let us consider the nonlinear system (3.20) modelling a group of $N = 3$ vehicles on ring roads of different length L. Suppose that $d_0 = l_v + d_s = 10\ m$ is fixed and the parameters are $b = 5\ s^{-1}$ and $V_{\max} = 10\ m/s$.

Simulation 1. $-1\ m \leq d - d_0 \leq 1\ m$
Suppose the ring road has length $L = 31.5\ m$, then $d = \frac{L}{N} = 10.5\ m$ and $d - d_0 = 0.5\ m$.

1. Case A. Suppose to start with the following inter-vehicle distances, depicted in Figure 3.6.
$$\Delta x_1(0) = 11.2\ m, \quad \Delta x_2(0) = 11.2\ m, \quad \Delta x_3(0) = 9.1\ m.$$
In this scenario, $\Delta x_1(0), \Delta x_2(0) > d_0 + 1\ m$, so their optimal velocity functions, V_{opt}^1 and V_{opt}^2, start in the high saturation region. On the contrary, $d_0 - 1\ m < \Delta x_3(0) < d_0 + 1\ m$, so the optimal velocity function V_{opt}^3 starts in the linearity region. In Figure 3.7 and Figure 3.8 are shown the trajectories of this simulation. The linearity region in Figure 3.7 is bounded by the red lines. Since $\Delta x_3 < d_0$, the distance between the 3^{rd} and the 1^{st} vehicle is not safe, so the optimal velocity of the 3^{rd} vehicle is low and the 3^{rd} vehicle brakes and its headway Δx_3 increases. It increases so much that it enters the high saturation region. As the 3^{rd} vehicle brakes, the distance

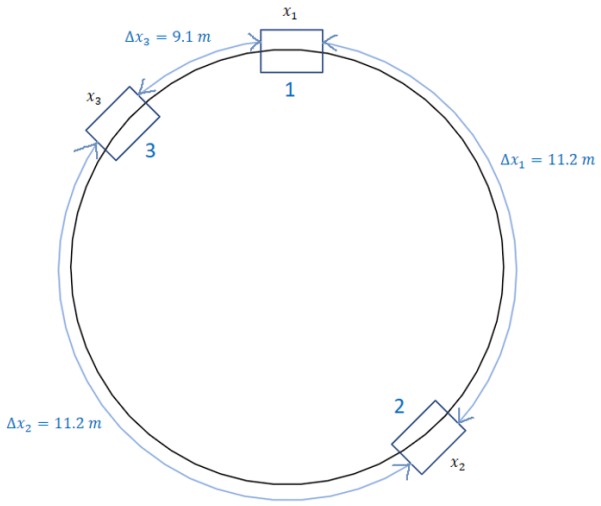

Figure 3.6: Initial positions in Simulation 1.A

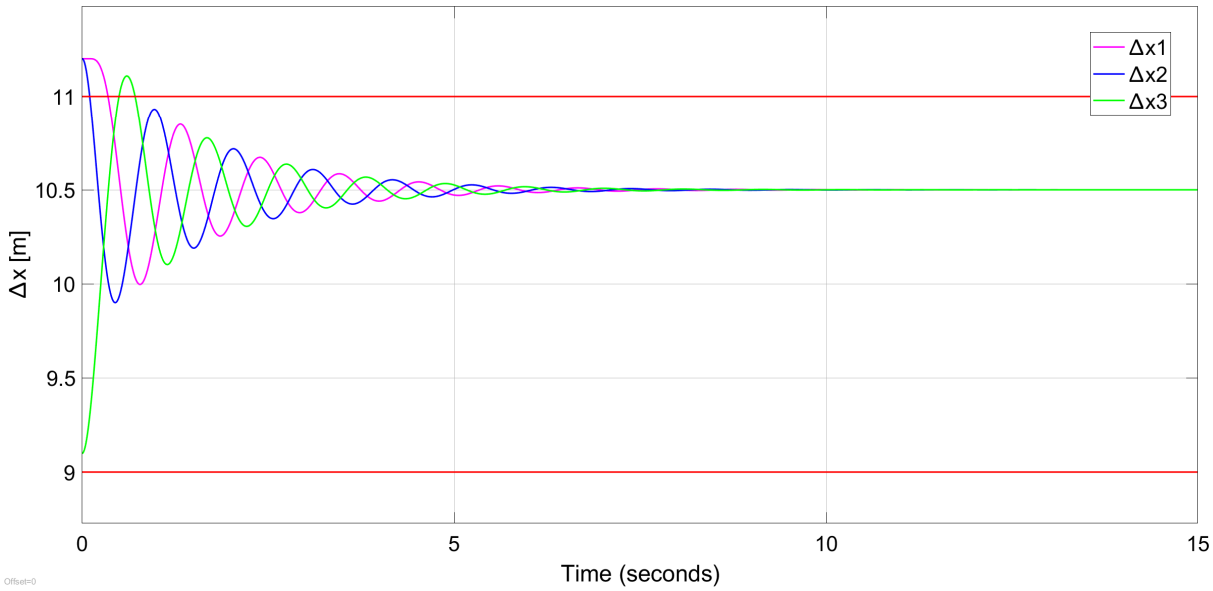

Figure 3.7: Inter-vehicle distances in Simulation 1.A

Δx_2 between the 3^{rd} and the 2^{nd} vehicle reduces and the optimal velocity function of the 2^{nd} vehicle decreases, leaves the saturation region and enters the linearity region. Since the 2^{nd} vehicle is braking, also the distance between the 2^{nd} and the 1^{st} vehicle, Δx_1, decreases and the velocity function of the 1^{st} vehicle reduces and enters the linearity region decreasing from $V_{\max}$. As the 1^{st} vehicle brakes, Δx_3 reduces and it enters the linearity region.
When all the velocity functions are in the linearity region, they converge to the uniform flow equilibrium. At the beginning of this simulation, $N-1$ vehicles were

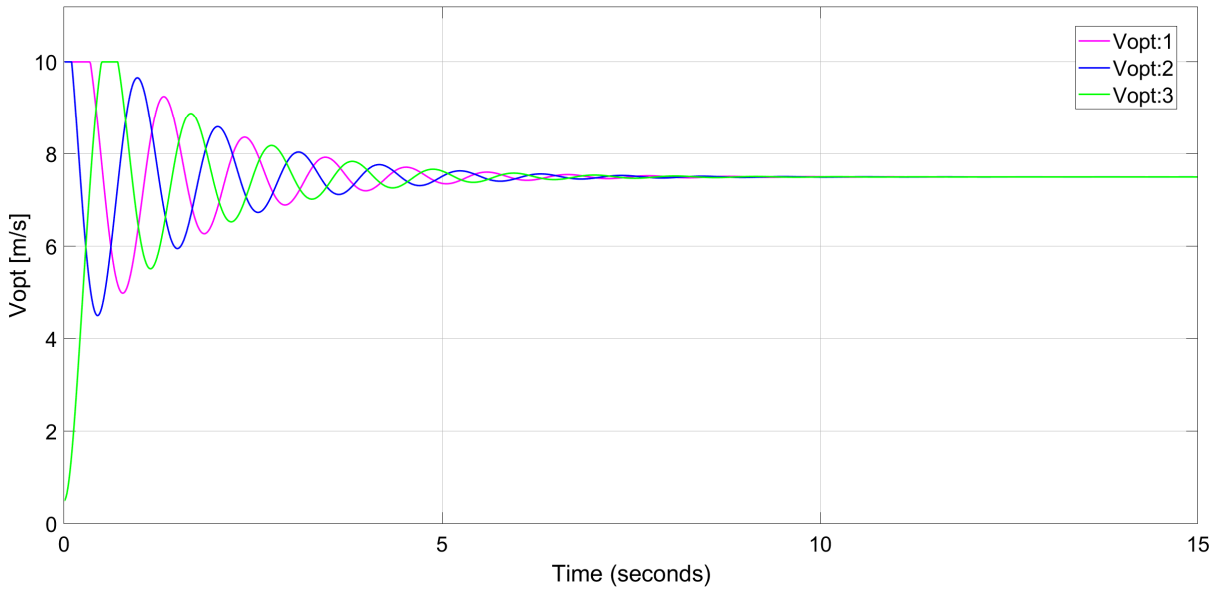

Figure 3.8: Optimal velocities in Simulation 1.A

in saturation region and just one started in the linearity region. Yet all saturation functions reach the linearity region. Since the parameters satisfy condition (3.36), the trajectories in the linearity region converge to the uniform flow equilibrium.

2. Case B. Suppose to start with the following initial inter-vehicle distances:

$$\Delta x_1(0) = 11.5\ m, \quad \Delta x_2(0) = 11.5\ m, \quad \Delta x_3(0) = 8.5\ m.$$

In this case, $\Delta x_1(0), \Delta x_2(0) > d_0 + 1\ m$, so their optimal velocity functions, V^1_{opt} and V^2_{opt}, start in the high saturation region. On the contrary, $\Delta x_3(0) < d_0 - 1\ m$, so the optimal velocity function V^3_{opt} starts in the low saturation region. The different saturations are shown in Figure 3.10. At the beginning, the 3^{rd} and the 1^{st} vehicle are very close, so the optimal velocity of the 3^{rd} vehicle saturates to zero and it brakes. Meanwhile, the distances between 2^{nd} and 1^{st} vehicle and 3^{rd} and 2^{nd} vehicle are large, so the 1^{st} and the 2^{nd} vehicle see a large headway in front of them. Their optimal velocity functions saturate to $V_{\max}$, so they speed up. The 3^{rd} vehicle brakes and the 2^{nd} and 1^{st} vehicle accelerate. At the same time, Δx_2 decreases and Δx_3 increases, as shown in Figure 3.9, while Δx_1 remains constant because both the 1^{st} and the 2^{nd} vehicle are travelling at the same speed, $V_{\max}$. As Δx_2 reduces, its optimal velocity function leaves the high saturation region and enters the linearity region (bounded by the red lines). As Δx_3 increases, its optimal velocity function leaves the low saturation region, enters the linearity region and reaches the high saturation region.
Finally, when all velocity functions are in the linearity region, the inter-vehicle distances converge to $d = \frac{L}{N}$ and the platoon reaches the uniform flow equilibrium, because the parameters of the model satisfy condition (3.36).

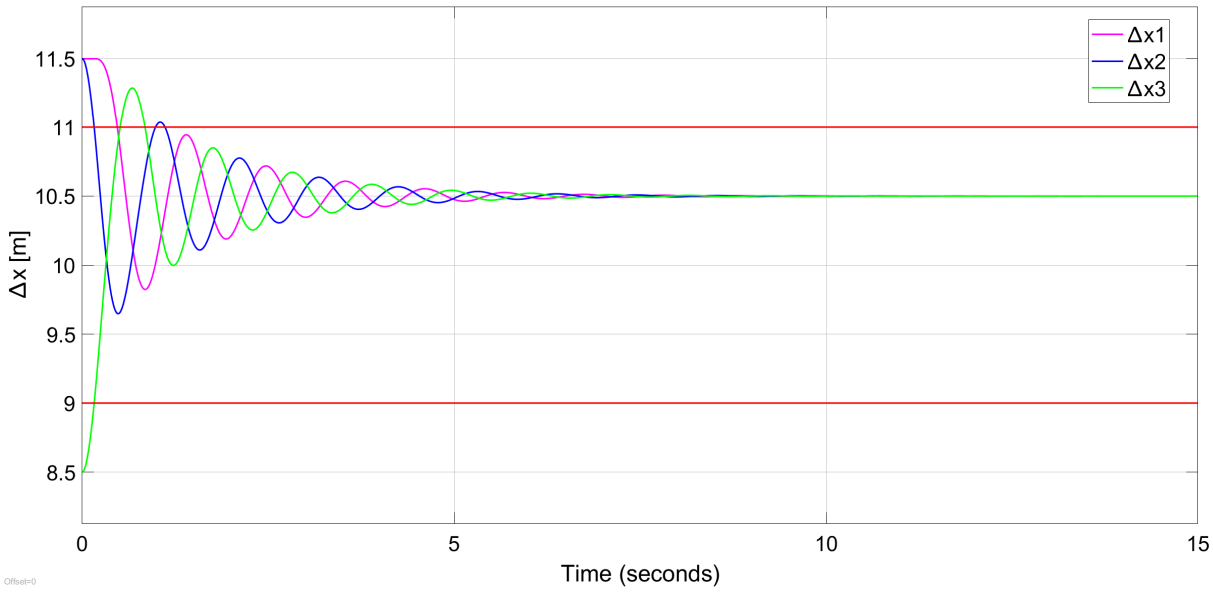

Figure 3.9: Inter-vehicle distances in Simulation 1.B

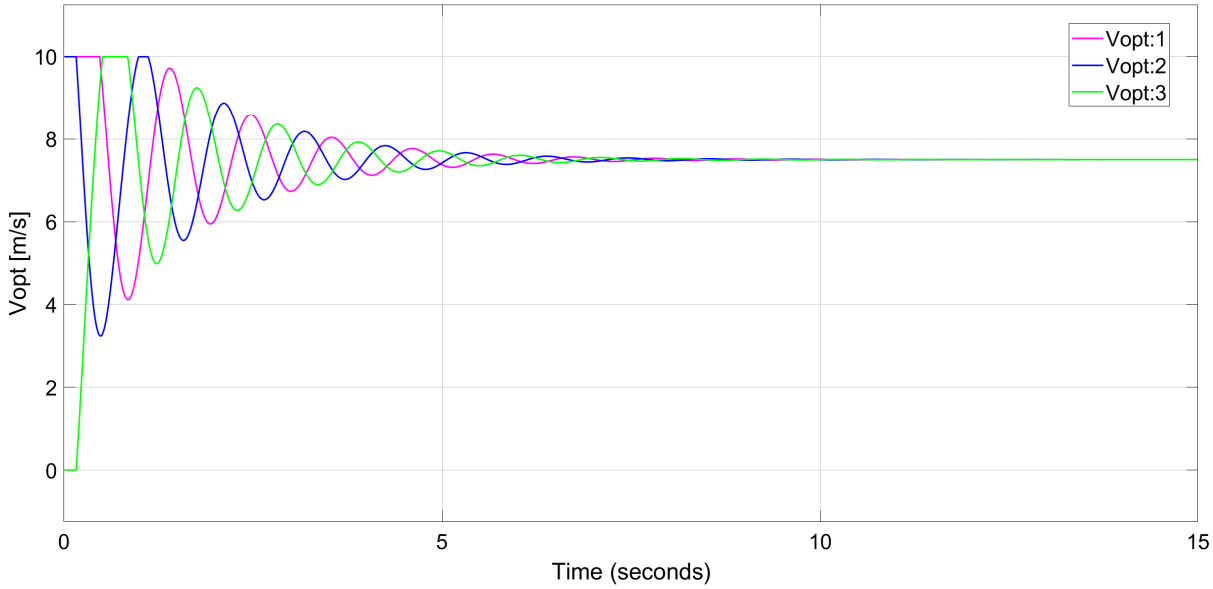

Figure 3.10: Optimal velocities in Simulation 1.B

Simulation 2. $d - d_0 > 1\ m$
Let us consider a ring road of length $L = 36\ m$, then $d = \frac{L}{N} = 12\ m$ and $d - d_0 = 2\ m$. Suppose to start with the following initial initial inter-vehicle distances:

$$\Delta x_1(0) = 10\ m, \quad \Delta x_2(0) = 10\ m, \quad \Delta x_3(0) = 16\ m.$$

Since $d_0 - 1\ m < \Delta x_1(0), \Delta x_2(0) < d_0 + 1\ m$, the initial optimal velocity functions V^1_{opt} and V^2_{opt} don't saturate and they lie in the linear region (bounded by the red lines), as shown in Figure 3.11. On the contrary, since $\Delta x_3(0) > d_0 + 1\ m$, V^3_{opt} saturates and it is equal to $V_{\max}$, as shown Figure 3.12. Since $V^3_{opt} = V_{\max}$, the 3^{rd} vehicle speeds up in order to decrease its distance with respect to the 1^{st} vehicle. As Δx_3 decreases, the distance Δx_2 between the 2^{nd} and 3^{rd} vehicle increases up to $d_0 + 1\ m = 11\ m$ and its velocity function enters the saturation region, so V^2_{opt} becomes equal to $V_{\max}$ and the 2^{nd} vehicle speeds up. Since the 2^{nd} vehicle accelerates, its distance with respect to the 1^{st} vehicle increases and even the V^1_{opt} enters the high saturation region and becomes equal to $V_{\max}$.
When all the optimal velocity functions lie in the high saturation region, the three vehicles travel at the same velocity, $V_{\max}$, and they don't regulate their velocity with the headway, so they don't reach the uniform flow equilibrium.

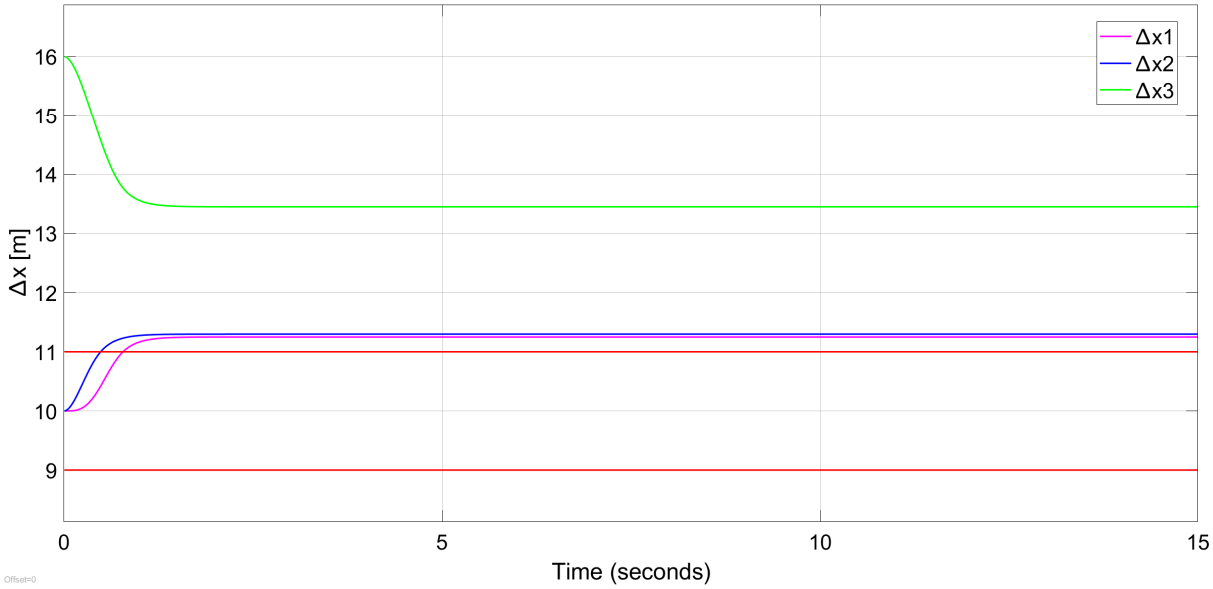

Figure 3.11: Inter-vehicle distances in Simulation 2

Simulation 3. $d - d_0 < -1\ m$
Let us consider a ring road of length $L = 24\ m$, then $d = \frac{L}{N} = 8\ m$ and $d - d_0 = -2\ m$. Suppose to start with the following initial initial inter-vehicle distances:

$$\Delta x_1(0) = 9.5\ m, \quad \Delta x_2(0) = 9.5\ m, \quad \Delta x_3(0) = 5\ m.$$

Since $d_0 - 1\ m < \Delta x_1(0), \Delta x_2(0) < d_0 + 1\ m$, the initial optimal velocity functions V^1_{opt} and V^2_{opt} lie in the linear region (bounded by the red lines), as shown in Figure 3.13. On the contrary, since $\Delta x_3(0) < d_0 - 1\ m$, the headway of the 3^{rd} vehicle is not safe, so V^3_{opt} saturates to zero, as shown Figure 3.14. Since its velocity function saturates to zero, the 3^{rd} vehicle brakes and stops, so its distance with respect to the 1^{st} vehicle, Δx_3, increases and the distance with respect to the 2^{nd} vehicle, Δx_2, decreases. As the 3^{rd} vehicle stops, also the 2^{nd} brakes and enters the low saturation region, as well as the 1^{st} vehicle does.

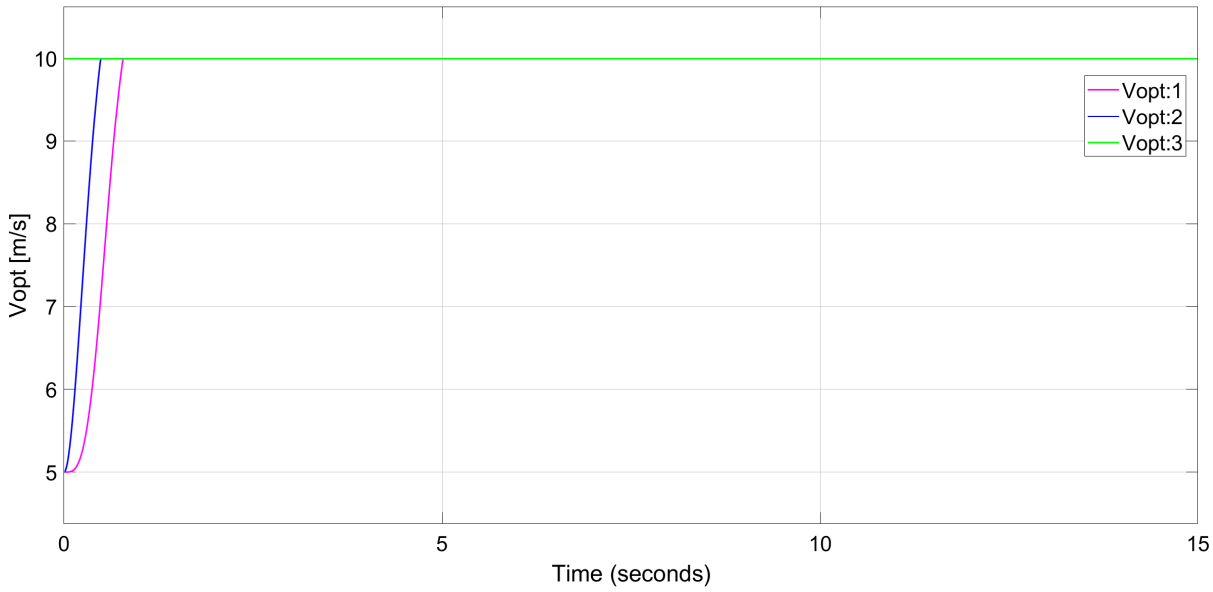

Figure 3.12: Optimal velocities in Simulation 2

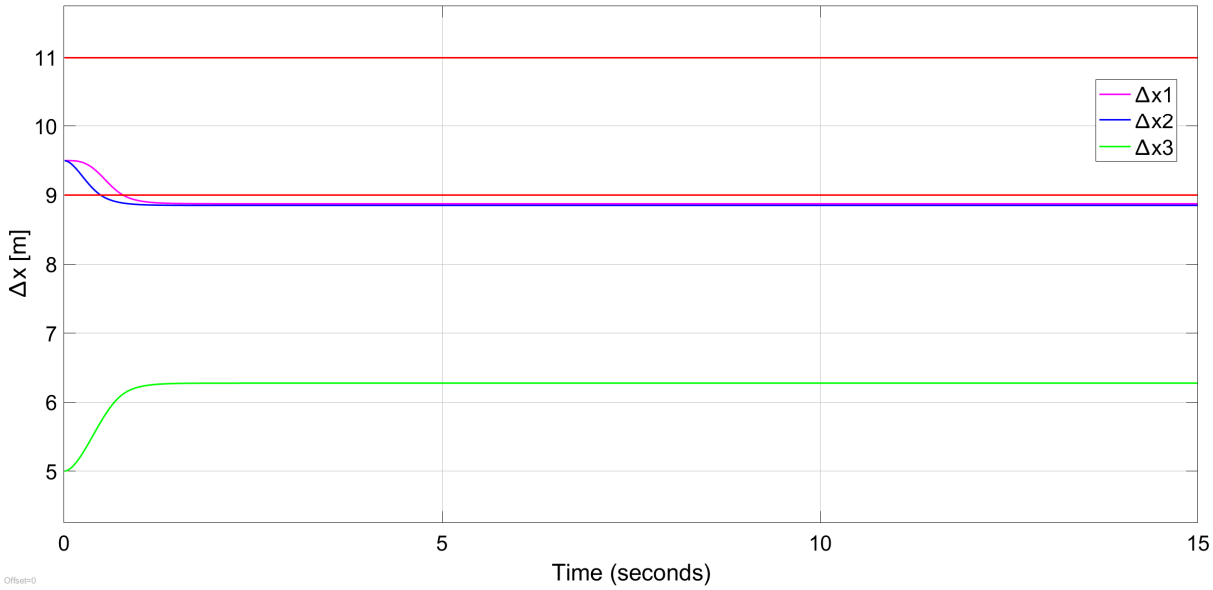

Figure 3.13: Inter-vehicle distances in Simulation 3

Finally, all the velocity functions lie in the low saturation region, so the vehicles are still and their inter-vehicle distances are different from d. Thus, the group of vehicles doesn't reach the uniform flow equilibrium.

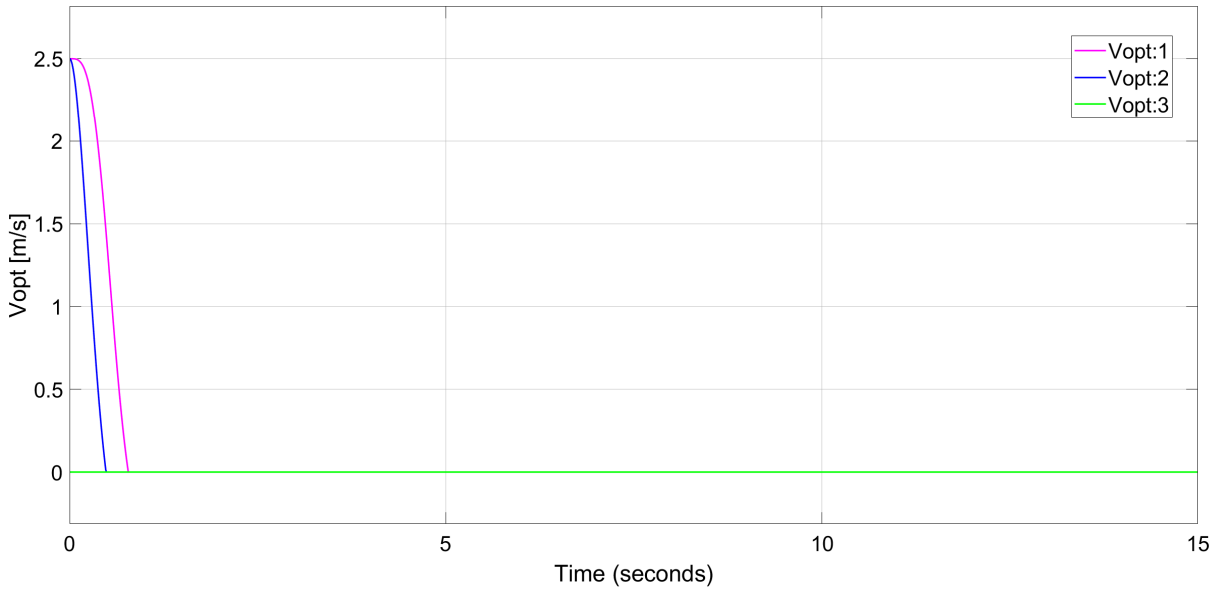

Figure 3.14: Optimal velocities in Simulation 3

3.3 Comparison of the linear models

The linearized Bando Optimal Velocity model around the uniform flow equilibrium (3.12) and the Optimal Velocity model with saturation function in the linearity region (3.35) share similar state equations. From the expression of the characteristic polynomial of the Jacobian matrix $\tilde{J}$ of the former, we derive a necessary and sufficient condition (3.18) on the parameters to guarantee that the uniform flow equilibrium is asymptotically stable. Being (3.12) an approximation of the nonlinear model (3.10) around an equilibrium point, the stability condition concerns a neighborhood of the uniform flow equilibrium and its satisfaction guarantees local stability. The Optimal Velocity model with saturation function in the linearity region is described by matrix $A + BK$ and the uniform flow is the only equilibrium point in this working condition. By noticing that $A + BK$ is similar to $\tilde{J}$, we derive a similar necessary and sufficient condition (3.36) that guarantees the asymptotically stability of the uniform flow equilibrium in the linearity region. Since the (3.35) is not an approximation, because the model is linear in the linearity region, the stability properties of $A + BK$ hold in the whole linearity region and not just in a neighborhood of the uniform flow equilibrium.
Fixing the number of vehicles and $d_0 = l_v + d_s$, the stability condition of the linearized Bando model involves the parameters b, $V_{\max}$ and $d = \frac{L}{N}$. Instead, provided that the state and $d - d_0$ are such that the model with saturation (3.24) works in the linearity region, the stability of the uniform flow equilibrium depends only on b and $V_{\max}$.
On the contrary, if the Optimal Velocity model with saturation function works in one of the two saturation regions, the behaviour of the model changes. The velocity functions saturate either to zero or to $V_{\max}$, so the vehicles don't regulate their velocities on the basis of the headways and the main feature of Bando traffic modelling fails. In these two scenarios, the system (3.37) is linear and it is described just by matrix A. It has several

equilibrium points, in which the relative velocities are zero and the spacing errors with respect to the desired distance at the uniform flow equilibrium are whatever. As shown in the previous section, depending on $d - d_0$, the trajectories of the model (3.24) can converge to the linearity region or to one of the two saturation regions, whatever are the initial conditions. They converge to the saturation regions if $d - d_0 > 1\ m$ or $d - d_0 < -1\ m$. Therefore, fixing d_0 and N, if the length L of the ring road is too long or too short, either the velocities of all vehicles are equal to $V_{\max}$ or the vehicles stop. In both cases, the velocity functions don't depend on the headways anymore and the vehicle distances may be anyone. This characteristic concerns only the Optimal Velocity model with saturation function, because in the Bando Optimal Velocity model the hyperbolic tangent never saturates and the vehicles always regulate their velocities on the basis of the headways. In the Bando model, if $|d - d_0|$ is very high, it means that, as the vehicles tend to the uniform flow equilibrium, the vehicle distances tend to d and the corresponding velocity functions tend to $V_{\max}$. Nevertheless, they do not saturate. Moreover, increasing $|d - d_0|$, the eigenvalues of the linearized Bando model around the uniform flow equilibrium tend to the imaginary axis. So, even if the stability condition (3.18) holds, the convergence to the equilibrium is slow.

Chapter 4

Stability and safety analysis of the Optimal Velocity model with saturation

4.1 Linear systems subject to saturated control law

In [23] a very deep study is carried out about linear systems subject to saturated inputs. These systems in open loop are linear, but, when they are fed with a feedback control law, physical constraints of the actuators make the control signal to be bounded.
In Figure 4.1 is shown the control system.
Depending on its amplitude, the control signal $\nu(t)$ provided to the actuator may be amplified or saturated to a minimum value or a maximum value, which depends on the physical construction of the actuator. The signal coming out from the actuator can be modelled by a saturation function as

$$u(t) = \text{sat}(\nu(t)),$$

where $u(t)$ and $\nu(t) \in \mathbb{R}^m$ and $\text{sat}(\nu(t))$ is a vector function whose rows are defined in (4.1) and shown in Figure 4.2.

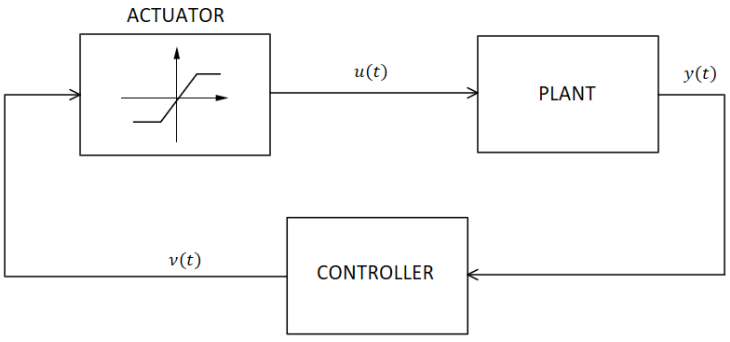

Figure 4.1: Closed-loop system

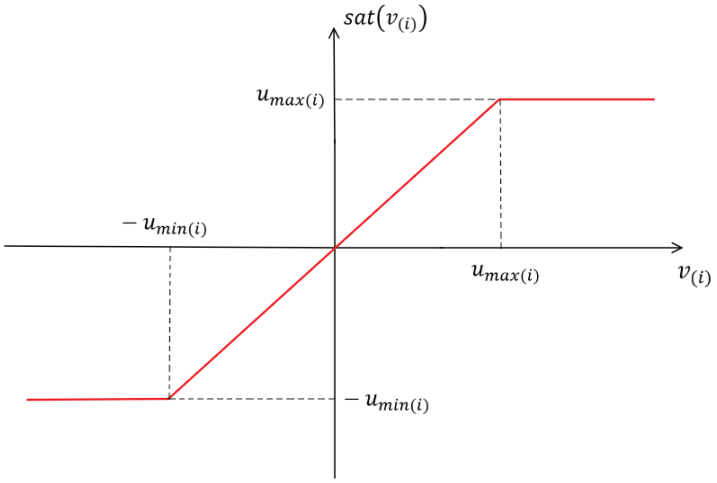

Figure 4.2: Saturation function

$$\text{sat}(\nu_{(i)}) = \begin{cases} -u_{\min(i)}, & \text{if } \nu_{(i)} < -u_{\min(i)} \\ \nu_{(i)}, & \text{if } -u_{\min(i)} \leq \nu_{(i)} \leq u_{\max(i)} \\ u_{\max(i)}, & \text{if } \nu_{(i)} > u_{\max(i)} \end{cases} \tag{4.1}$$

$\forall\ i = 1, ..., m.$
Let us suppose that the system in open loop is linear

$$\dot{x}(t) = Ax(t) + Bu(t), \tag{4.2}$$

where $x \in \mathbb{R}^n$ is the state vector and $u \in \mathbb{R}^m$ is the control signal provided by the actuator. Suppose that all states can be measured and that the signal provided by the controller and subject to saturation is

$$\nu(t) = Kx(t),$$

where $K \in \mathbb{R}^{m \times m}$ is a known constant matrix. Then, the control input fed to the linear system is

$$u(t) = \text{sat}(Kx(t)).$$

Thus, the closed-loop system (4.2) is

$$\dot{x}(t) = Ax(t) + B\,\text{sat}(Kx(t)). \tag{4.3}$$

It is clear that the saturation introduced by the actuator makes the whole closed loop system nonlinear. Nevertheless, a nonlinear system like (4.3) shows some particular characteristics that allow to study interesting system properties (i.e. stability) in a simple way with respect to generic nonlinear systems.

Region of linearity
When $x(t)$ is such that $-u_{\min(i)} \leq \nu_{(i)} \leq u_{\max(i)},\ \forall\ i = 1, ..., m,\ \nu(t)$ is not saturated. It follows that

$$\text{sat}(Kx(t)) = Kx(t) \tag{4.4}$$

and the closed loop system (4.3) is linear and equal to

$$\dot{x}(t) = (A + BK)x(t). \tag{4.5}$$

When (4.4) is true, the system lies in the region of linearity, which is defined as

$$R_L = S(K,\ u_{\min},\ u_{\max}) = \{x \in \mathbb{R}^n : -u_{\min} \preccurlyeq Kx(t) \preccurlyeq u_{\max}\}. \tag{4.6}$$

It is important to notice that, even if the trajectories of (4.3) start in R_L, they may go out of it. Furthermore, even if the linear system (4.5) is asymptotically stable (i.e. $(A + BK)$ has all eigenvalues with negative real part), the whole nonlinear system (4.3) may be unstable. This is true also if the initial conditions of (4.3) lie within the region of linearity.

Region of Asymptotic Stability

If the linear system (4.5) is asymptotically stable, the convergence of the trajectories of (4.3) depends on the initial conditions. The region of attraction R_A for system (4.3) is the set of points $x \in \mathbb{R}^n$ such that, if the trajectories start with initial conditions $x(0) = x$, they asymptotically converge to the origin.

$$R_A = \{x \in \mathbb{R}^n :\ x(t,\ x(0)) \to 0 \text{ as } t \to 0\} \tag{4.7}$$

Since the region of attraction is difficult to evaluate and basically it might be identified only through many simulations, it is possible to consider its inner approximation, as the region of asymptotic stability (RAS). Then, if $(A + BK)$ is asymptotically stable and the trajectories of system (4.3) start within the region of asymptotic stability, they asymptotically converge to the origin.

Lyapunov functions may be employed to estimate the region of asymptotic stability towards the origin. Let $V(x)$ be a Lyapunov function, then the surface

$$L_s(V,\ c) = \{x \in \mathbb{R}^n :\ V(x) = c,\ c > 0\} \tag{4.8}$$

is called a Lyapunov surface or level surface. For different values of c the same Lyapunov function defines different level surfaces, as shown in Figure 4.3.

If $\dot{V}(x) \leq 0$, it means that, when a trajectory crosses a Lyapunov surface $V(x) = c$, it cannot come out again (i.e. the level surface is invariant). In this case, the origin is stable because the trajectories cannot go far away from it, they move inside a set defined by

$$S(V,\ c) = \{x \in \mathbb{R}^n :\ V(x) \leq c\}. \tag{4.9}$$

If $\dot{V}(x) < 0$, it means that the trajectories enter into inner surfaces with a smaller c and, as c decreases, surfaces shrink to the origin, so the trajectories converge to the origin as $t \to \infty$. If the origin is asymptotically stable, that is $\dot{V}(x) < 0$, any trajectory that starts inside $S(V,\ c)$ for sure converges to the origin (i.e. the level surface is invariant and contractive). Thus, $S(V,\ c)$ is an estimate of the region of asymptotic stability.

Actually, $S(V,\ c)$ is for sure contained inside a RAS, but this region may be far larger than $S(V,\ c)$, that is why this method to define the RAS is conservative.

Region of Asymptotic Stability through sector nonlinearity

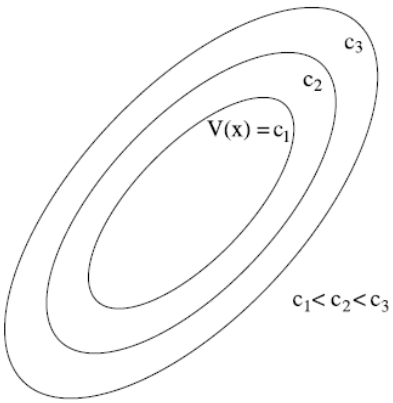

Figure 4.3: Lyapunov surfaces

Let us consider a generic linear system, where the feedback control input is affected by saturation

$$\dot{x}(t) = Ax(t) + B\,\mathrm{sat}(Kx(t)) \tag{4.10}$$

and define the dead-zone nonlinear vector function (4.11).

$$\phi(v(t)) = \mathrm{sat}(v(t)) - (v(t)). \tag{4.11}$$

Each row of $\phi(v(t))$ is represented in Figure 4.4, where $i = 1, ..., m$.
If it is possible to inscribe each element of $\phi(v(t))$ in a local sector, some local conditions can be stated, that may be useful to analyse the stability of system (4.10).
The local sector where the dead-zone nonlinearity is inscribed is shown in Figure 4.5 in dashed line, where $\lambda_{(i)} \leq 1$.

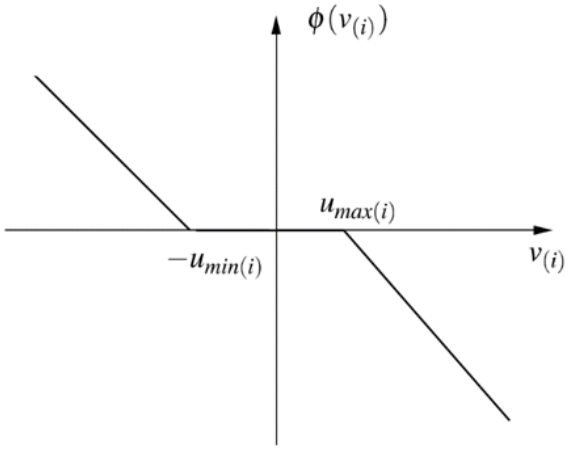

Figure 4.4: Dead-zone nonlinearity

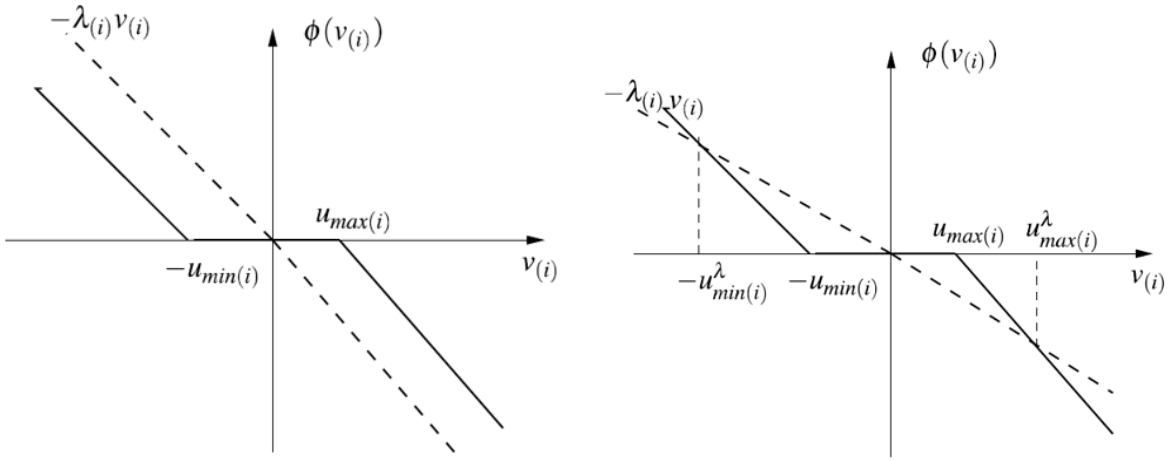

(a) (b)

Figure 4.5: Global sector (a) and local sector (b)

If the dead-zone nonlinearity belongs to the local sector $sec[0, -\lambda_{(i)}]$, it means:

$$-\lambda_{(i)}v_{(i)} \leq \phi(v_{(i)}) \leq 0, \quad \text{for} \quad 0 \leq v_{(i)} \leq \frac{u_{\max(i)}}{1-\lambda_{(i)}} = u^{\lambda}_{\max(i)}$$

$$0 \leq \phi(v_{(i)}) \leq -\lambda_{(i)}v_{(i)}, \quad \text{for} \quad -u^{\lambda}_{\min(i)} = \frac{-u_{\min(i)}}{1-\lambda_{(i)}} \leq v_{(i)} \leq 0$$

If $\lambda_{(i)} = 1$, the sector becomes global $sec[0, -1]$ and the dead-zone nonlinearity function $\phi(v)$ is entirely contained in this sector.
Thanks to the belonging of the nonlinearity to global or local sectors, in [23] the authors state the following results.

Lemma 4.1. *(Global sector condition)*
For any $v \in \mathbb{R}^m$, $\phi(v)$ satisfies the following inequality

$$\phi(v)^T T(\phi(v) + v) \leq 0 \tag{4.12}$$

for any diagonal positive definite matrix $T \in \mathbb{R}^{m\times m}$.

Lemma 4.2. *(Classical local sector condition)*
If $v \in S(v,\ u^{\lambda}_{\max},\ u^{\lambda}_{\min}) = \{v \in \mathbb{R}^m :\ -u^{\lambda}_{\min} \preccurlyeq v \preccurlyeq u^{\lambda}_{\max}\}$, $\phi(v)$ satisfies

$$\phi(v)^T T(\phi(v) + \Lambda v) \leq 0 \tag{4.13}$$

where $\Lambda \in \mathbb{R}^{m\times m}$ is a diagonal matrix, whose elements are $\lambda_{(i)}$ and $T \in \mathbb{R}^{m\times m}$ is any diagonal positive definite matrix.

This sector condition applies not only to the dead-zone function (4.11), but to any nonlinearity that belongs to the local sector shown in Figure 4.5. So, when it is used to prove the stability of system (4.10), it ensures the stability of any system whose nonlinearity

belongs to the same local sector.
In the particular case where $v(t) = Kx(t)$, Lemma 4.2 becomes:
if $x \in S(K,\ u^{\lambda}_{\max},\ u^{\lambda}_{\min}) = \{x \in \mathbb{R}^n :\ -u^{\lambda}_{\min} \preccurlyeq Kx \preccurlyeq u^{\lambda}_{\max}\}$, $\phi(v)$ satisfies the following inequality:

$$\phi(Kx)^T T(\phi(Kx) + \Lambda Kx) \leq 0 \tag{4.14}$$

Lemma 4.3. *(Generalized local sector condition)*
If $v, \omega \in S(v-\omega,\ u_{\max},\ u_{\min}) = \{v, \omega \in \mathbb{R}^m :\ -u_{\min} \preccurlyeq v - \omega \preccurlyeq u_{\max}\}$, *then* $\phi(v)$ *satisfies*

$$\phi(v)^T T(\phi(v) + \omega) \leq 0 \tag{4.15}$$

for any diagonal positive definite $T \in \mathbb{R}^{m\times m}$.

Sector condition (4.15) is a generalization of (4.13), but it applies specifically to the dead-zone nonlinearity function (4.11).
In the particular case where $v(t) = Kx(t)$, Lemma 4.3 becomes:
if $x \in S(K-G,\ u_{\max},\ u_{\min}) = \{x \in \mathbb{R}^n :\ -u_{\min} \preccurlyeq (K-G)x \preccurlyeq u_{\max}\}$, then $\phi(v)$ satisfies the following inequality

$$\phi(Kx)^T T(\phi(Kx) + Gx) \leq 0 \tag{4.16}$$

When G is such that $G = \Lambda K$, sector condition (4.16) is equal to the classical condition (4.13).

Asymptotic stability analysis through quadratic Lyapunov functions

As already said, global and local sector conditions may be useful to state theorems for the stability analysis of systems. In particular, if the dead-zone nonlinearity function (4.11) belongs to a global or local sector, it satisfies some sector condition that may be employed to state stability properties of system (4.10).
Let us rewrite system (4.10) as

$$\dot{x}(t) = (A + BK)x(t) + B\phi(Kx(t)), \tag{4.17}$$

where $\phi(Kx(t))$ is the dead-zone nonlinearity defined in (4.11).
In [23], an important result is stated on asymptotic stability of system (4.17), employing the generalized sector condition (4.16) and considering quadratic Lyapunov functions as

$$V(x) = x^T P x.$$

Proposition 4.1. *If there exist* $W \in \mathbb{R}^{n\times n}$ *symmetric and positive definite,* $S \in \mathbb{R}^{m\times m}$ *symmetric and positive definite and* $Z \in \mathbb{R}^{m\times n}$ *such that they satisfy LMIs (4.18) and (4.19) in* W, S *and* Z, *then the ellipsoid*

$$\mathcal{E}(P,1) = \{x \in \mathbb{R}^n :\ x^T P x \leq 1\},$$

where $P = W^{-1}$, *is a region of asymptotic stability for system (4.10).*

$$\begin{bmatrix} W(A+BK)^T + (A+BK)W & BS - Z^T \\ SB^T - Z & -2S \end{bmatrix} < 0 \tag{4.18}$$

$$\begin{bmatrix} W & WK_{(i)}^T - Z_{(i)}^T \\ K_{(i)}W - Z_{(i)} & u_{0(i)}^2 \end{bmatrix} \geq 0, \ i = 1, ..., m, \tag{4.19}$$

where $K_{(i)}^T$ *and* $Z_{(i)}^T$ *are the transpositions of the i-th rows of* K *and* Z *respectively.*

The satisfaction of condition (4.19) ensures that the ellipsoid $\mathcal{E}(P,1)$ is included in the polyhedral set

$$S(|K - G|, u_0) = \{x \in \mathbb{R}^n : \ -u_0 \preccurlyeq (K - G)x \preccurlyeq u_0\}.$$

By choosing $v = Kx$ and $\omega = Gx$ and applying Lemma 4.3, for any $x \in S(|K - G|, u_0)$ sector condition (4.16) becomes:

$$2\phi(Kx)^T T(\phi(Kx) + Gx) \leq 0. \tag{4.20}$$

If this condition is true, the following relation is satisfied:

$$\dot{V}(x) \leq \dot{V}(x) - 2\phi(Kx)^T T(\phi(Kx) + Gx) \tag{4.21}$$

The satisfaction of inequality (4.18) implies that $\dot{V}(x) - 2\phi(Kx)^T T(\phi(Kx) + Gx) < 0$, then it follows that $\dot{V}(x) < 0$. Thus, $x \in \mathcal{E}(P,1) \subseteq S(|K - G|, u_0)$, asymptotically converges to the origin.

A result similar to Proposition 4.1 can be derived employing local classical sector conditions. In this case, the constraints to satisfy are Bilinear Matrix Inequalities in the decision variables and their practical handling may be more difficult with respect to LMIs.

In Proposition 4.2 is stated the condition to satisfy in order for system (4.10) to be globally asymptotically stable.

Proposition 4.2. *If there exist* $W \in \mathbb{R}^{n \times n}$ *symmetric and positive definite and* $S \in \mathbb{R}^{m \times m}$ *diagonal positive definite such that they satisfy (4.22) then the origin is globally asymptotically stable for system (4.10).*

$$\begin{bmatrix} W(A + BK)^T + (A + BK)W & BS - WK^T \\ SB^T - KW & -2S \end{bmatrix} < 0 \tag{4.22}$$

If condition (4.22) is true, the region of attraction of system (4.10) is the whole state space.

4.2 Ellipsoidal estimate of the region of asymptotic stability

The Optimal Velocity model with saturation function may be considered as a linear system subject to saturated control law. Having substituted the hyperbolic tangent of the Bando model with a piecewise function, the resulting nonlinearity is exactly the saturation function depicted in Figure 4.2.

With the aim of applying the techniques described in [23], let us consider the Optimal Velocity model in error coordinates in order to study the region of asymptotic stability of the origin (i.e. uniform flow equilibrium) and let us consider its reduced version in order to guarantee the property of asymptotic stability within the region of linearity.
The model that will be analyzed is (4.23), whose state vector is (4.24).

$$\begin{cases} \dot{z}_i = y_i, \quad \forall\ i = 1, ..., N-1 \\ \dot{y}_i = b\left[V_{\max}\frac{\text{sat}(z_{i+1}+d-d_0)-\text{sat}(z_i+d-d_0)}{1+\tanh(d_0)} - y_i\right], \quad \forall\ i = 1, ..., N-2 \\ \dot{y}_{N-1} = b\left[V_{\max}\frac{\text{sat}\left(-\sum_{i=1}^{N-1} z_i+d-d_0\right)-\text{sat}(z_{N-1}+d-d_0)}{1+\tanh(d_0)} - y_{N-1}\right], \\ \dot{y}_N = b\left[V_{\max}\frac{\text{sat}(z_1+d-d_0)-\text{sat}\left(-\sum_{i=1}^{N-1} z_i+d-d_0\right)}{1+\tanh(d_0)} - y_N\right] \end{cases} \tag{4.23}$$

$$\mathbf{x} = [z_1, z_2, ..., z_{N-1}, y_1, y_2, ..., y_N]^T \in \mathbb{R}^{2N-1} \tag{4.24}$$

System (4.23) cannot be written as (4.26), unless we choose to put $d = d_0$. This choice leads to consider a particular situation, where the ring road has a specific length such that when the vehicles are equally spaced, their inter-vehicle distance equals the safety distance. Nevertheless, the presence of $d - d_0$ would introduce a bias in the definition of the saturation function and no change of variables is able to cancel it. For this reason, let us consider $d = d_0$ and system (4.25), which can be written as (4.26).

$$\begin{cases} \dot{z}_i = y_i, \quad \forall\ i = 1, ..., N-1 \\ \dot{y}_i = \frac{bV_{\max}}{1+\tanh(d_0)}\,\text{sat}\,(z_{i+1}) - \frac{bV_{\max}}{1+\tanh(d_0)}\,\text{sat}\,(z_i) - by_i, \quad \forall\ i = 1, ..., N-2 \\ \dot{y}_{N-1} = \frac{bV_{\max}}{1+\tanh(d_0)}\,\text{sat}\left(-\sum_{i=1}^{N-1} z_i\right) - \frac{bV_{\max}}{1+\tanh(d_0)}\,\text{sat}\,(z_{N-1}) - by_{N-1}, \\ \dot{y}_N = \frac{bV_{\max}}{1+\tanh(d_0)}\,\text{sat}\,(z_1) - \frac{bV_{\max}}{1+\tanh(d_0)}\,\text{sat}\left(-\sum_{i=1}^{N-1} z_i\right) - by_N \end{cases} \tag{4.25}$$

$$\dot{\mathbf{x}}(t) = A\mathbf{x}(t) + B\,\text{sat}(K\mathbf{x}(t)), \tag{4.26}$$

where

$$A = \begin{bmatrix} 0 & A_{zy} \\ 0 & -bI_N \end{bmatrix},$$

with I_N the identity matrix $\in \mathbb{R}^{N\times N}$ and

$$A_{zy} = \begin{bmatrix} 1 & & & (0) & 0 \\ & 1 & & & \vdots \\ & & \ddots & & \vdots \\ (0) & & & 1 & 0 \end{bmatrix} \in \mathbb{R}^{N-1\times N},$$

$$B = \begin{bmatrix} 0_{N-1 \times N} \\ B_{yz} \end{bmatrix} \in \mathbb{R}^{2N-1 \times N},$$

where

$$B_{yz} = \frac{bV_{\max}}{1 + \tanh(d_0)} \begin{bmatrix} -1 & 1 & & & (0) \\ & -1 & 1 & & \\ & & \ddots & \ddots & \\ (0) & & & -1 & 1 \\ 1 & 0 & \dots & 0 & -1 \end{bmatrix} \in \mathbb{R}^{N \times N}$$

and

$$K = \begin{bmatrix} K_{yz} & 0_{N \times N} \end{bmatrix} \in \mathbb{R}^{N \times 2N-1},$$

where

$$K_{yz} = \begin{bmatrix} 1 & & & (0) \\ & 1 & & \\ & & \ddots & \\ (0) & & & 1 \\ -1 & \dots & \dots & -1 \end{bmatrix} \in \mathbb{R}^{N \times N-1}.$$

Thanks to the choice of the Reduced Optimal Velocity model, if the parameters satisfy condition (3.36), $A + BK$ is asymptotically stable, thus system (4.25) is asymptotically stable in its region of linearity. This fact allows to compute an underestimate of its region of asymptotic stability, so that all the trajectories of (4.25) that start within this set asymptotically converge to the origin (i.e. uniform flow equilibrium).

Having substituted the hyperbolic tangent with the saturation function, depicted in Figure 2.10, each row of our $\text{sat}(K\mathbf{x}(t))$ vector in (4.26) is the same saturation function shown in Figure 4.2, where the values defining the piecewise function are

$$u_{\max(i)} = u_{\min(i)} = 1.$$

Moreover, $\text{sat}(K\mathbf{x}(t))$ is a vector function $\in \mathbb{R}^N$.
Our model may be equivalently rewritten as

$$\dot{\mathbf{x}}(t) = (A + BK)\mathbf{x}(t) + B\phi(K\mathbf{x}(t)), \tag{4.27}$$

where each row of $\phi(K\mathbf{x}(t)) \in \mathbb{R}^N$ is the dead-zone nonlinearity depicted in Figure 4.4.
Our objective is to exploit the results described in [23] and summarized in Section 4.1 in order to characterize the region of asymptotic stability of our model (4.25).

Global stability
In order to see if the region of attraction of (4.25) is the whole state space and so it is globally asymptotically stable, it is sufficient to look for any matrix W and S satisfying the LMI (4.22). Thus, the problem is defined, but there exists no feasible solution to LMI (4.22), leading to the conclusion that the origin (i.e. uniform flow equilibrium) is not globally asymptotically stable.
For this reason, we look for an estimate of the region of asymptotic stability of system

(4.25).

Local stability
Proposition 4.1 in Section 4.1 allows to compute an invariant and contractive ellipsoid which underestimates the region of asymptotic stability, so that, if the trajectories of system (4.25) start within that ellipsoid, for sure they converge to the origin.
The procedure consists in finding a feasible solution for LMIs (4.18) and (4.19) in $W = P^{-1}$, S and Z. Condition (4.18) ensures that the derivative of the Lyapunov function of system (4.25) is negative if $\mathbf{x} \in S(|K-G|, u_0)$, and (4.19) ensures that ellipsoid $\mathcal{E}(P,1)$ is included in $S(|K-G|, u_0)$ where the dead-zone nonlinearity satisfies a local sector condition.
LMIs (4.18) and (4.19) are provided to a suitable solver, where $m = N$, $n = 2N-1$ and $u_{0(i)} = u_{\max(i)} = 1$.
Since the ellipsoids are an underestimate of the region of asymptotic stability, in order to find the best estimate, the objective is to maximize the volume of $\mathcal{E}(P,1) \in \mathbb{R}^{2N-1}$. With this aim, the maximization of the volume is performed by maximizing $\log(\det(P^{-1}))$. Then the optimization problem is defined as

$$\begin{aligned} &\text{maximize} && \log(\det(W)) \\ &\text{subject to} && \text{inequalities (4.18), (4.19)} \end{aligned} \tag{4.28}$$

Example 4.1. *Let us consider a group of $N = 5$ vehicles, with $b = 10\ s^{-1}$, $V_{\max} = 10\ m/s$ and $d_0 = 10\ m$. Since $d = d_0$, the length of the ring road is fixed to $L = 50\ m$.*
With these parameters the stability constraint (3.36) is satisfied, then the eigenvalues of $A+BK$ have negative real part and the origin is an asymptotically stable equilibrium point for model (4.25). The state vector is

$$\boldsymbol{x} = [z_1, z_2, ..., z_4, y_1, y_2, ..., y_5]^T \in \mathbb{R}^9.$$

We compute the maximum-volume ellipsoid $\mathcal{E}(P,1) \in \mathbb{R}^9$ by solving problem (4.28). To have an idea of the size of the ellipsoid, in Figure 4.6 and Figure 4.7 are shown the sections of $\mathcal{E}(P,1)$ onto (z_1, z_2) and (y_1, y_2) respectively. By choosing any (z_i, z_j), $\forall\ i \neq j$, the sections of $\mathcal{E}(P,1)$ are equal to the ellipse in Figure 4.6 and the sections of $\mathcal{E}(P,1)$ onto (y_i, y_j), $\forall\ i \neq j$, are equal to the ellipse in Figure 4.7.
Thus, starting with any initial condition $\boldsymbol{x}(0) \in \mathcal{E}(P,1)$, the trajectories of system (4.25) will converge to the origin (i.e. uniform flow equilibrium).

4.3 Dependence of the RAS on the model parameters

In Section 3.2 we saw that the parameters of model (3.24) affect the stability of the uniform flow equilibrium point when the model works in the linearity region. If the state $\mathbf{x}(t)$ and $d - d_0$ are such that the model works in the linearity region and b and $V_{\max}$ satisfy the constraint (3.36), then the uniform flow is the only equilibrium point and it is asymptotically stable. For a given number of vehicles and a fixed d_0, the stability constraint is satisfied for high values of b and low values of $V_{\max}$. In this section we study the dependence of the volume of the estimate of the region of asymptotic stability for model (3.24) on these parameters and find out if the increase of b and the reduction of $V_{\max}$ improve not only

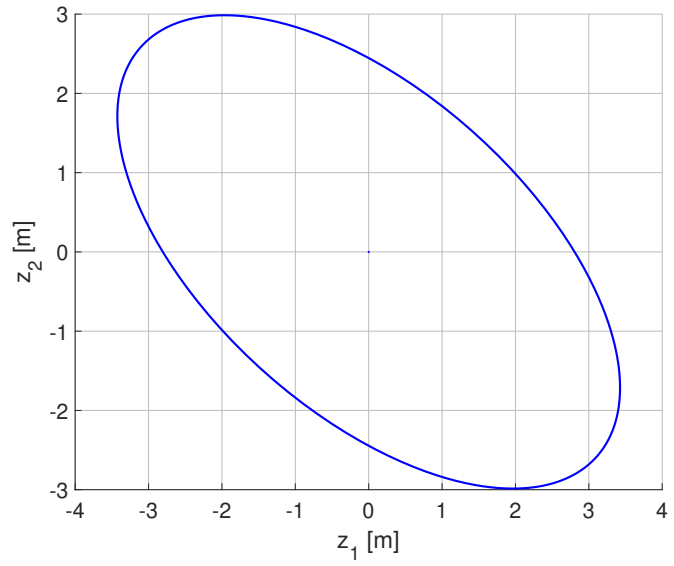

Figure 4.6: Section of $\mathcal{E}(P,1)$ onto (z_1, z_2)

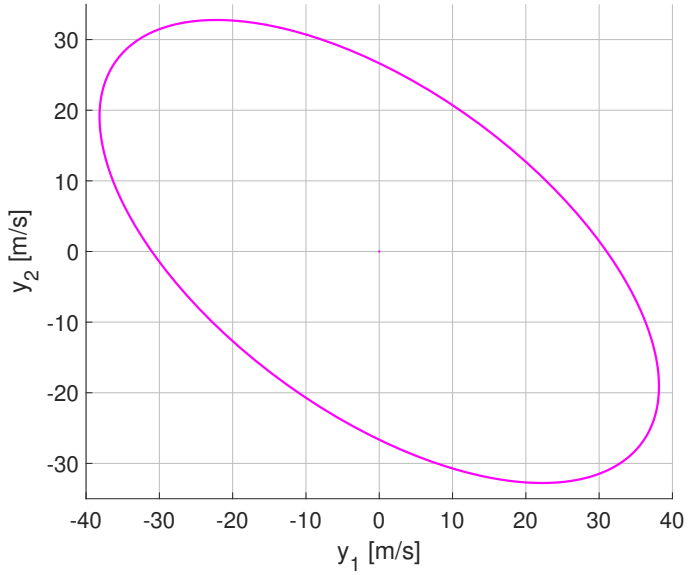

Figure 4.7: Section of $\mathcal{E}(P,1)$ onto (y_1, y_2)

the satisfaction of the stability constraint in the linear framework but also lead to an improvement of the ellipsoidal estimates in the nonlinear framework.
In order to study the dependence of the volume of the ellipsoidal estimates on the parameters, we consider the nonlinear model (4.25) and solve the optimization problem (4.28) for different couples of values b and $V_{\max}$. We focus on the model in which $d = d_0$ because it

can be written as (4.26). Moreover, we saw in Section 3.2 that if $d = d_0$ the trajectories of (4.25) converge to the linearity region for any initial condition and the stability constraint (3.36) holds exactly in the linearity region.
For a group of $N = 5$ vehicles we fix $d_0 = 10\ m$ and consider a ring road of length $L = 50\ m$, so that $d = \frac{L}{N}$ is equal to d_0. Let us fix $V_{\max} = 10\ m/s$, compute the ellipsoidal estimate $\mathcal{E}(P,1)$ for different values of b and project it on subspaces generated by bases of the state variables. In Table 4.1 are shown the ranges of the state variables belonging to $\mathcal{E}(P,1)$. Increasing b leads to ellipsoidal estimates of the RAS with larger volume. The ellipsoids

Table 4.1: Dependence of the ellipsoidal estimate of the RAS on b. Increasing b, the size of $\mathcal{E}(P,1)$ increases. $V_{\max} = 10\ m/s$, $d = d_0$ and $N = 5$.

$b\ [s^{-1}]$	Ranges of z_i and $y_i \in \mathcal{E}(P,1)$
$b = 10$	$-6.98\ m \leq z_i \leq 6.98\ m$ $-77\ m/s \leq y_i \leq 77\ m/s$
$b = 20$	$-10.85\ m \leq z_i \leq 10.85\ m$ $-169\ m/s \leq y_i \leq 169\ m/s$
$b = 30$	$-14.2\ m \leq z_i \leq 14.2\ m$ $-289\ m/s \leq y_i \leq 289\ m/s$

are inner-approximations, so we can't state if an increase of b makes the volume of the RAS of system (4.25) increase, but we get a larger set of initial conditions from which we are sure the trajectories of the model converge to the uniform equilibrium. Finally, we perform the same analysis fixing $b = 10\ s^{-1}$ and determine the ellipsoidal estimates of the RAS for different values of $V_{\max}$. For each value we project $\mathcal{E}(P,1)$ onto subspaces of the state variables and in Table 4.2 are shown the ranges of the state variables belonging to the ellipsoids. By increasing $V_{\max}$, the volume of the ellipsoidal estimates of the RAS

Table 4.2: Dependence of the ellipsoidal estimate of the RAS on $V_{\max}$. Increasing $V_{\max}$, the size of $\mathcal{E}(P,1)$ decreases. $b = 10\ s^{-1}$, $d = d_0$ and $N = 5$.

$V_{\max}\ [\frac{m}{s}]$	Ranges of z_i and $y_i \in \mathcal{E}(P,1)$
$V_{\max} = 5$	$-14.2\ m \leq z_i \leq 14.2\ m$ $-144\ m/s \leq y_i \leq 144\ m/s$
$V_{\max} = 10$	$-6.98\ m \leq z_i \leq 6.98\ m$ $-77\ m/s \leq y_i \leq 77\ m/s$
$V_{\max} = 15$	$-3.74\ m \leq z_i \leq 3.74\ m$ $-47\ m/s \leq y_i \leq 47\ m/s$

decreases. Again, we can't be sure that the volume of the RAS of system (4.25) reduces as $V_{\max}$ increases, but an increase of $V_{\max}$ leads to a smaller set of initial conditions for which we are sure the trajectories of the model converge to the unifrom flow equilibrium.
In conclusion, even if we cannot determine the actual region of asymptotic stability for the model (4.25), we can state that high values of b and low values of $V_{\max}$ improve the satisfaction of the stability constraint (3.36) of the linear system around the uniform flow equilibrium and enlarge the ellipsoidal estimates of the RAS of the nonlinear model.

Therefore, they lead to the determination of wider sets of initial conditions for which the trajectories of the nonlinear model are ensured to converge to the uniform flow equilibrium.

In the Optimal Velocity model with saturation function

$$\begin{cases} \dot{x}_i = v_i, \quad \forall\ i = 1, ..., N \\ \\ \dot{v}_i = b\left[V_{\max}\frac{\text{sat}(x_{i+1}-x_i-d_0)\ +\ \tanh(d_0)}{1\ +\ \tanh(d_0)} - v_i\right], \quad \forall\ i = 1, ..., N \end{cases} \tag{4.29}$$

b is a weight which represents the sensitivity of the driver. If the velocity v_i of one vehicle is too low with respect to the optimal velocity computed on the basis of the headway, then this vehicle should accelerate in order to reduce the gap in front of it. With constant $V_{opt}(x_{i+1} - x_i) > 0$, a higher b leads to a higher acceleration, then it means that the driver reacts faster. The same is true when the headway is too short, the optimal velocity should be lower than the current velocity of the vehicle and it must brake. The deceleration may be faster or slower on the basis of weight b. Therefore, b represents the time reaction of the driver when he needs to update its velocity on the basis of the headway in front of it. A platoon with a high b coefficient is more reactive, while a low value of b means that the drivers react slowly. It's reasonable to think that a reactive platoon is able to keep the uniform flow equilibrium more easily with respect to a less sensitive group of vehicles. Therefore, it is reasonable that if b is larger the stability of the uniform flow equilibrium is better. Moreover, this evidence is shown both in the linear framework and in the estimate of the RAS of the nonlinear model.
$V_{\max}$ is the maximum value of the velocity function, therefore it is the maximum absolute velocity the vehicles can reach. In order to understand this dependence on $V_{\max}$, let us simulate a platoon of $N = 5$ vehicles travelling on a ring road of length $L = 50\ m$, such that $d_0 = 10\ m$ equals d. Let us choose $b = 10\ s^{-1}$ and simulate model (4.29) starting with the same initial conditions and with two different values of $V_{\max}$.

1. $V_{\max} = 5\ m/s$
   As shown in Figure 4.8, the trajectory of only one vehicle (2^{nd}) starts in the linearity region (bounded by the red lines) and the other four vehicles start in one of the two saturation regions. Anyway, since $-1\ m \leq d - d_0 \leq 1\ m$, all the trajectories reach the linearity region and converge to the uniform flow equilibrium because the parameters satisfy the stability condition (3.36).

2. $V_{\max} = 15\ m/s$
   In Figure 4.9 are shown the relative distances of the model with the same initial conditions and a higher value of $V_{\max}$. At the beginning of the simulation, the vehicles close long distances and increase short distances in less time with respect to the previous case. This is because, with the same inter-vehicle distance and with the same actual velocity, a higher value of $V_{\max}$ leads to a higher time derivative of the velocity. Therefore, with a higher $V_{\max}$, when the inter-vehicle distance is too long, the acceleration is larger, and, when the inter-vehicle distance is too short, the deceleration is stronger. Even if the closing of long distances and the opening of short distances is faster, a higher value of $V_{\max}$ makes more difficult to adjust the velocity of one vehicle when it approaches its preceding one. With the same headway, the

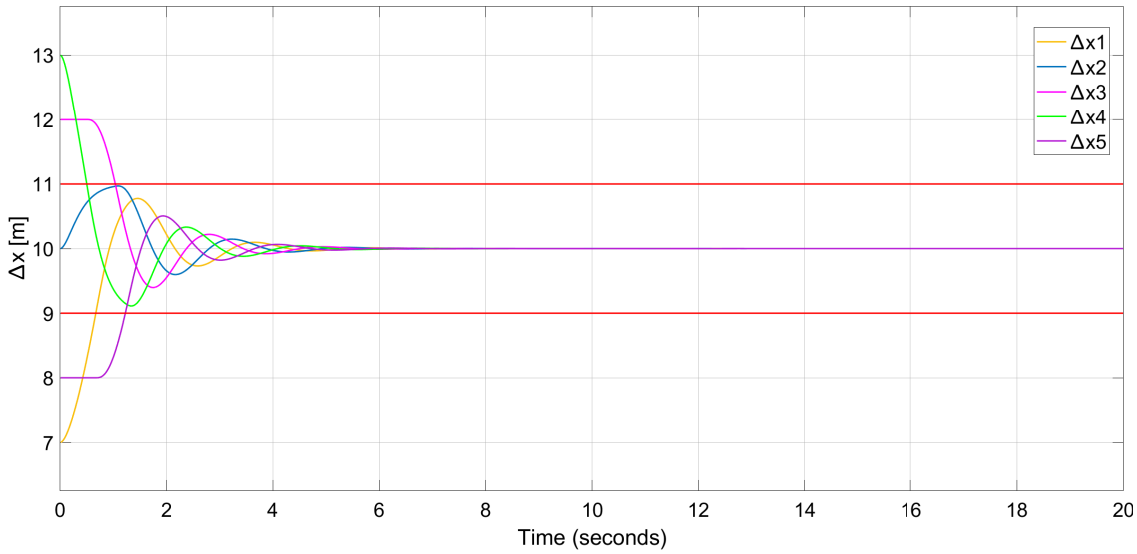

Figure 4.8: Relative distances of the group of 5 vehicles when $V_{\max} = 5\ m/s$

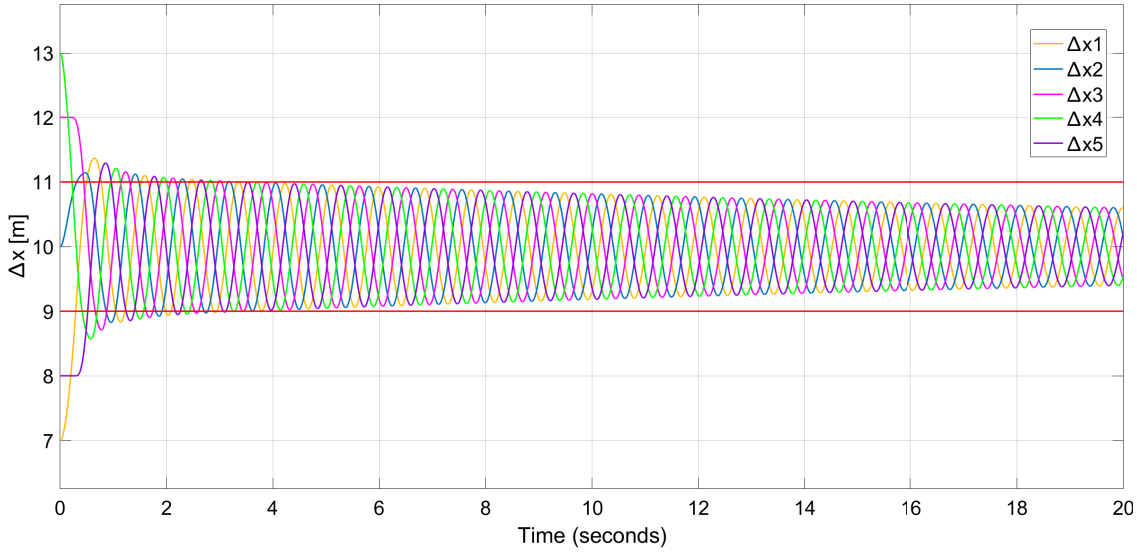

Figure 4.9: Relative distances of the group of 5 vehicles when $V_{\max} = 15\ m/s$

magnitude of the optimal velocity function is larger, so brakings and accelerations are stronger and less gentle than before and this causes periodic oscillations of the velocity. Anyway, since also in this scenario the parameters satisfy condition (3.36), the trajectories reach the uniform flow equilibrium in more time than before, as shown in Figure 4.10.

As shown in Figures 4.8-4.9, at least when $d = d_0$, a lower value of $V_{\max}$ improves the stability of the model. In the linear framework it helps the satisfaction of the stability condition (3.36) and leads to eigenvalues of the linear system with more negative real part.

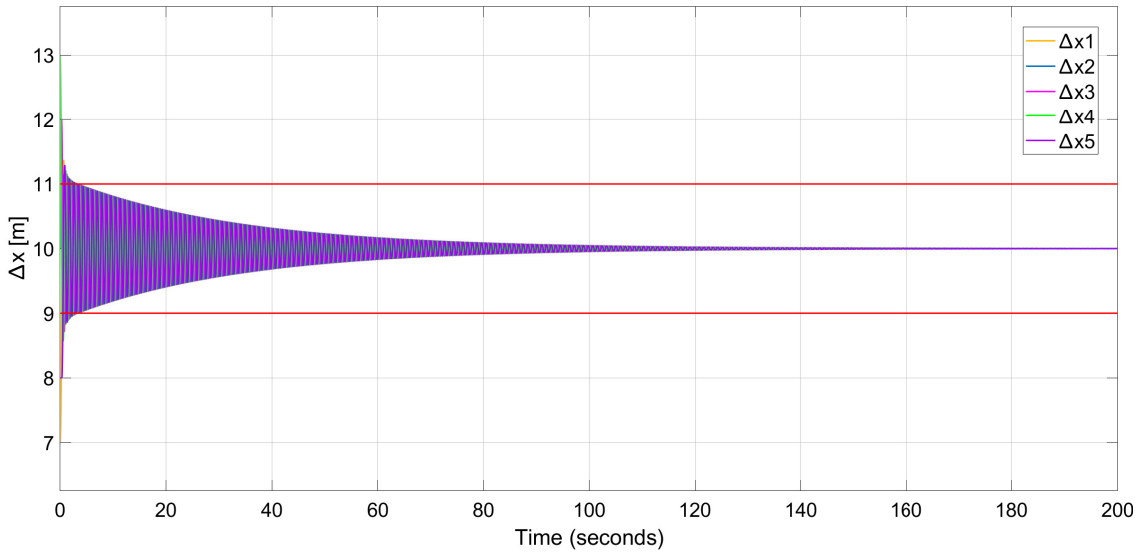

Figure 4.10: Relative distances of the group of 5 vehicles when $V_{\max} = 15\ m/s$

In the nonlinear framework, by decreasing $V_{\max}$, the ellipsoidal estimates of the RAS of the model (4.25) has a larger volume, so we get a wider set of initial conditions from which the trajectories are ensured to converge to uniform flow equilibrium.

4.4 Safe region of asymptotic stability

If it is possible to compute an invariant and contractive set within a 'safety area' for system (4.25), not only its trajectories starting in this set asymptotically converge to the origin (i.e. the uniform flow equilibrium), but the inter-vehicles distances Δx_i of the cars are lower bounded during the whole travel.
The objective is to find the maximum-volume region of asymptotic stability for the system (4.25) lying within a polytope that forces a bound on the spacing errors z_i. In this way, bounding z_i to a minimum value prevents the collision between two adjacent vehicles.

In general, as explained in [23], if one wants to inscribe the ellipsoid $\mathcal{E}(P,1) = \{x \in \mathbb{R}^n : \ x^T P x \leq 1\}$, in a symmetric polytope as

$$S(|Q|, \rho) = \{x \in \mathbb{R}^n : \ |Qx| \preccurlyeq \rho\} = \{x \in \mathbb{R}^n : \ |Q_{(i)}x| \leq \rho, \ \forall i\}, \tag{4.30}$$

the following inequality must be satisfied for each element of vector ρ:

$$Q_{(i)} P^{-1} Q_{(i)}^T \leq \rho_{(i)}^2, \ \forall i, \tag{4.31}$$

where $Q_{(i)}^T$ is the transpose of the i-th row of Q.
LMIs (4.31) are included in the set of constraints of the optimization problem (4.28), in order to find the maximum-volume ellipsoid included in a safety symmetric polytope (4.30) that ensures asymptotic convergence to the origin.

For example, one can impose a bound on the minimum and the maximum inter-vehicle distance Δx_i:

$$d_{\min} \leq \Delta x_i \leq d_{\max}, \tag{4.32}$$

where $d_{\min}$ is the safety distance and $d_{\max}$ is the maximum allowed inter-vehicle distance. Condition (4.32) is equivalent to the following constraints on the spacing errors:

$$d_{\min} - d \leq z_i \leq d_{\max} - d, \tag{4.33}$$

where d is the desired distance between two consecutive vehicles.
Suppose L and N are such that $d = 10\ m$, $d_{\min} = 8\ m$ and $d_{\max} = 12\ m$, then the safety range for z_i is symmetric:

$$-2\ m \leq z_i \leq 2\ m. \tag{4.34}$$

The matrix inequalities (4.31) are added to the optimization problem, where Q is defined as follows. Since the polytope is such that

$$\begin{cases} Q_{(i)}x \leq \rho_{(i)} \\ Q_{(i)}x \geq -\rho_{(i)} \end{cases}$$

and the safety ranges are defined in (4.33), where $d_{\min} - d = -(d_{\max} - d)$, then

$$Q = \begin{bmatrix} I_{N-1} & 0_{N\times N} \end{bmatrix} \in \mathbb{R}^{N-1\times 2N-1},$$

where I_{N-1} is the identity matrix $\in \mathbb{R}^{N-1\times N-1}$ and

$$\rho = \begin{bmatrix} d_{\max} - d \\ d_{\max} - d \\ \vdots \\ d_{\max} - d \end{bmatrix} \in \mathbb{R}^{N-1}.$$

The resulting optimization problem is then

$$\begin{aligned} &\text{maximize} && \log(\det(W)) \\ &\text{subject to} && \text{inequalities (4.18), (4.19), (4.31).} \end{aligned} \tag{4.35}$$

Example 4.2. *Let us solve (4.35) for a group of $N = 5$ vehicles with the same parameters as Example 4.1, $b = 10\ s^{-1}$, $V_{\max} = 10\ m/s$, $d_0 = 10\ m$ and $L = 50\ m$, and choose $d_{\min} = 8\ m$ and $d_{\max} = 12\ m$. In this way, the relative distances are bounded by*

$$8\ m \leq \Delta x_i \leq 12\ m. \tag{4.36}$$

Looking at the sections of the ellipsoid on subspaces generated by the z_i variables, the constraints (4.34) are satisfied, as shown in Figure 4.11. Being $\mathcal{E}(P,1)$ an invariant and contractive set, if the trajectories of system (4.25) are initialized inside it, they remain within this set and converge to the origin.
Therefore, the vehicles whose behaviour is modelled by (4.25) do not collide, as their minimum inter-vehicle distance is lower and upper bounded.
In Figure 4.12 are shown the relative distances of a group of 5 vehicles with $b = 10\ s^{-1}$, $V_{\max} = 10\ m/s$ and $d = d_0 = 10\ m$. The initial conditions in error coordinates belong to $\mathcal{E}(P,1)$ and the relative distances lie in the safety range defined in (4.36).

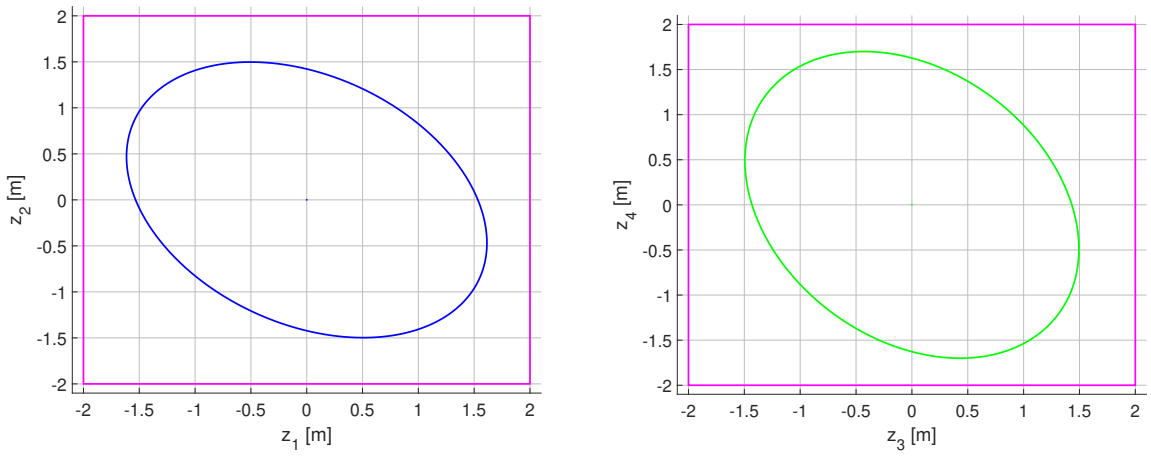

(a) (z_1, z_2) *subspace* (b) (z_3, z_4) *subspace*

Figure 4.11: Sections of the safe $\mathcal{E}(P,1)$ and $S(|Q|, \rho)$ onto (z_i, z_j)

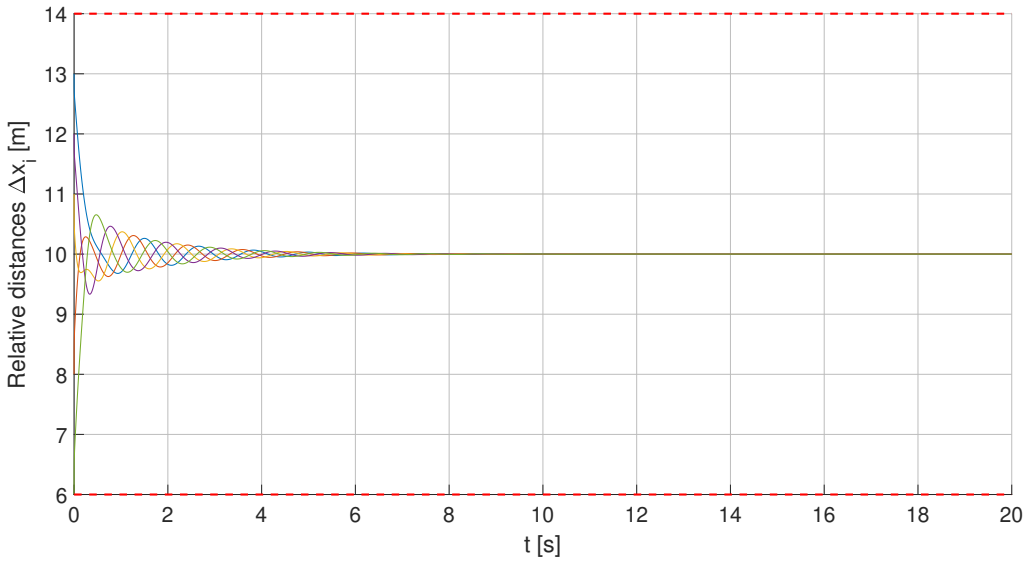

Figure 4.12: Evolution of the vehicle distances with respect to time. Starting the trajectories within $\mathcal{E}(P,1)$ included in the safety polytope, the distances are lower and upper bounded

Chapter 5

Stability and safety analysis of the Bando Optimal Velocity model

5.1 LTI systems with Neural Network Controller

In article [24], a method to compute an underestimate of the region of attraction is carried out for discrete time systems with Neural Network Controllers. In this section, the same analysis is developed for continuous time systems.

Let us consider the continuous time LTI plant

$$\dot{x}(t) = Ax(t) + Bu(t), \tag{5.1}$$

where $x \in \mathbb{R}^n$ is the state and $u \in \mathbb{R}^m$ is the input.
In general, the controller π is an ℓ - layer Neural Network defined by

$$\omega^0(t) = x(t) \tag{5.2a}$$

$$\omega^i(t) = \phi^i(W^i\omega^{i-1}(t) + b^i),\ i = 1, ..., \ell \tag{5.2b}$$

$$u(t) = W^{\ell+1}\omega^\ell(t) + b^{\ell+1}, \tag{5.2c}$$

where $\omega^i \in \mathbb{R}^{n_i}$ are the activation outputs of each i-th layer. Each activation ω^i depends on a weight matrix $W^i \in \mathbb{R}^{n_i \times n_{i-1}}$, a bias vector $b^i \in \mathbb{R}^{n_i}$ and an activation function vector

$$\phi^i(v) = [\varphi(v_1), ..., \varphi(v_{n_i})]^T \in \mathbb{R}^{n_i},$$

where each element $\varphi(\nu)$ is a particular scalar function. For instance, $\varphi(\nu) = \tanh(\nu)$.
By defining the input vector to the activation function ω^i as

$$v^i(t) = W^i\omega^{i-1}(t) + b^i, \quad i = 1, ..., \ell,$$

the output of each layer is

$$\omega^i(t) = \phi^i(v^i(t)).$$

Thus, each layer, $i = 1, ..., \ell$, has its own set of n_i activation functions, $\phi^i(v)$, its own input vector $v^i \in \mathbb{R}^{n_i}$ and its own output vector $\omega^i \in \mathbb{R}^{n_i}$. Let us put together all the inputs and outputs of all the layers:

$$v_\phi = [v^1, ..., v^\ell]^T \in \mathbb{R}^{n_\phi},$$
$$\omega_\phi = [\omega^1, ..., \omega^\ell]^T \in \mathbb{R}^{n_\phi},$$

where $n_\phi = n_1 + n_2 + ... + n_\ell$, and collect all activation functions together:

$$\phi(v_\phi) = [\phi^1(v^1), ..., \phi^\ell(v^\ell)]^T \in \mathbb{R}^{n_\phi}.$$

Thus $\omega_\phi(t) = \phi(v_\phi(t))$. The controller defined in (5.2) can be rewritten as (5.3), where linear and nonlinear parts are split up.

$$\begin{bmatrix} u(t) \\ v_\phi(t) \end{bmatrix} = N \begin{bmatrix} x(t) \\ \omega_\phi(t) \\ 1 \end{bmatrix} \tag{5.3a}$$

$$\omega_\phi(t) = \phi(v_\phi(t)), \tag{5.3b}$$

where

$$N = \begin{bmatrix} N_{ux} & N_{u\omega} & N_{ub} \\ N_{vx} & N_{v\omega} & N_{vb} \end{bmatrix}$$

A local sector condition on the activation function $\phi(v)$ may be used to carry out a stability analysis for system (5.1)-(5.2).
Let us consider a generic equilibrium point

$$x^* = Ax^* + Bu^*$$

$$u^* = \pi(x^*).$$

(x^*, u^*) must satisfy equation (5.3), then

$$\begin{bmatrix} u_* \\ v_* \end{bmatrix} = N \begin{bmatrix} x_* \\ \omega_* \\ 1 \end{bmatrix}, \tag{5.4a}$$

$$\omega_* = \phi(v_*). \tag{5.4b}$$

Therefore, the equilibrium point is $(x_*, u_*, v_*, \omega_*)$.

Consider $\varphi(\nu) = \tanh(\nu)$, shown in blue solid line in Figure 5.1. In $\underline{\nu} \leq \nu \leq \bar{\nu}$, $\tanh(\nu)$ lies within the two green dashed lines, defining the local sector $[\alpha, \beta]$, where $\alpha \leq \beta$. In sector $[\alpha, \beta]$, $\varphi(\nu)$ satisfies the following inequality.

$$(\varphi(\nu) - \alpha\nu)(\beta\nu - \varphi(\nu)) \geq 0, \tag{5.5}$$

where $\underline{\nu} = -\bar{\nu}$, $\beta = 1$ and $\alpha = \frac{\tanh(\bar{\nu})}{\bar{\nu}}$.

The local sector constraint (5.5) is centered in $(\nu, \varphi(\nu)) = (0,0)$ and it is useful to evaluate stability of (x_*, u_*) such that $(\nu_*, \varphi(\nu_*)) = (0,0)$.

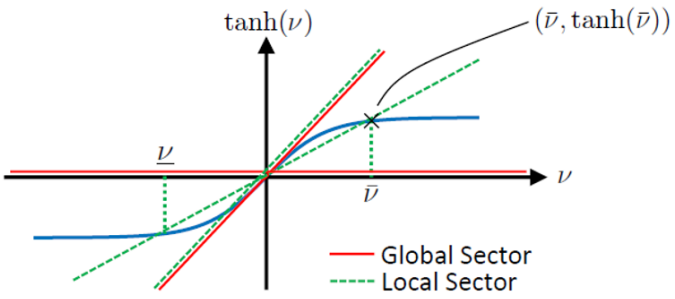

Figure 5.1: Local sector on tanh

According to the choice of the equilibrium point where we want to evaluate stability, it is required to define offset local conditions for any generic $(\nu_*, \varphi(\nu_*))$.

Let us consider $\varphi(\nu) = \tanh(\nu)$, shown in blue solid line in Figure 5.2. In $\underline{\nu} \leq \nu \leq \bar{\nu}$), $\tanh(\nu)$ lies within the offset local sector $[\alpha, \beta]$ around v_*, where $\alpha \leq \beta$ and $\underline{\nu} = -\bar{\nu}$, if it satisfies the inequality (5.5).

$$(\Delta\varphi(\nu) - \alpha\Delta\nu)(\beta\Delta\nu - \Delta\varphi(\nu)) \geq 0, \tag{5.6}$$

where $\Delta\varphi(\nu) = \varphi(\nu) - \varphi(\nu_*)$ and $\Delta\nu = \nu - \nu_*$.
For example $\beta = 1$ and $\alpha = \min\left\{\frac{\tanh(\bar{\nu})-\tanh(\nu_*)}{\bar{\nu}-\nu_*}, \frac{\tanh(\nu_*)-\tanh(\underline{\nu})}{\nu_*-\underline{\nu}}\right\}$.

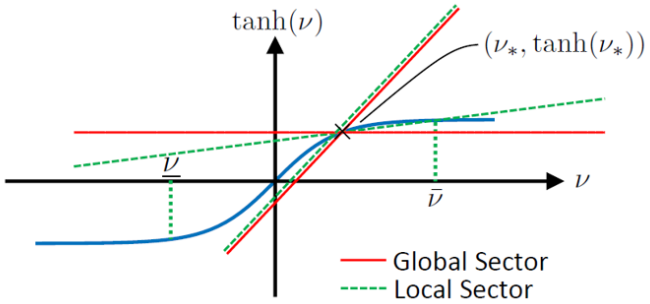

Figure 5.2: Offset local sector on tanh

Let us assume that, for $v_i \in [\underline{v_i}, \bar{v_i}]$, each activation function $\varphi(v_i)$ lies locally in the sector $[\alpha_i, \beta_i]$, for $i = 1, ..., n_\phi$. Then the local sectors can be put together in vectors α_ϕ and β_ϕ. In [24] the authors state the following lemma.

Lemma 5.1. *Given $\bar{v}$, $\underline{v}$, v_*, α_ϕ, β_ϕ, where $\alpha_\phi \preccurlyeq \beta_\phi$, $\underline{v} \preccurlyeq v_* \preccurlyeq \bar{v}$ and $\omega_* = \phi(v_*)$. Let us assume $v_\phi \in [\underline{v}, \bar{v}]$ and ϕ lies in the local sector $[\alpha_\phi, \beta_\phi]$ around v_* element-wise for any v_ϕ. Then*

$$\begin{bmatrix} v_\phi - v_* \\ \omega_\phi - \omega_* \end{bmatrix}^T \Psi_\phi^T M_\phi(\lambda) \Psi_\phi \begin{bmatrix} v_\phi - v_* \\ \omega_\phi - \omega_* \end{bmatrix} \geq 0 \tag{5.7}$$

$\forall\ v_\phi \in [\underline{v}, \bar{v}]$ *and* $\omega_\phi = \phi(v_\phi)$, *where* $\lambda \in \mathbb{R}^{n_\phi}$ *and* $\lambda(i) \geq 0$,

$$\Psi_\phi = \begin{bmatrix} \operatorname{diag}(\beta_\phi) & -I_{n_\phi} \\ -\operatorname{diag}(\alpha_\phi) & I_{n_\phi} \end{bmatrix},$$

$$M_\phi(\lambda) = \begin{bmatrix} 0_{n_\phi} & \operatorname{diag}(\lambda) \\ \operatorname{diag}(\lambda) & 0_{n_\phi} \end{bmatrix},$$

where I_{n_ϕ} *and* 0_{n_ϕ} *are the identity matrix and the zero matrix* $\in \mathbb{R}^{n_\phi \times n_\phi}$.

The satisfaction of the local sector condition (5.5) or the more general offset local sector condition (5.6) applies in the computation of an inner approximation of the region of attraction for system (5.1)-(5.2).
In [24] the authors state a theorem that allows to estimate the region of attraction for a discrete system. In a similar way, we state the same theorem for a continuous control system.

Theorem 5.1. *Let us consider a system with plant (5.1) and Neural Network Controller (5.2) with equilibrium point* $(x_*, u_*, v_*, \omega_*)$. *Assume* $\alpha_\phi, \beta_\phi \in \mathbb{R}^{n_\phi}$ *are such that* ϕ *satisfies the offset local sector condition (5.6) around* $(v_*, \phi(v_*))$. *Let* $v^1 \in [\underline{v}^1, \bar{v}^1]$, $v^1 \in \mathbb{R}^{n_1}$, *be the first element of vector* v_ϕ *and* $\underline{v}^1 = 2v^1_* - \bar{v}^1$, *where* $v^1_* \in [\underline{v}^1, \bar{v}^1]$ *is the first element of the equilibrium value* v_*.
Let us define the following matrices

$$R_V = \begin{bmatrix} I_n & 0_{n \times n_\phi} \\ N_{ux} & N_{u\omega} \end{bmatrix},\ R_\phi = \begin{bmatrix} N_{vx} & N_{v\omega} \\ 0_{n_\phi \times n} & I_{n\phi} \end{bmatrix},$$

where n *is the dimension of the state vector. If there exist a symmetric positive definite matrix* $P \in \mathbb{R}^{n \times n}$ *and a vector* $\lambda \in \mathbb{R}^{n_\phi}$, *where* $\lambda(i) \geq 0$, *satisfying*

$$R_V^T \begin{bmatrix} A^T P - PA & PB \\ B^T P & 0 \end{bmatrix} R_V + R_\phi^T \Psi_\phi^T M_\phi(\lambda) \Psi_\phi R_\phi < 0 \tag{5.8}$$

$$\begin{bmatrix} (\bar{v}^1_{(i)} - v^1_{*_{(i)}})^2 & W^1_{(i)} \\ {W^1_{(i)}}^T & P \end{bmatrix} \geq 0,\ i = 1, ..., n_1, \tag{5.9}$$

where W^1 *is the weight matrix of the first layer,* $W^1_{(i)}$ *is the i-th row of* W^1, $v^1_{*_{(i)}}$ *and* $\bar{v}^1_{(i)}$ *are the i-th elements of* v^1_* *and* $\bar{v}^1$ *respectively. Then*

$$\mathcal{E}(P, x_*) = \{x \in \mathbb{R}^n :\ (x - x_*)^T P (x - x_*) \leq 1\}$$

is an inner approximation of the region of attraction of system (5.1)-(5.2).

Proof. The satisfaction of LMIs (5.9) guarantees that

$$\mathcal{E}(P, x_*) \subseteq S(W^1, \bar{v}^1) = \{x \in \mathbb{R}^n :\ \underline{v}^1 \preccurlyeq v^1 \preccurlyeq \bar{v}^1\} = \{x \in \mathbb{R}^n :\ \underline{v}^1 - v^1_* \preccurlyeq W^1(x - x_*) \preccurlyeq \bar{v}^1 - v^1_*\}.$$

Let us consider the following quadratic Lyapunov function candidate

$$V(x - x_*) = (x - x_*)^T P (x - x_*),\ P > 0.$$

To establish the result, we show that for all $x \in (\mathcal{E}(P, x_*) \setminus \{x_*\})$

$$\dot{V}(x - x_*) = (\dot{x} - x_*)^T P(x - x_*) + (x - x_*)^T P(\dot{x} - x_*) < 0.$$

$$\dot{V}(x - x_*) =$$

$$(x-x_*)^T A^T P(x-x_*)+(u-u_*)^T B^T P(x-x_*)+(x-x_*)^T PA(x-x_*)+(x-x_*)^T PB(u-u_*)$$

Which can be written in the following matrix form:

$$\dot{V}(x - x_*) = \begin{bmatrix}(x - x_*)^T & (u - u_*)^T\end{bmatrix} \begin{bmatrix}A^T P + PA & PB \\ B^T P & 0\end{bmatrix} \begin{bmatrix}x - x_* \\ u - u_*\end{bmatrix}.$$

Pre-and-post multiply LMI (5.2) by $[(x - x_*)^T \ (\omega_\phi - \omega_*)^T]$ and its transpose.

$$\begin{bmatrix}(x - x_*)^T & (\omega_\phi - \omega_*)^T\end{bmatrix} R_V^T \begin{bmatrix}A^T P + PA & PB \\ B^T P & 0\end{bmatrix} R_V \begin{bmatrix}x - x_* \\ \omega_\phi - \omega_*\end{bmatrix} + \begin{bmatrix}v_\phi - v_* \\ \omega_\phi - \omega_*\end{bmatrix}^T \Psi_\phi^T M_\phi(\lambda) \Psi_\phi \begin{bmatrix}v_\phi - v_* \\ \omega_\phi - \omega_*\end{bmatrix} < 0$$

which is equivalent to

$$\begin{bmatrix}(x - x_*)^T & (\omega_\phi - \omega_*)^T\end{bmatrix} \begin{bmatrix}I_n & N_{ux} \\ 0_{nxn_\phi} & N_{u\omega}\end{bmatrix} \begin{bmatrix}A^T P + PA & PB \\ B^T P & 0\end{bmatrix} \begin{bmatrix}I_n & 0_{nxn_\phi} \\ N_{ux} & N_{u\omega}\end{bmatrix} \begin{bmatrix}x - x_* \\ \omega_\phi - \omega_*\end{bmatrix}$$

$$+ \begin{bmatrix}v_\phi - v_* \\ \omega_\phi - \omega_*\end{bmatrix}^T \Psi_\phi^T M_\phi(\lambda) \Psi_\phi \begin{bmatrix}v_\phi - v_* \\ \omega_\phi - \omega_*\end{bmatrix} < 0$$

where the terms in blue are $[(x - x_*)^T \ (u - u_*)^T]$ and its transpose. Thus

$$\begin{bmatrix}(x - x_*)^T & (u - u_*)^T\end{bmatrix} \begin{bmatrix}A^T P + PA & PB \\ B^T P & 0\end{bmatrix} \begin{bmatrix}x - x_* \\ u - u_*\end{bmatrix} + \begin{bmatrix}v_\phi - v_* \\ \omega_\phi - \omega_*\end{bmatrix}^T \Psi_\phi^T M_\phi(\lambda) \Psi_\phi \begin{bmatrix}v_\phi - v_* \\ \omega_\phi - \omega_*\end{bmatrix} < 0$$

where the terms in red are equivalent to $\dot{V}(x - x_*)$.

$$\dot{V}(x - x_*) + \begin{bmatrix}v_\phi - v_* \\ \omega_\phi - \omega_*\end{bmatrix}^T \Psi_\phi^T M_\phi(\lambda) \Psi_\phi \begin{bmatrix}v_\phi - v_* \\ \omega_\phi - \omega_*\end{bmatrix} < 0$$

where, from Lemma 5.1, for $x \in S(W^1, \bar{v}^1)$ the term in green is ≥ 0.
It follows that, for $x \in \mathcal{E}(P, x_*) \subseteq S(W^1, \bar{v}^1)$, $x \neq x_*$,

$$\dot{V}(x - x_*) < 0.$$

□

5.2 Ellipsoidal estimate of the region of attraction

5.2.1 Local sector condition on tanh

The results of [24] are applied to the Optimal Velocity model (5.10) in error coordinates with N vehicles on a ring road of length L.

$$\begin{cases} \dot{z}_i = y_i, \quad \forall\ i = 1, ..., N-1 \\ \dot{y}_i = b\left[V_{\max}\frac{\tanh(z_{i+1}+d-d_0)-\tanh(z_i+d-d_0)}{1+\tanh(d_0)} - y_i\right], \quad \forall\ i = 1, ..., N-2 \\ \dot{y}_{N-1} = b\left[V_{\max}\frac{\tanh\left(-\sum_{i=1}^{N-1} z_i+d-d_0\right)-\tanh(z_{N-1}+d-d_0)}{1+\tanh(d_0)} - y_{N-1}\right] \\ \dot{y}_N = b\left[V_{\max}\frac{\tanh(z_1+d-d_0)-\tanh\left(-\sum_{i=1}^{N-1} z_i+d-d_0\right)}{1+\tanh(d_0)} - y_N\right] \end{cases} \tag{5.10}$$

In this section, we consider the particular case where L is such that $d = \frac{L}{N} = d_0$ and the reason is that, with this choice, the local sector condition on tanh will be centered in the origin. The model becomes equal to (5.11).

$$\begin{cases} \dot{z}_i = y_i, \quad \forall\ i = 1, ..., N-1 \\ \dot{y}_i = b\left[V_{\max}\frac{\tanh(z_{i+1})-\tanh(z_i)}{1+\tanh(d_0)} - y_i\right], \quad \forall\ i = 1, ..., N-2 \\ \dot{y}_{N-1} = b\left[V_{\max}\frac{\tanh\left(-\sum_{i=1}^{N-1} z_i\right)-\tanh(z_{N-1})}{1+\tanh(d_0)} - y_{N-1}\right] \\ \dot{y}_N = b\left[V_{\max}\frac{\tanh(z_1)-\tanh\left(-\sum_{i=1}^{N-1} z_i\right)}{1+\tanh(d_0)} - y_N\right] \end{cases} \tag{5.11}$$

First of all, the nonlinear system (5.11) may be rewritten as

$$\dot{\mathbf{x}} = A\mathbf{x}(t) + Bu(t) = A\mathbf{x}(t) + B\tanh(K\mathbf{x}(t)), \tag{5.12}$$

where the state vector is

$$\mathbf{x} = [z_1, z_2, ..., z_{N-1}, y_1, y_2, ..., y_N]^T \in \mathbb{R}^n,$$

$$A = \begin{bmatrix} 0 & A_{zy} \\ 0 & -bI_N \end{bmatrix} \in \mathbb{R}^{2N-1 \times 2N-1},$$

with I_N the identity matrix $\in \mathbb{R}^{N \times N}$ and

$$A_{zy} = \begin{bmatrix} 1 & & & (0) & 0 \\ & 1 & & & \vdots \\ & & \ddots & & \vdots \\ (0) & & & 1 & 0 \end{bmatrix} \in \mathbb{R}^{N-1 \times N},$$

$$B = \begin{bmatrix} 0_{N-1 \text{x} N} \\ B_{yz} \end{bmatrix} \in \mathbb{R}^{2N-1 \times N},$$

where

$$B_{yz} = \frac{bV_{\max}}{1 + \tanh(d_0)} \begin{bmatrix} -1 & 1 & & & (0) \\ & -1 & 1 & & \\ & & \ddots & \ddots & \\ (0) & & & -1 & 1 \\ 1 & 0 & \dots & 0 & -1 \end{bmatrix} \in \mathbb{R}^{N \times N}$$

and

$$K = \begin{bmatrix} K_{yz} & 0_{N \times N} \end{bmatrix} \in \mathbb{R}^{N \times 2N-1},$$

where

$$K_{yz} = \begin{bmatrix} 1 & & & (0) \\ & 1 & & \\ & & \ddots & \\ (0) & & & 1 \\ -1 & \dots & \dots & -1 \end{bmatrix} \in \mathbb{R}^{N \times N-1}.$$

System (5.12) may be considered as a plant (5.1), driven by a 1-layer controller π (5.13).

$$\omega^0(t) = \mathbf{x}(t) \tag{5.13a}$$

$$\omega^1(t) = \phi^1(W^1\omega^0(t) + b^1) \tag{5.13b}$$

$$u(t) = W^2\omega^1(t) + b^2 \tag{5.13c}$$

Since there is only one layer, $v_\phi = v^1 \in \mathbb{R}^{n_1}$ and $\omega_\phi = \omega^1 \in \mathbb{R}^{n_1}$ and the only activation function vector is

$$\phi(v_\phi) = \phi^1(v) = [\varphi(v_1), ..., \varphi(v_{n_1})]^T \in \mathbb{R}^{n_1}.$$

So, $n_\phi = n_1 = N$.
The nonlinearity is given by

$$\omega^1(t) = \phi^1(v^1(t)) = \phi^1(W^1\omega^0(t)) = \phi^1(W^1\mathbf{x}(t)) = \tanh(W^1\mathbf{x}(t)) = \tanh(K\mathbf{x}(t)),$$

so

$$W^1 = K \text{ and } b^1 = 0$$

Then

$$u(t) = W^2\omega^1(t) + b^2 = W^2 \tanh(K\mathbf{x}(t)) + b^2.$$

But, since from (5.12) $u(t) = \tanh(K\mathbf{x}(t))$, then

$$W^2 = I_N \text{ and } b^2 = 0,$$

where I_N is the identity matrix $\in \mathbb{R}^{N\times N}$.
Since

$$\omega^1 = \phi^1(v^1) = \tanh(K\mathbf{x}) = \begin{bmatrix} \tanh(z_1) \\ \tanh(z_2) \\ \vdots \\ \tanh(z_{N-1}) \\ \tanh(-z_1 - z_2 - ... - z_{N-1}) \end{bmatrix} \in \mathbb{R}^N,$$

then $n_1 = N$. Having defined W^1 and W^2, let us compute matrix N.

$$\begin{bmatrix} u(t) \\ v^1(t) \end{bmatrix} = N \begin{bmatrix} x(t) \\ \omega^1(t) \\ 1 \end{bmatrix} = \begin{bmatrix} 0_{N\times 2N-1} & W^2 & 0 \\ K & 0_{N\times N} & 0 \end{bmatrix} \begin{bmatrix} x(t) \\ \omega^1(t) \\ 1 \end{bmatrix} \tag{5.14}$$

Let us compute an under-estimate of the region of attraction of system (5.11) using the method described in [24], where the equilibrium point is given by

$$x_* = Ax_* + Bu_*$$

$$u_* = \pi(x_*)$$

Since we are interested in a region of attraction around $\mathbf{x} = 0$ (i.e. uniform flow equilibrium), $x_* = 0$ and the corresponding input at the equilibrium is $u_* = 0$.
Finally, (x_*, u_*) must satisfy (5.4) and (5.14), therefore

$$v_* = v_*^1 = W^1 x_* = 0$$

and

$$\omega_* = \omega_*^1 = \phi^1(v_*^1) = \tanh(v_*^1) = 0.$$

Then, the equilibrium point is $(x_*, u_*, v_*, w_*) = (0,0,0,0)$ and the local sectors $[\alpha_\phi, \beta_\phi]$ are centered in the origin as in Figure 5.1.

In order to determine the ellipsoidal estimates of the region of attraction, we choose the vector $\bar{v}^1$, in which the hyperbolic tangent satisfies the local sector condition (5.5).
Therefore, the ellipsoidal estimates will be included in the following polyhedral set.

$$\mathcal{E}(P,0) \subseteq S(K, \bar{v}^1) = \{x \in \mathbb{R}^{2N-1} : \ -\bar{v}^1 \preccurlyeq K\mathbf{x} \preccurlyeq \bar{v}^1\}$$

Being the ellipsoidal estimates inner-approximations of the region of attraction of model (5.11), to determine the best approximation, we maximize the volume of $\mathcal{E}(P,0) \in \mathbb{R}^{2N-1}$. The maximization of the size of the ellipsoids is performed by minimizing the trace of matrix P. Therefore, the best approximation is determined solving the following optimization problem.

$$\begin{aligned} &\text{minimize} && \text{trace}(P) \\ &\text{subject to} && \text{inequalities (5.8), (5.9)} \end{aligned} \tag{5.15}$$

Example 5.1. *Let us consider a platoon of $N = 5$ vehicles driving on a ring road of length $L = 50\ m$, in which the safety distance is $d_0 = l_v + d_s = 10\ m$. Since $d = L/N$ is equal to d_0, the group of vehicles is modelled as (5.11). These parameters satisfy the stability constraint (3.18), so the origin is an asymptotically stable equilibrium point for the model. The state vector is*

$$\boldsymbol{x} = [z_1, z_2, z_3, z_4, y_1, y_2, y_3, y_4, y_5]^T \in \mathbb{R}^9$$

Suppose the model parameters are $b = 20\ s^{-1}$ and $V_{\max} = 5\ m/s$ and suppose the levels of the local sectors are

$$\bar{v}^1 = [3\ 3\ 3\ 3\ 3] \in \mathbb{R}^5.$$

The hyperbolic tangent is inscribed in the local sector shown in Figure 5.3.
We compute the maximum-volume ellipsoid $\mathcal{E}(P,0) \in \mathbb{R}^9$ by solving problem (5.15). To

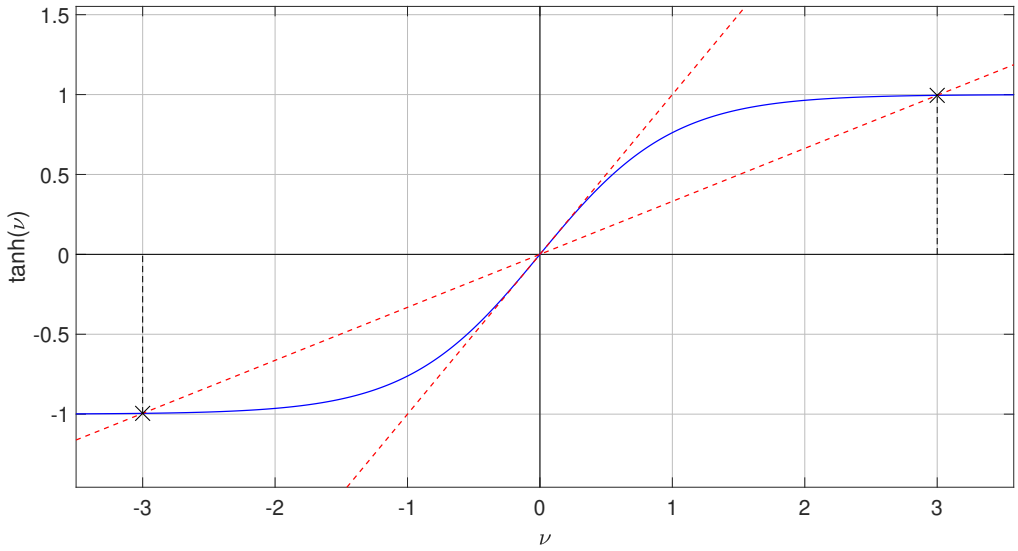

Figure 5.3: Local sector with $\bar{\nu} = 3$

have an idea of the size of the ellipsoid, in Figure 5.4 and 5.5 are shown the sections of the ellipsoid onto (z_1, z_2) and (y_1, y_2) respectively.
Having chosen $\bar{v}_i^1 = 3\ \forall\ i = 1, ...,5$, since

$$\mathcal{E}(P,0) \subseteq S(K, \bar{v}^1) = \{x \in \mathbb{R}^9 :\ -\bar{v}^1 \preccurlyeq K\boldsymbol{x} \preccurlyeq \bar{v}^1\}$$

and

$$K = \begin{bmatrix} 1 & 0 & 0 & 0 & 0 & 0 & 0 & 0 & 0 \\ 0 & 1 & 0 & 0 & 0 & 0 & 0 & 0 & 0 \\ 0 & 0 & 1 & 0 & 0 & 0 & 0 & 0 & 0 \\ 0 & 0 & 0 & 1 & 0 & 0 & 0 & 0 & 0 \\ -1 & -1 & -1 & -1 & 0 & 0 & 0 & 0 & 0 \end{bmatrix} \in \mathbb{R}^{5\times 9},$$

the following constraints hold on z_i.

$$-3 \leq z_i \leq 3,\ \forall i = 1, ...,4$$

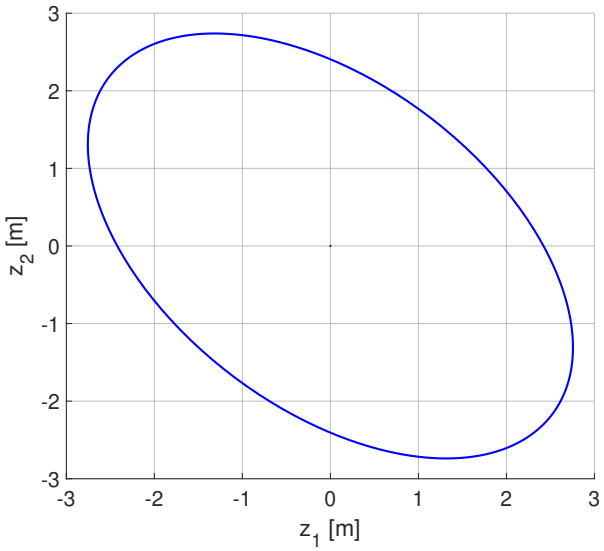

Figure 5.4: Section of $\mathcal{E}(P,0)$ onto (z_1, z_2) when $\bar{v}_i^1 = 3$

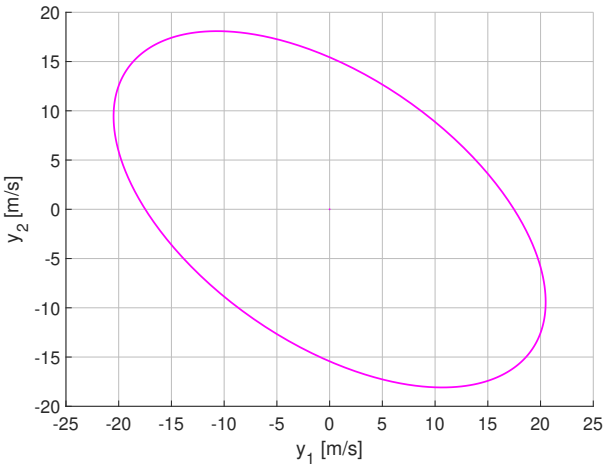

Figure 5.5: Section of $\mathcal{E}(P,0)$ onto (y_1, y_2) when $\bar{v}_i^1 = 3$

This means that vector $\bar{v}^1$ limits the size of the ellipsoidal estimate with respect to z_i, as shown in Figure 5.4. Therefore, the larger is $\bar{v}^1$, the wider is the maximum-volume ellipsoid and the better is the estimate.
Nevertheless, increasing too much the values of vector $\bar{v}^1$ to enlarge the local sector may lead to infeasible solutions to problem (5.15). For this reason, we determine the best estimate of the region of attraction of the model (5.11) by choosing the highest $\bar{v}^1$ for which a feasible solution to (5.15) exists.

With the same model parameters as before, the highest value of $\bar{v}^1_{(i)}$ *for which the optimization problem is feasible is*

$$\bar{v}^1_{(i)} = 3.1308.$$

In Figure 5.6 is shown the section of the maximum-volume ellipsoid onto (z_1, z_2) *and in Figure 5.6 the section onto* (y_1, y_2)*. As expected, since the defined polyhedral set* $S(K, \bar{v}^1)$ *is wider, the volume of the ellipsoidal estimate is larger and, with* $b = 20\ s^{-1}$ *and* $V_{\max} = 5\ m/s$*, this is the best approximation of the region of attraction of model (5.11) we can obtain.*

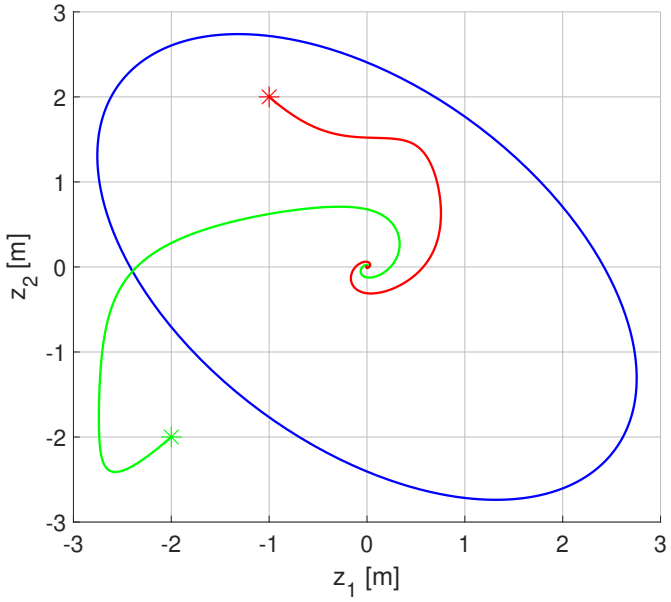

Figure 5.6: Section of $\mathcal{E}(P,0)$ (blue) onto (z_1, z_2) when $\bar{v}^1_i = 3.1308$, one trajectory (red) is initialized inside and one trajectory is initialized outside (green)

Since $\mathcal{E}(P,0)$ *is an invariant and contractive set, if the trajectories are initialized inside it, they remain within the ellipsoid and converge to the origin. In Figures 5.6-5.7 are shown the projections of one trajectory (red) that starts inside* $\mathcal{E}(P,0)$*. Being* $\mathcal{E}(P,0)$ *an underestimate of the region of attraction, there are trajectories that converge to the origin but don't start from the ellipsoid. In Figures 5.6-5.7 the green curves are the projections of one trajectory that doesn't start from* $\mathcal{E}(P,0)$ *and yet it converges to the origin.*
Looking at the sections, we cannot state whether one point x_* *belongs to* $\mathcal{E}(P,0)$ *or not. To know if it belongs to the ellipsoid, we have to check if*

$$x_*^T P x_* \leq 1.$$

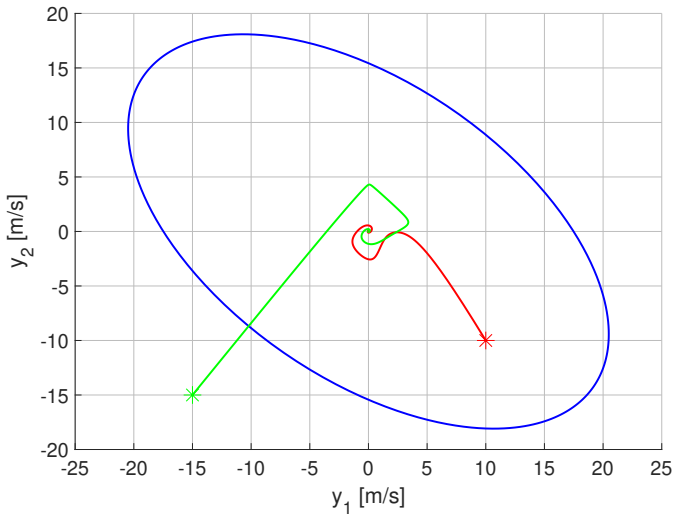

Figure 5.7: Section of $\mathcal{E}(P,0)$ (blue) onto (y_1, y_2) when $\bar{v}_i^1 = 3.1308$, one trajectory (red) is initialized inside and one trajectory is initialized outside (green)

5.2.2 Offset local sector condition on tanh

With respect to what has been done in Section 5.2.1, here we focus on the general case where L is such that $d \neq d_0$. The nonlinear model is then

$$\begin{cases} \dot{z}_i = y_i, \quad \forall\ i = 1, ..., N-1 \\ \dot{y}_i = b\left[V_{\max}\frac{\tanh(z_{i+1}+d-d_0)-\tanh(z_i+d-d_0)}{1+\tanh(d_0)} - y_i\right], \quad \forall\ i = 1, ..., N-2 \\ \dot{y}_{N-1} = b\left[V_{\max}\frac{\tanh\left(-\sum_{i=1}^{N-1} z_i+d-d_0\right)-\tanh(z_{N-1}+d-d_0)}{1+\tanh(d_0)} - y_{N-1}\right] \\ \dot{y}_N = b\left[V_{\max}\frac{\tanh(z_1+d-d_0)-\tanh\left(-\sum_{i=1}^{N-1} z_i+d-d_0\right)}{1+\tanh(d_0)} - y_N\right] \end{cases} \tag{5.16}$$

The nonlinear system (5.16) may be rewritten as

$$\dot{\mathbf{x}} = A\mathbf{x}(t) + Bu(t) = A\mathbf{x}(t) + B\tanh(K\mathbf{x}(t) + \bar{d}), \tag{5.17}$$

where $\bar{d} = (d - d_0)\mathbf{1}_N \in \mathbb{R}^N$ and $\mathbf{x} \in \mathbb{R}^{2N-1}$, $A \in \mathbb{R}^{2N-1\times 2N-1}$, $B \in \mathbb{R}^{2N-1\times N}$ and $K \in \mathbb{R}^{N\times 2N-1}$ are the same quantities defined in Section 5.2.1. The only difference is the presence of $\bar{d}$ in the nonlinear functions. As well as before, system (5.17) may be considered as a plant (5.1) driven by a 1-layer controller π (5.18).

$$\omega^0(t) = \mathbf{x}(t) \tag{5.18a}$$

$$\omega^1(t) = \phi^1(W^1\omega^0(t) + b^1) \tag{5.18b}$$

$$u(t) = W^2\omega^1(t) + b^2 \tag{5.18c}$$

Since there is only one layer, $v_\phi = v^1 \in \mathbb{R}^{n_1}$ and $\omega_\phi = \omega^1 \in \mathbb{R}^{n_1}$ and the only activation function vector is

$$\phi(v_\phi) = \phi^1(v) = [\varphi(v_1), ..., \varphi(v_{n_1})]^T \in \mathbb{R}^{n_1}.$$

So, $n_\phi = n_1 = N$.
The nonlinearity is given by

$$\omega^1(t) = \phi^1(v^1(t)) = \phi^1(W^1\omega^0(t)+b^1) = \phi^1(W^1\mathbf{x}(t)+b^1) = \tanh(W^1\mathbf{x}(t)+b^1) = \tanh(K\mathbf{x}(t)+\bar{d}),$$

so

$$W^1 = K \text{ and } b^1 = \bar{d}$$

Then

$$u(t) = W^2\omega^1(t) + b^2 = W^2\tanh(K\mathbf{x}(t)) + b^2.$$

But, since from (5.17) $u(t) = \tanh(K\mathbf{x}(t) + \bar{d})$, then

$$W^2 = I_N \text{ and } b^2 = 0,$$

where I_N is the identity matrix $\in \mathbb{R}^{N\times N}$. As before $n_1 = N$. We can compute matrix N:

$$\begin{bmatrix} u(t) \\ v^1(t) \end{bmatrix} = N \begin{bmatrix} x(t) \\ \omega^1(t) \\ 1 \end{bmatrix} = \begin{bmatrix} 0_{N\times 2N-1} & W^2 & 0 \\ K & 0_{N\times N} & \bar{d} \end{bmatrix} \begin{bmatrix} x(t) \\ \omega^1(t) \\ 1 \end{bmatrix} \tag{5.19}$$

Let us compute an under-estimate of the region of attraction of system (5.16) using the method described in [24], where the equilibrium point is given by

$$x_* = Ax_* + Bu_*$$

$$u_* = \pi(x_*)$$

Since we are interested in a region of attraction around $\mathbf{x} = 0$ (i.e. uniform flow equilibrium), $x_* = 0$ and the corresponding input at the equilibrium is $u_* = \tanh(\bar{d})$.
Finally, (x_*, u_*) must satisfy (5.4) and (5.19), therefore

$$v_* = v_*^1 = W^1x_* + b^1 = b^1 = \bar{d}$$

and

$$\omega_* = \omega_*^1 = \phi^1(v_*^1) = \tanh(v_*^1) = \tanh(\bar{d}).$$

Then, the equilibrium point is $(x_*, u_*, v_*, w_*) = (0, \tanh(\bar{d}), \bar{d}, \tanh(\bar{d}))$ and the local sectors $[\alpha_\phi, \beta_\phi]$ are centered in $(\bar{d}, \tanh(\bar{d}))$

In order to determine the ellipsoidal estimates of the region of attraction, we choose the vector $\bar{v}^1$, in which the hyperbolic tangent satisfies the offset local sector condition (5.5). Therefore, the ellipsoidal estimates will be included in the following polyhedral set.

$$\mathcal{E}(P,0) \subseteq S(K, \bar{v}^1) = \{x \in \mathbb{R}^n : \underline{v}^1 - v_* \preccurlyeq Kx \preccurlyeq \bar{v}^1 - v_*\}$$

Being the ellipsoidal estimates inner-approximations of the region of attraction of model (5.16), to determine the best approximation, we maximize the volume of $\mathcal{E}(P,0) \in \mathbb{R}^{2N-1}$. The maximization of the size of the ellipsoids is performed solving the same optimization problem (5.15) as before and trying to choose the largest values of $\bar{v}^1 - v_*$ and $|\underline{v}^1 - v_*|$. Now the local sectors are not centered in the origin, because they are translated towards one of the two flat regions of tanh dependently on the sign of $d - d_0$. With respect to the case where the local sectors are centered in the origin, this feature leads to lower maximum levels $\bar{v}^1 - v_*$ (and $|\underline{v}^1 - v_*|$) for which the optimization problem is feasible and so to ellipsoidal estimates with smaller volume. The main reason of the reduction of $\bar{v}^1 - v_*$ as the local sectors move away from the origin is due to the flat branches of the hyperbolic tangent. Keeping the same difference $\bar{v}^1 - v_*$, as v_* moves towards one of the two branches, it means that the local sector tends to be global. Since global stability doesn't hold for model (5.16), the result is that the optimization problem (5.15) is unfeasible. Therefore, with the same choice of b and $V_{\max}$, if the local sectors are not centered in the origin, the resulting ellipsoidal estimates of the region of attraction of model (5.16) have a smaller volume. This means that, if $d < d_0$ or $d > d_0$, the estimates of the region of attraction are smaller than the estimates of the region of attraction of the model (5.16) when $d = d_0$.
Finally, the maximum value of $\bar{v}^1 - v_*$ for which the optimization problem (5.15) is feasible reduces as the number of vehicles increases. The dependence of the size of the ellipsoids on $|d - d_0|$ and N reflects the worsening of stability as these two parameters increase that was shown in the linear framework in Section 3.1.

Example 5.2. *Let us consider a platoon of $N = 5$ vehicles driving on a ring road of length $L = 55$ m, in which the safety distance is $d_0 = l_v + d_s = 10$ m. Therefore $d = d_0 = 1$ m and the offset local sectors are centered in $v_* = 1$ m. Suppose the model parameters are $b = 20$ s^{-1} and $V_{\max} = 5$ m/s as in Example 5.1.*
The maximum value of $\bar{v}^1$ for which problem (5.15) admits a feasible solution is such that

$$\bar{v}^1 - v_* = 0.36.$$

Therefore, the maximum ellipsoidal estimate of the region of attraction that lies in the polyhedral set $S(K, \bar{v}^1)$ has a quite small volume and its sections onto (z_1, z_2) and (y_1, y_2) are depicted in Figure 5.8 and Figure 5.9.

5.3 Dependence of the ROA on the model parameters

In Section 3.1 we saw that the parameters affect the eigenvalues of the linearized model (3.12) around the origin and if they satisfy the condition (3.18) then the uniform flow equilibrium is asymptotically stable. The parameters affect also the size of the ellipsoidal estimate of the ROA of the nonlinear model (3.10) around the origin. By fixing $d = d_0$, the local sectors are centered in the origin and they provide the widest ellipsoidal estimates, while choosing $d > d_0$ leads to relatively smaller ellipsoids. Therefore, we fix $d = d_0$ and compute the ellipsoidal estimates for different values of b and $V_{\max}$ and see that they affect the maximum value of $\bar{v}_{(i)}$ for which problem (5.15) is feasible. In particular, increasing b and reducing $V_{\max}$ help the satisfaction of the stability constraint and lead to larger $\bar{v}_{(i)}$ and so to ellipsoidal estimates with larger volume.

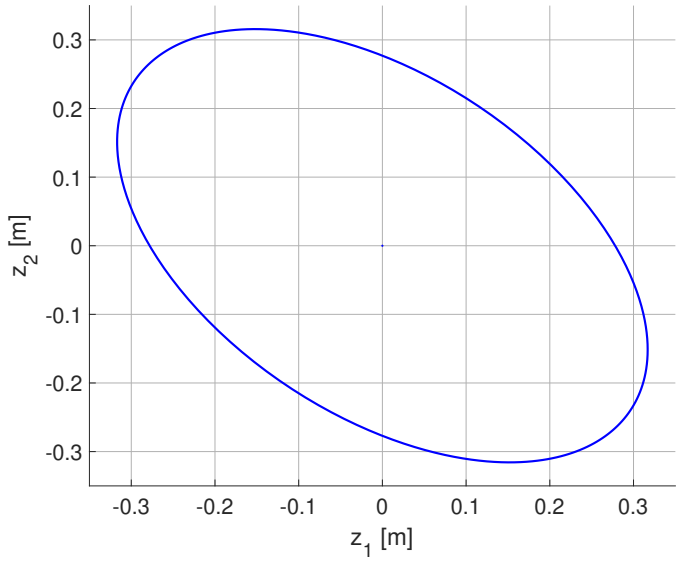

Figure 5.8: Section of $\mathcal{E}(P,0)$ onto (z_1, z_2) when $\bar{v}^1 - v_* = 0.36$

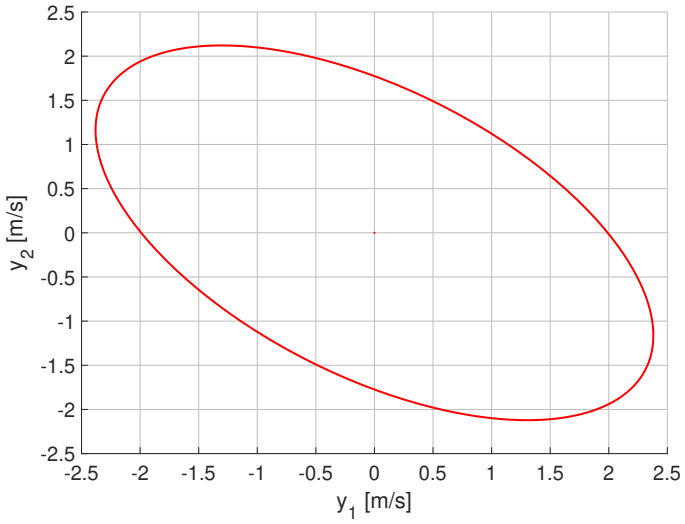

Figure 5.9: Section of $\mathcal{E}(P,0)$ onto (y_1, y_2) when $\bar{v}^1 - v_* = 0.36$.

For a group of $N = 5$ vehicles we fix $d_0 = 10\ m$ and consider a ring road of length $L = 50\ m$, so that $d = \frac{L}{N}$ equals d. Let us fix $V_{\max} = 10\ m/s$, compute $\mathcal{E}(P,0)$ for different values of b and project it on subspaces generated by bases of the state variables. In Table 5.1 are shown the ranges of the state variables belonging to $\mathcal{E}(P,0)$. As expected, by increasing b, the volume of the ellipsoidal estimate of the ROA increases. The ellipsoids are inner-approximations, so we can't state whether tuning b actually makes the ROA enlarge, but a larger b allows to get to a wider set of initial conditions for which we are sure the

Table 5.1: Dependence of the ellipsoidal estimate of the ROA on b. Increasing b, the levels $\bar{v}$ increases and the size of $\mathcal{E}(P,0)$ increases. $V_{\max} = 10\ m/s$, $d = d_0$ and $N = 5$.

$b\ [s^{-1}]$	Vector $\bar{v}$	Ranges of z_1 and $y_1 \in \mathcal{E}(P,0)$
$b = 10$	$\bar{v}_{(i)} = 1.3040$	$-1.304\ m \leq z_1 \leq 1.304\ m$ $-10.32\ m/s \leq y_1 \leq 10.32\ m/s$
$b = 20$	$\bar{v}_{(i)} = 2.4421$	$-2.442\ m \leq z_1 \leq 2.442\ m$ $-23.85\ m/s \leq y_1 \leq 23.85\ m/s$
$b = 30$	$\bar{v}_{(i)} = 2.8906$	$-2.888\ m \leq z_1 \leq 2.888\ m$ $-33.08\ m/s \leq y_1 \leq 33.08\ m/s$

trajectories of (3.10) converge to the uniform flow equilibrium. Finally, we compute the ellipsoidal estimates by solving (5.15) fixing $b = 20\ s^{-1}$ with different values of $V_{\max}$. The ellipsoids are projected on subspaces generated by bases of the state variables. In Table 5.2 are shown the ranges of the state variables belonging to $\mathcal{E}(P,0)$. Even if we can only

Table 5.2: Dependence of the ellipsoidal estimate of the ROA on $V_{\max}$. Increasing $V_{\max}$, the levels $\bar{v}$ decreases and the size of $\mathcal{E}(P,0)$ decreases. $b = 20\ s^{-1}$, $d = d_0$ and $N = 5$.

$V_{\max}\ [\frac{m}{s}]$	Vector $\bar{v}$	Ranges of z_1 and $y_1 \in \mathcal{E}(P,0)$
$V_{\max} = 5$	$\bar{v}_{(i)} = 3.1308$	$-3.127\ m \leq z_1 \leq 3.127\ m$ $-21.04\ m/s \leq y_1 \leq 21.04\ m/s$
$V_{\max} = 10$	$\bar{v}_{(i)} = 2.4421$	$-2.442\ m \leq z_1 \leq 2.442\ m$ $-23.85\ m/s \leq y_1 \leq 23.85\ m/s$
$V_{\max} = 20$	$\bar{v}_{(i)} = 1.3030$	$-1.303\ m \leq z_1 \leq 1.303\ m$ $-20.16\ m/s \leq y_1 \leq 20.16\ m/s$

determine an estimate of the region of attraction of the model (3.10), we see that high values of b and low values of $V_{\max}$ improve the satisfaction of the stability constraint (3.18) of the linearized model around the uniform flow equilibrium and lead to the determination of wider sets of initial conditions for which the trajectories of the nonlinear model are ensured to converge to the uniform flow equilibrium.

In the Optimal Velocity model

$$\begin{cases} \dot{x}_i = v_i, \quad \forall\ i = 1, ..., N \\ \dot{v}_i = b\left[V_{opt}\left(x_{i+1} - x_i\right) - v_i\right], \quad \forall\ i = 1, ..., N \end{cases} \tag{5.20}$$

b is the sensitivity of the driver. Therefore, with the same headway and same absolute velocity v_i, a vehicle with larger b reacts faster. As consequence, an increase of b improves the stability of the uniform flow equilibrium and this feature is shown both in the linear and nonlinear framework.
$V_{\max}$ is the maximum value of the velocity function and we see that, when $d = d_0$, larger values of $V_{\max}$ affect the trajectories of the nonlinear model in a similar way as seen in Section 4.3. We simulate system (5.20) modelling a group of $N = 5$ vehicles on a ring road

of length $L = 50\ m$, where $d_0 = l_v + d_s = 10\ m$. We select $b = 10\ s^{-1}$ and choose two values of $V_{\max}$, keeping the same initial conditions.

1. $V_{\max} = 5\ m/s$
   As shown in Figure 5.10, the trajectories of the nonlinear converge to the uniform flow equilibrium because the parameters satisfy the stability condition (3.18) where $\kappa_5 = 0.7639$.

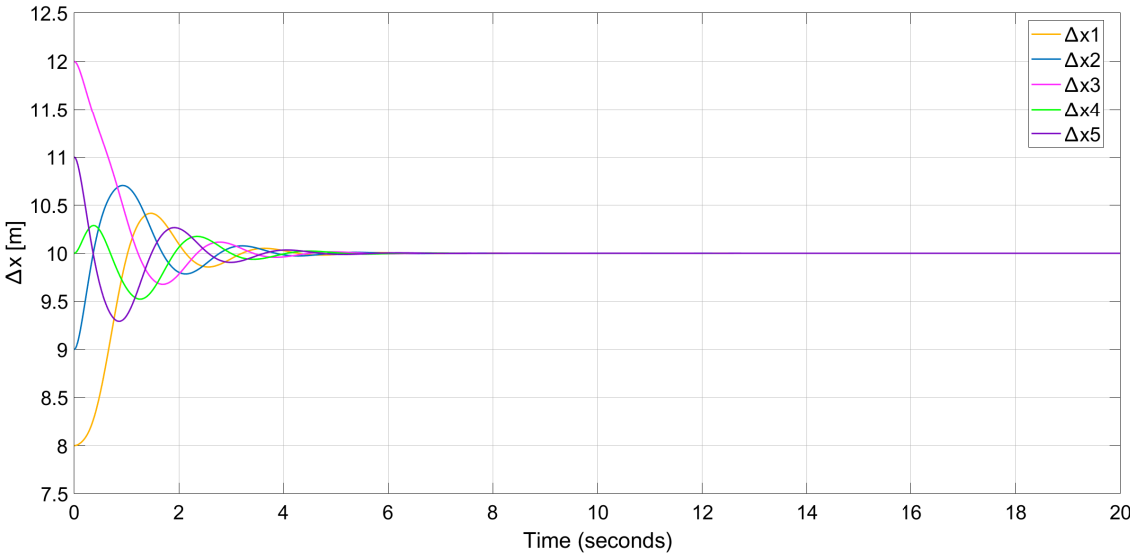

Figure 5.10: Relative distances of the group of 5 vehicles when $V_{\max} = 5\ m/s$

2. $V_{\max} = 15\ m/s$
   As well as for the model with saturation function in Section 4.3, a larger value of $V_{\max}$ helps in closing long distances and opening short distances in less time. Nevertheless, it leads to oscillations of the velocity functions and of the inter-vehicle distances because it is more difficult to brake and accelerate gently when the distances are too short or too long respectively. As a result, the convergence to the uniform flow equilibrium takes more time. Anyway, since the parameters satisfy constraint (3.18), the trajectories reach the equilibrium, as shown in Figure 5.12.

5.4 Safe region of attraction

In the same way as in Section 4.4 for the Optimal Velocity model with saturation, we can determine an ellipsoidal estimate of the region of attraction of the Optimal Velocity model (5.16) that lies in a safety polytope that forces a lower bound on the inter-vehicle distances. This leads to determine a contractive and invariant set such that, if the trajectories of the model are initialized in this set, they converge to the uniform flow equilibrium and collision is avoided.
The procedure consists in adding the LMIs (5.21) to the optimization problem (5.15), so that the ellipsoidal estimate is included in (5.22). In this way, we force a lower (and upper)

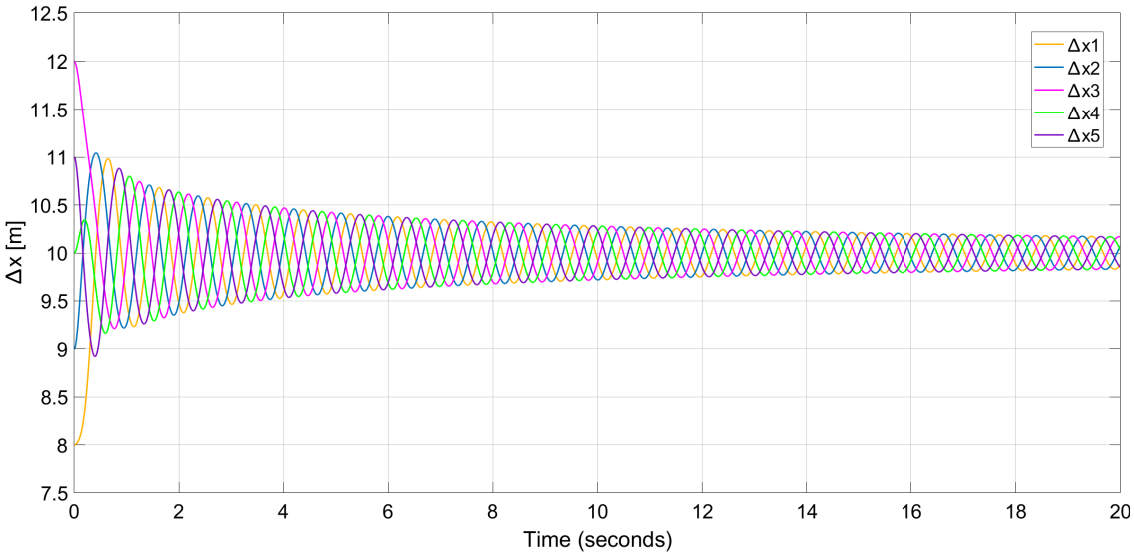

Figure 5.11: Relative distances of the group of 5 vehicles when $V_{\max} = 15\ m/s$

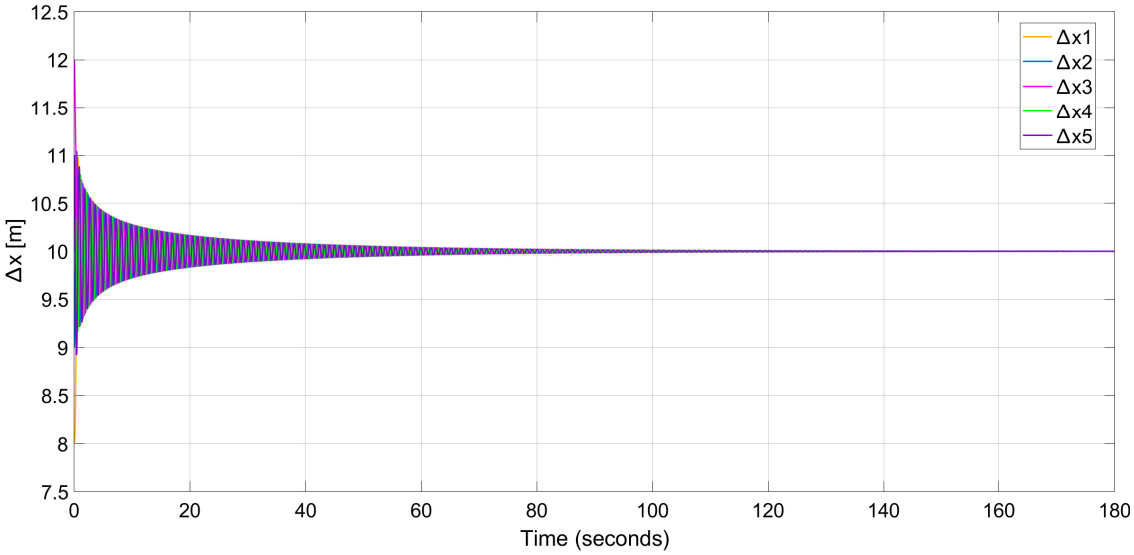

Figure 5.12: Relative distances of the group of 5 vehicles when $V_{\max} = 15\ m/s$

bound on the inter-vehicle distances (5.24) by imposing a lower (and upper) bound on the inter-vehicle distances (5.23).

$$\begin{bmatrix} P & Q_{(i)}^T \\ Q(i) & \rho_{(i)}^2 \end{bmatrix} \geq 0,\ \forall\ i, \tag{5.21}$$

where

$$Q = \begin{bmatrix} I_{N-1} & 0_{N\times N} \end{bmatrix} \in \mathbb{R}^{N-1\times 2N-1},$$

where I_{N-1} is the identity matrix $\in \mathbb{R}^{N-1\times N-1}$ and

$$\rho = \begin{bmatrix} d_{\max} - d \\ d_{\max} - d \\ \vdots \\ d_{\max} - d \end{bmatrix} \in \mathbb{R}^{N-1}.$$

$$S(|Q|, \rho) = \{x \in \mathbb{R}^n : \ |Qx| \preccurlyeq \rho\} = \{x \in \mathbb{R}^n : \ |Q_{(i)}x| \leq \rho, \ \forall i\}, \tag{5.22}$$

$$d_{\min} - d \leq z_i \leq d_{\max} - d, \tag{5.23}$$

$$d_{\min} \leq \Delta x_i \leq d_{\max}, \tag{5.24}$$

The resulting optimization problem that maximizes the volume of the ellipsoidal estimate of the region of attraction for model (5.16) included in the safety polytope is (5.25).

$$\begin{aligned} &\text{minimize} \quad \text{trace}(P) \\ &\text{subject to} \quad \text{inequalities (5.8), (5.9), (5.21)} \end{aligned} \tag{5.25}$$

Example 5.3. *Let us suppose to deal with the same model in Example 5.1 in Section 5.2.1, where $N = 5$ and the parameters are $b = 20\ s^{-1}$, $V_{\max} = 5\ m/s$ and $d_0 = 10\ m$. To get the maximum-volume ellipsoidal estimate, consider that the length of the ring road is such that the inter-vehicle distances at the uniform flow equilibrium, d, is equal to d_0.*
Suppose to force the following lower bound on the inter-vehicle distances:

$$d_{\min} = 8\ m.$$

In order to get a symmetric polytope $S(|Q|, \rho)$, $d_{\max} = 12\ m$, so that

$$8\ m \leq \Delta x_i \leq 12\ m, \tag{5.26}$$

$$-2\ m \leq z_i \leq 2\ m. \tag{5.27}$$

We define matrix Q and vector ρ, solve the optimization problem (5.25) and compute the maximum-volume ellipsoidal estimate $\mathcal{E}(P,0)$ of the ROA contained in the safety polytope $S(|Q|, \rho)$. The resulting ellipsoid is smaller with respect to the one computed in Example 5.1 and its section onto (z_1, z_2) is shown in Figure 5.13. Therefore, initializing the trajectories of (5.11) in this smaller ellipsoid, they converge to the uniform flow equilibrium and the vehicle distances are bounded between 8 m and 12 m and the vehicles don't collide. In Figure 5.14 are shown the relative distances of a group of 5 vehicles with $b = 20\ s^{-1}$, $V_{\max} = 10\ m/s$ and $d = d_0 = 10\ m$. The initial conditions in error coordinates belong to $\mathcal{E}(P,0)$ and the relative distances lie in the safety range defined in (5.26).

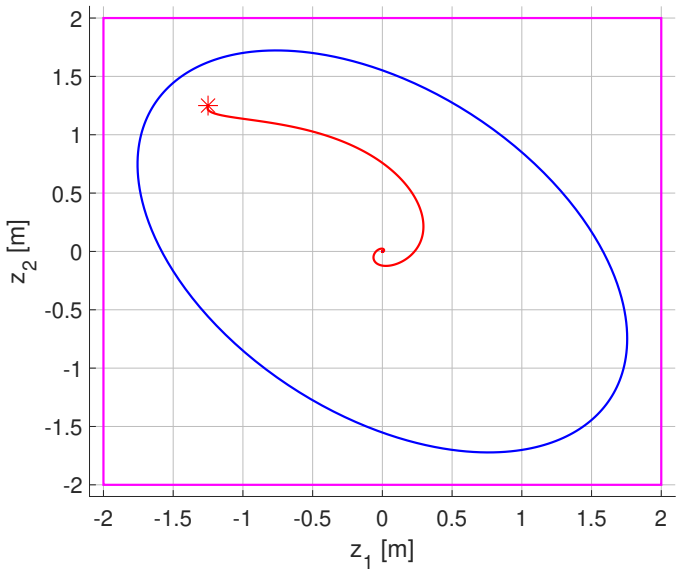

Figure 5.13: Section of $\mathcal{E}(P,0)$ (blue) onto (z_1, z_2), projection of $S(|Q|, \rho)$ (pink) and one trajectory (red) of the model

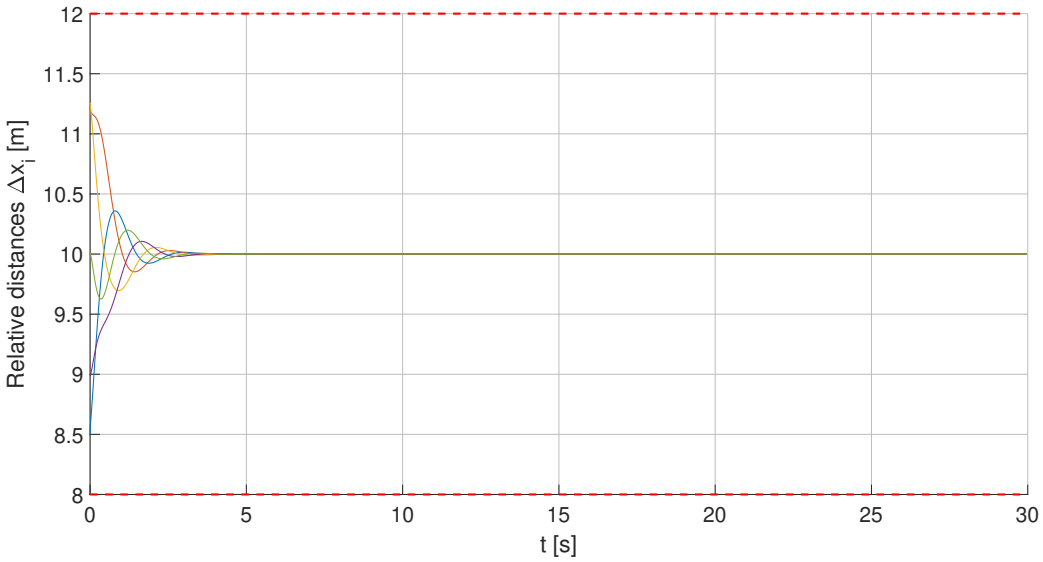

Figure 5.14: Evolution of the vehicle distances with respect to time. Starting the trajectories within $\mathcal{E}(P,0)$ included in the safety polytope, the distances are lower and upper bounded

Chapter 6

Conclusion and future work

6.1 Summary and comparison of the models

Experimental evidence on a ring road shows that the presence of a small number of autonomous vehicles (AVs) is able to dampen stop-and-go waves, avoid huge oscillations of the speed and prevent accidents of a group of human-driven vehicles. Being unclear by which mechanism AVs can improve the behaviour of human-driven vehicles so far, this work aims to analyse the properties of a group of N vehicles on a ring road.
Traffic flow is described by the nonlinear Bando Optimal Velocity model and the analysis focuses on the stability of the uniform flow equilibrium and on the safety of the trajectories of the vehicles. Being the hyperbolic tangent of the Bando model similar to a bounded piecewise linear function, called saturation function, we substitute it and define a simplified traffic model. The resulting Optimal Velocity model with saturation is piecewise linear and we carry out the same analyses for both the models.
As a first step, the stability analysis of the uniform flow equilibrium is performed on the linearization of the Bando model rewritten in the spacing errors and relative velocities. Since the linearized model shows a structural zero eigenvalue, the objective is to remove it. As the vehicles travel on a closed ring, one spacing error is written as function of the others, the state vector is reduced and the linearization around the uniform flow equilibrium doesn't have any structural zero eigenvalue anymore. Depending on the choice of the parameters of the model, the uniform flow equilibrium may be stable or unstable. The application of Routh stability criterion on the linearization of the reduced model of groups of three, four and five vehicles allows to state a necessary and sufficient condition on the parameters that ensures asymptotic stability of the uniform flow equilibrium. Anyway, the purpose is to state a result on a generic group of N vehicles. From the non-reduced linearized model of a group of N vehicles, we derive the expression of the characteristic polynomial and apply previous results from the literature. We come up with a necessary and sufficient condition on the roots of the characteristic polynomial and notice that it is the generalization of the conditions derived from Routh criterion. The equilibrium may become unstable if the gap between the safety distance d_0 and the inter-vehicle distance d at the equilibrium is low, the sensitivity of the driver b reduces or the maximum of the velocity function $V_{\max}$ increases. Moreover, if the difference between the safety distance and the inter-vehicle distance at the equilibrium increases, then the stability condition

holds and the eigenvalues of the linearized model have negative real part. Nevertheless, the eigenvalues tend to the imaginary axis, so the uniform flow equilibrium is asymptotically stable but the convergence to the equilibrium is slow. Lastly, the number of vehicles of the model affects stability, too. Increasing N and the length L of the ring road such that $d = \frac{L}{N}$ is constant, the eigenvalues of the linearized model tend to the imaginary axis, slowing down the convergence of the trajectories to the equilibrium.
The study of the stability of the uniform flow equilibrium in the linear framework is carried out on the Optimal Velocity model with saturation, too. Having replaced the hyperbolic tangent with the saturation function, the velocity function may be linear with the headway or it may either saturate to zero or to the maximum value $V_{\max}$. By simulating the model, it is seen that when all velocity functions saturate to $V_{\max}$ or all saturate to zero, the vehicles travel with constant velocity and with any inter-vehicle distances. So, they don't reach the uniform flow equilibrium. On the contrary, if the velocity function of at least one vehicle doesn't lie in the same saturation region of the others or it lies in the linearity region, it is able to make the other velocity functions enter the linearity region. The convergence of the trajectories to the linearity region or the saturation regions depends on the difference between d and d_0. When $-1\ m \leq |d - d_0| \leq 1\ m$, for any initial condition the velocity functions will converge to the linearity region, otherwise they saturate to $V_{\max}$ or to zero. When the velocity functions are linear with the respective headways, the whole model is linear and the uniform flow is the only equilibrium point. Moreover, the analysis of this linear model leads to a necessary and sufficient condition on the parameters similar to the condition derived for the linearization of Bando model. On the contrary, if all velocity functions saturate to $V_{\max}$ or to zero, the model has several equilibrium points that are unstable.
The main purpose of this work focuses on the analysis of the Optimal Velocity models in the nonlinear framework. In particular, it deals with the ellipsoidal under-estimate of the region of attraction of the uniform flow equilibrium. Therefore, we determine a set of initial conditions from which the trajectories of the model are ensured to converge to the uniform flow equilibrium.
In the particular case where $d = d_0$, the Optimal Velocity model with saturation function may be considered as an LTI plant fed with a saturated control input. Therefore, we apply the results from the literature about these particular systems, define local sector constraints and compute ellipsoidal under-estimates of the region of asymptotic stability (RAS) of the uniform flow by solving a set of LMIs. The Bando Optimal Velocity model may be considered as an LTI plant fed with a Neural Network controller with one layer. A recent study in the literature describes a method to determine ellipsoidal estimates of the region of attraction (ROA) of the equilibrium points of LTI systems with Neural Network controllers, based on local sector conditions and the solution of LMIs. We apply this procedure to our model and compute inner-approximations of the ROA of the uniform flow equilibrium for the Bando Optimal Velocity model. In order to determine the best approximation of the RAS and of the ROA for the two models, we define and solve two optimization problems that aim to maximize the volume of the ellipsoidal estimates.
For both models, from numerical analysis, we study how the parameters affect the size of the ellipsoidal estimates. We notice that the volume of the ellipsoids decreases as the drivers' sensitivity b reduces and $V_{\max}$ increases. Being the ellipsoids under-estimates, we

cannot state whether the RAS and the ROA reduce by changing these parameters. Nevertheless, if b decreases and $V_{\max}$ increases, the ellipsoidal set that ensures asymptotic convergence to the equilibrium shrinks. As a result, the influence of these parameters on stability of the linearized model is confirmed in the nonlinear framework, too. Moreover, for the Bando model, if $d > d_0$ (or $d < d_0$), the corresponding local sectors where tanh is inscribed move towards the flat area of the hyperbolic tangent and the volume of the resulting ellipsoidal estimates decreases. The fact that the size of the ellipsoids reduces as $|d - d_0|$ increases reflects the worsening of the real part of the eigenvalues of the linearized model around the uniform flow equilibrium.
Lastly, being the ellipsoidal estimates invariant sets, we exploit this property to determine a set of initial conditions from which the trajectories of the vehicles can start and the don't collide. By adding to the optimization problems constraints on the minimum (and maximum) spacing errors, we inscribe the ellipsoids in a polytope that forces a lower bound on the inter-vehicle distances. Therefore, not only the trajectories of the models that start within the ellipsoidal estimates converge to the origin, but the distance between each couple of vehicles is lower bounded and collision is avoided. The identification of sets of initial conditions from which the inter-vehicle distances are lower bounded during the whole travel fits into the context of road safety.

Comparison of the Optimal Velocity models

Both the Bando Optimal Velocity model and the Optimal Velocity model with saturation function are microscopic traffic models featuring a nonlinear bounded velocity function which depends on the distance with respect to the preceding vehicle. Since the velocity function of the latter is piecewise linear, the model with saturation function is a simplification of the Bando model and in the different working conditions it can be studied as an LTI system. Nevertheless, the model with saturation introduces a drawback, because when the ring road is too long or too short the velocity functions saturate to zero or to $V_{\max}$. Therefore, the vehicles don't regulate their velocities with respect to the current headways and the main principle of the Optimal Velocity traffic modelling fails. This unwanted scenario is a feature of the saturation function alone and it doesn't show off in the Bando model because the hyperbolic tangent never saturates. So, in the Bando model, the vehicles always regulate their velocities on the basis of the headways.
The analyses of the models in the nonlinear framework through the estimate of the region of attraction of the uniform flow equilibrium are similar. In the nonlinear model with saturation function, we assume that the length of the ring road is such that the inter-vehicle distance d at the uniform flow equilibrium equals the safety distance $d_0 = l_v + d_s$. This assumption allows to rewrite the model in a suitable matrix form shown in [23] and determine ellipsoidal estimates of the region of asymptotic stability of the uniform flow equilibrium via the definition of local sector conditions on the nonlinearity of the model. On the contrary, for the Bando model, we don't make any assumption on the parameters. We compute an estimate of the region of attraction of the uniform flow equilibrium through the definition of local sector conditions on the hyperbolic tangent. The size of the ellipsoidal estimates is affected by the sensitivity of the drivers b and by the maximum value of the velocity functions $V_{\max}$ and, as expected, the dependence is the same for both models. Despite the computation of the ellipsoidal estimates for both models is based on the satisfaction of

the nonlinearities of local sector conditions, in the Bando model the method shown in [24] requires to choose 'a priori' the level vectors $\bar{v}$ that define the local sectors. Then, in order to maximize the size of the estimate, we aim to choose the largest level vectors. In the model with saturation, this choice is not needed, since the optimization problem already maximizes the width of the local sectors.

6.2 Improvement of the analyses and future work

The objective of the ellipsoidal estimates is to determine the widest approximation of the region of attraction of the uniform flow equilibrium for the two models. Nevertheless, the analysis of both models shows some limitations.

Limiting choice of the parameters in the model with saturation

In the Optimal Velocity model with saturation function, having reduced the state vector, the only case where the model can be written in the suitable form described in [23] is when the length L of the ring road is such that $d = \frac{L}{N}$ equals $d_0 = l_v + d_s$. As a result, the ellipsoidal estimate of the RAS applies to this particular choice, while it would be interesting to estimate the RAS for any length of the ring road. A possible way to solve this limitation is to inscribe the dead-zone nonlinearity (or the saturation function itself) in a local sector that is not centered in the origin in order to extend the method to LTI system subject to saturated control input featuring a bias in the argument of the saturation function.

Conservativeness of the estimate in the Bando model

The estimate of the ROA of the Bando Optimal Velocity model is not limited to a particular choice of the parameters, because it is sufficient to employ offset local sector constraints on the hyperbolic tangent. The main drawback in the Bando model is that the size of the ellipsoids is limited by the choice of the level vectors $\bar{v}$ defining the local sectors. Especially if $d \neq d_0$, the largest levels for which a feasible solution exists can be very low and lead to relatively small local sectors. Therefore, the size of the resulting ellipsoids is low and the estimates are conservative with respect to the actual region of attraction. The reason why choosing larger $\bar{v}$ vectors lead to no feasible solutions is due to the flat branches of the hyperbolic tangent that defines the nonlinearity of the model. Thus, the profile of the nonlinear function employed to define the model introduces some conservativeness in the estimation of the region of attraction. Nevertheless, we may consider other microscopic traffic models [25] that belong to the family of Optimal Velocity models featuring more complex nonlinear functions other than the hyperbolic tangent. The method described in [24] involving local sector conditions applies to any kind of nonlinearity. Therefore, the same method can apply to any Optimal Velocity model where the nonlinearity is different from the hyperbolic tangent. Employing other nonlinear functions or defining local sector conditions not directly on them but on their linear combinations may lead to better ellipsoidal estimates of the region of attraction.

Further analyses

With the aim of refining the stability analysis of groups of vehicles on a ring road, one possible way is to describe the dynamics by other or more complex mathematical models. As an example, it is a common choice in the literature [10],[12],[20] to combine the Follow-the-leader model and the Optimal Velocity model. The resulting model is a weighted function of the two mathematical descriptions and the addition of the Follow-the-leader model may provide a more complete characterization of traffic dynamics.
In the objective of providing the explanation to the effectiveness of the introduction of autonomous vehicles (AVs) among human-driven ones on ring roads [10], the study of the dynamic traffic model may consider the introduction of external signals representing the AVs. In this framework, a possible improvement of the stability analysis could be the evaluation of the effect that an external signal has on the region of attraction of an equilibrium point. Moreover, the effective results of AVs on the behaviour of human-driven vehicles may be investigated on further properties other than stability. For instance, the effect that AVs have on the improvement of the behaviour of the rest of vehicles should be sought in the context of the reachability or controllability analysis.

Bibliography

[1] Sugiyama, Y., Fukui, M., Kikuchi, M., Hasebe, K., Nakayama, A., Nishinari, K., Yukawa, S.: Traffic jams without bottlenecks – experimental evidence for the physical mechanism of the formation of a jam. New J. Phys. 10 (3), 033001. (2008)

[2] Papageorgiou, M., Kotsialos, A.: Freeway Ramp Metering: an overview. Intelligent Transportation Systems, IEEE Transactions on. 3. 271- 281. 10.1109/TITS.2002.806803. (2003)

[3] Hadj-Salem, H., Blosseville, J. M., Papageorgiou, M.: ALINEA: a local feedback control law for on-ramp metering; a real-life study. Third International Conference on Road Traffic Control, London, UK, 1990, pp. 194-198. (1990)

[4] Smulders, S.: Control of freeway traffic flow by variable speed signs. Transportation Research Part B: Methodological, 24, issue 2, p. 111-132. (1990)

[5] Hegyi, A., De Schutter, B., Hellendoorn, J.: Optimal Coordination of Variable Speed Limits to Suppress Shock Waves. Intelligent Transportation Systems, IEEE Transactions on. 6. 102 - 112. 10.1109/TITS.2004.842408. (2005)

[6] Gomes, G., Horowitz, R.: Optimal freeway ramp metering using the asymmetric cell transmission model. Transportation Research Part C: Emerging Technologies. 14. 244-262. (2006)

[7] Ioannou, P.,Xu, X., Eckert, S., Clemons D., Sieja, T.: Intelligent cruise control: theory and experiment. Proceedings of 32nd IEEE Conference on Decision and Control, San Antonio, TX, USA, 1993, pp. 1885-1890 vol.2, doi: 10.1109/CDC.1993.325521. (1993)

[8] Rajamani, R., Choi, S. B., Law, B. K., Hedrick, J. K., Prohaska, R., and Kretz, P.: Design and Experimental Implementation of Longitudinal Control for a Platoon of Automated Vehicles. ASME. J. Dyn. Sys., Meas., Control. September 2000; 122(3): 470–476. (1998)

[9] Darbha, S., Rajagopal, K.: Intelligent cruise control systems and traffic fow stability. UC Berkeley: California Partners for Advanced Transportation Technology. (1998)

[10] Stern, R. E., Cui, S., Delle Monache, M. L., Bhadani, R., Bunting, M., Churchill, M., Hamilton, N., Haulcy, R., Pohlmann, H., Wu, F., Piccoli, B., Seibold, B., Sprinkle, J., Work, D. B. : Dissipation of stop-and-go waves via control of autonomous vehicles: Field experiments, Transportation Research Part C: Emerging Technologies, Volume 89, Pages 205-221, ISSN 0968-090X. (2018)

[11] Bekiaris-Liberis, N., Roncoli, C., Papageorgiou, M.: Highway Traffic State Estimation with Mixed Connected and Conventional Vehicles Using Speed Measurements. In Proceedingsof the IEEE International Conference on Intelligent Transportation Systems: Smart Mobility for Safety and Sustainability, ITSC 2015 (Vol. 2015-October, pp. 2806-2811). (2015)

[12] Delle Monache, M. L., Liard, T., Piccoli, B., Stern, R., Work, D.: Traffic Reconstruction Using Autonomous Vehicles. SIAM Journal on Applied Mathematics. 79. 1748-1767. 10.1137/18M1217000. (2018)

[13] Wang, M., Daamen, W., Hoogendoorn, S.P., van Arem, B.: Connected variable speed limits control and car-following control with vehicle-infrastructure communication to resolve stop-and-go waves. J. Intell. Transport. Syst. 20 (6), 559–572 (2016)

[14] van de Weg, G., Hegyi, A., Hellendoorn, H., Shladover, S.E.: Cooperative systems based control for integrating ramp metering and variable speed limits. In: Transportation Research Board 93rd Annual Meeting, number 14-1432. (2014)

[15] Lighthill, M. J., Whitham, G. B.: On Kinematic Waves. II. A Theory of Traffic Flow on Long Crowded Roads. Proceedings of the Royal Society A: Mathematical, Physical and Engineering Sciences, vol. 229, no. 1178, pp. 317–345. (1955)

[16] Richards, P. I.: Shock waves on the highway. Operations Research, vol. 4, no. 1, pp. 42–51. (1956)

[17] Pipes, L.A.: An operational analysis of traffic dynamics. J. Appl. Phys. 24(3), 274–281 (1953)

[18] Reuschel, A.: Vehicle movements in a platoon with uniform acceleration or deceleration of the lead vehicle. Zeitschrift des Oesterreichischen Ingenieur-und Architekten-Vereines 95, 50–62 (1950)

[19] Bando, M., Hasebe, K., Nakayama, A., Shibata, A., Sugiyama, Y.: Dynamical model of traffic congestion and numerical simulation. Phys. Rev. E 51(2), 35–1042 (1995)

[20] Giammarino, V., Baldi, S., Frasca, P., Delle Monache, M. L.: Traffic Flow on a Ring With a Single Autonomous Vehicle: An Interconnected Stability Perspective. IEEE Transactions on Intelligent Transportation Systems. PP. 1-11. 10.1109/TITS.2020.2985680 (2020)

[21] Routh, E. J.: A treatise on the stability of a given state of motion, particularly steady motion. p. 127. (1877)

[22] Hurwitz, A.: Ueber die Bedingungen, unter welchen eine Gleichung nur Wurzeln mit negativen reellen Theilen besitzt. Mathematische Annalen, vol. 46, pp. 273–284. (1895)

[23] Tarbouriech, S., Garcia, G., Gomes da Silva Jr., J.M., Queinnec, I.: Stability and stabilization of linear systems with saturating actuators. London: Springer. (2011)

[24] Yin, H., Seiler, P., Arcak, M.: Stability analysis using quadratic constraints for systems with neural network Controllers. ArXiv, vol. abs/2006.07579 (2020)

[25] Helbing, D., Tilch, B.: Generalized Force Model of Traffic Dynamics. Physical review. E, Statistical physics, plasmas, fluids, and related interdisciplinary topics. 58. 10.1103/PhysRevE.58.133 (1998)